Cyclic Behavior of Small Scale Shear Panels Containing Fiber Reinforced Rubber Concrete

A Thesis

Presented to the

Graduate Faculty of the

University of Louisiana at Lafayette

In Partial Fulfillment of the

Requirements for the Degree

Master of Science

Dylan W. Broussard

Fall 2015

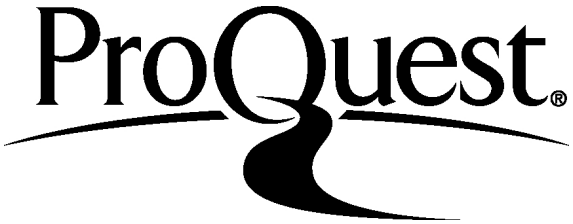

Cyclic Behavior of Small Scale Shear Panels
Containing Fiber Reinforced Rubber Concrete

Dylan W. Broussard

APPROVED:

Kenneth McManis, Co-chair Head and Professor of Civil Engineering	Chris Carroll, Co-chair Assistant Professor of Civil Engineering Saint Louis University
Mohammad Jamal Khattak Associate Professor of Civil Engineering	Russell C. Hibbeler Professor of Civil Engineering
Mary Farmer-Kaiser Dean of the Graduate School	

ACKNOWLEDGMENTS

I would like to extend my thanks to Dr. McManis, Dr. Khattak, and Dr. Hibbeler in helping me to achieve success in my graduate school research. I would especially like to thank my advisor, Dr. Chris Carroll, for his guidance and encouragement throughout the process. In addition, I would like to gratefully acknowledge the support provided by the Louisiana Board of Regents through the Board of Regents Support Fund – Research Competiveness Subprogram (RCS), Contract No. LEQSF (2013-16)-RD-A-12.

This project could not have been accomplished without the dedicated help of my fellow graduate and undergraduate classmates including Michelle Campbell, Dylan Hardy, Nick Helminger, Brant Jones, and Algy Semien. A special thanks to Mr. Mark Leblanc for his laboratory assistance for this project and to fellow graduate classmate Jacob Benton for his help throughout the research project. I would also like to thank my parents, family, and friends for their support as well.

TABLE OF CONTENTS

LIST OF TABLES

LIST OF FIGURES

Appendix A Figures

Appendix B Figures

LIST OF ABBREVIATIONS

a	Shear span length (in)
$A_{v,vert}$	Area of vertical reinforcement (in^2)
$A_{v,horiz}$	Area of horizontal reinforcement (in^2)
A_c	Area of concrete resisting shear transfer (in^2)
A_{cv}	Gross area of concrete bounded by web thickness and length of section in direction of shear force (in^2)
A_g	Area of gross concrete (in^2)
A_s	Area of tensile steel (in^2)
A_{sw}	Area of web reinforcement per row (in^2)
A_v	Area of shear reinforcement (in^2)
A_{vf}	Area of shear-friction reinforcement perpendicular to shear-friction plane (in^2)
b	Width of compression face of member (in)
C	Compressive force of concrete (kips)
c	Distance from extreme compression fiber to neutral axis (in)
d_b	Effective beam depth (mm)
d_f	Diameter of fiber (mm)
E	Modulus of elasticity (ksi)
f'_c	Ultimate concrete compressive strength (psi)
f'_{sp}	Split cylinder strength (Mpa)
f_y	Yield strength (ksi)
F	Load (kips)
F_1	Fiber factor

h	Height of member (in)
h_w	Height of wall (in)
H	Height of potentiometer rectangle (in)
I	Moment of inertia (lb/ft^2)
k	Effective length factor for compression members
l_f	Fiber length (mm)
l	Length of span (in)
l_w	Length of wall (in)
M_{max}	Flexural strength of wall (k-in)
M_n	Nominal moment (k-in)
M_u	Factored moment (k-in)
N_n	Nominal axial load (kips)
N_u	Factored axial load (kips)
r	Radius of gyration (in)
s	Reinforcement spacing (in)
T	Tensile force (kips)
v	Average shear stress (psi)
V_c	Shear capacity of beam (kips)
V_f	Fiber volume fraction
V_{max}	Probable shear demand (k-in)
V_n	Nominal shear (kips)
V_{nb}	Shear at base of wall (kips)
V_s	Shear strength provided by horizontal reinforcement (kips)

V_u	Factored shear (kips)
α	Contribution of the concrete to shear strength
β	Bond factor relating to the shape and surface characteristics of the fiber
β_1	Concrete strength adjustment factor
Υ	Shear strain (rad)
Δ	Lateral displacement (in)
λ	Concrete modification factor
μ	Percentage of σ_{cr} experienced after first crack
ρ	Tensile reinforcement ratio
ρ_l	Vertical reinforcement ratio
ρ_t	Horizontal reinforcement ratio
ρ_w	Web reinforcement ratios
σ_{cr}	Critical stress for buckling (psi)
τ	Fiber matrix interfacial bond
ψ	Concrete modification factor for shear strength
ϕ	Strength reduction factor
δ	Drift
δ_u	Design displacement (in)

CHAPTER 1: Introduction

1.1 Introduction and Purpose

Concrete properties, behaviors, and characteristics have been studied and experimented upon extensively over the past half century. With significant advances in technology over that time, the demand for specific applications of concrete has risen. Along with the design demands, the price of the building materials for these projects is also a factor to consider. Because of this, recycled materials used for sustainable design have been viewed as a viable option. Recycled materials such as fly ash and silica fume are now commonly found in concrete applications, and further research has been and is being done on how to utilize more recycled materials during construction.

One recycled item with numerous studies is recycled tires. Millions of scrap tires are generated each year in the United States alone and ultimately end up in landfills. These scrap tires can be recycled and used as both fine and coarse aggregate replacement in concrete (U.S. Environmental Protection Agency, 2013). Although research has shown that recycled tires in concrete decreases the strength and workability, it is viewed as a viable option for its ductile behavior and increased toughness in comparison to conventional concrete of the same strength (Eldin & Senouci, Rubber-Tire Particles As Concrete Aggregate, 1993), (Khatib & Bayomy, 1999), (Topçu I. B., 1995), (Toutanji, The Use of Rubber Tire Particles in Concrete to Replace Mineral Aggregate, 1996). The characteristics of rubber concrete are desirable for the use in structural applications subjected to extreme events such as seismic activity but no studies to date have investigated its behavior in a structural application. Research has also shown that the addition of other materials such as fibers can increase ductility and toughness significantly. The type, size, orientation, and amount of fiber added to a concrete will

ultimately determine its overall behavior. Fibers have also been found to increase shear strength, increase damage tolerance, and mitigate crack progression by bridging the cracks (Parra-Montesinos & Chompreda, 2007). The drawbacks of adding fibers to concrete are that they increase unit weight (steel), decrease workability, and can be expensive. Similar ductile behavior found in fiber reinforced concrete and rubber concrete can also be achieved with the addition and modification of the structures reinforcing steel but this can often complicate designs and increase the cost of the project.

Considerable research has also been done on structures subjected to extreme events such as seismic activity. This research has led to a better understanding of the desired characteristics and design of reinforced concrete shear walls which are used as the primary element to resist lateral loads in a structure, especially in seismic regions. The seismic design of reinforced concrete shear walls is detailed in Chapter 21 of the ACI Building Code (ACI Committee 318, 2011). The code details the requirements for reinforcement in the web and boundary areas as well as special considerations for additional reinforcement. The requirement for reinforcement in these walls can be an issue when the wall is considered a "low-rise" wall due to the congestion and construction issues the reinforcement in a small area can cause. Low-rise walls must be able to resist large shear demands due to its aspect ratio. Reinforced concrete low-rise shear walls can also be hindered by the significant lack of sustainable drift.

Collectively, research on these three areas is abundant, but research on the addition of recycled rubber particles and fibers to concrete as well as their application in structural low-rise shear walls is scarce. Kim and Parra were the first to research the effects of fibers in low-rise shear walls subject to displacement reversals which yielded positive results (Kim &

Parra-Montesinos, 2003). Further research on fiber reinforced low-rise shear walls subject to displacement reversals was done by Athanasopoulou, Parra-Montesinos, Canbolat, and Jeyeraman (Athanasopoulou, 2010), (Parra-Montesinos, Canbolat, & Jeyeraman, 2006). In addition, there has been no research done on low-rise rubber concrete shear walls subjected to displacement reversals.

The characteristics shown by both the rubber particles and fibers can attempt to simplify the reinforcement in low-rise shear walls and increase energy dissipation, toughness, and ductility, all of which are desirable characteristics in seismic areas. These affects are detailed in the second section of this research. Shear walls subject to extreme loads in structures can benefit greatly if these properties can be improved upon by the addition of these materials. The scope of this research consisted of two main areas. The first focused on shear beams using 22 different mixes. The beams were placed in a MTS Universal Testing Machine supported by two plates and loaded until failure. The behavior and data output of both was then recorded and analyzed. The second was limited to rectangular cantilever low-rise walls with a span-to-length ratio of 1.25 constructed using four different concrete mixes. The four walls were subsequently tested under a reverse static cyclic loading.

1.2 Objectives

The purpose of this research was to determine if fibers and/or rubber particles are a viable option as a mix constituent in reinforced concrete structural shear walls.

1. Conclude the fresh and hardened concrete properties for 22 shear beam mixes and 4 shear wall mixes.
2. Determine the shear strength contributions for each shear beam mix.

3. Observe and determine the effects of the addition of fibers and rubber in concrete shear walls subject to reversed cyclic loads and if they are a viable addition to concrete shear walls.

1.3 Organization of Report

1. Literature Reviewed

   The literature review covered three main topics. The first topic concentrated on the properties and behavior of fibers. The second topic concentrated on the properties and behavior of rubber. The third and final topic concentrated on the design, properties, and behavior of structural shear walls.

2. Methodology and Experimental Studies

   This research project included the analysis of 22 shear beams which were loaded in a MTS Universal Testing Machine until failure along with the design, construction, and testing of four low-rise walls which were placed under reversed cyclic loadings. These walls were designed according to the 2011 ACI Code (ACI Committee 318, 2011). Fresh concrete tests including slump, air content, and unit weight as well as hardened concrete tests including compression tests, split tensile tests, and modulus of elasticity tests were performed on each mix. The main objective of this research was to observe the behavior and analyze the test data of the shear beams and shear walls constructed from mix compositions that included discontinuous steel fibers and rubber.

3. Results and Analysis

   An analysis was completed on the data from the shear beam specimens including fresh concrete properties, hardened concrete properties, the load versus displacement,

crack progression, and shear strength. Experimental tests were used to evaluate the behavior of the wall specimens including fresh concrete properties, hardened concrete properties, the load versus displacement hysteresis response, the damage and crack progression, the lateral load versus drift envelope, the shear strain, the sliding shear response, the wall dilations, the rotations, the stiffness retention capacity, the energy dissipation capacity, and the ductility.

4. Summary and Conclusion

The final section included a summary of the main ideas and topics from the study. This section also included a conclusion of the findings from the experimental part of the study based on the research objectives and recommendations for future research. By conducting this research we hoped to determine the behavior and properties of fiber reinforced rubber concrete shear walls and shear beams by looking at the data collected from our experiment and comparing it to past research and experiments.

CHAPTER 2: Literature Review

2.1 Fiber Reinforced Concrete

2.1.1 Types of Fibers

Fiber reinforced concrete (FRC) contains small and/or large discontinuous fibers that can be categorized by material type used, physical and chemical properties, and mechanical properties. Each fiber type displays its own unique set of properties that can be beneficial or detrimental in a given concrete matrix and application. The types of materials used for fibers are classified into three categories: 1) natural organic materials, 2) natural mineral materials, and 3) man-made. Natural organic materials include cellulose, sisal, jute, or bamboo. Natural mineral materials include asbestos or rock-wool, for example. Lastly, man-made fibers include materials such as steel, titanium, glass, carbon, polymers, or synthetics. Man-made fibers are most commonly used today because they are engineered to be far more effective than any natural organic or natural mineral fiber. The common types of man-made fibers include smooth steel fibers, hooked-end steel fibers, crimped steel fibers, twisted steel fibers, nylon fibers, polyethylene (Spectra) fibers, low-density polyethylene fibers, polypropylene fibers, and polyvinyl alcohol (PVA) fibers. The physical and chemical properties distinguishing fibers include density, surface roughness, chemical stability, non-reactivity with the cement matrix, fire resistance, and flammability. The mechanical properties differentiating fibers include tensile strength, elastic modulus, stiffness, ductility, elongation to failure, and surface adhesion (Naaman, 2003). The performance of an FRC not only depends on the fiber material chosen but also the geometry, fiber volume content, matrix properties, and interface properties (Kim, Naaman, & El-Tawil, 2008). Each fiber type

mentioned is susceptible to the effects of the entire concrete matrix. When choosing the fiber type, it should be selected based on the properties of the concrete desired and its application.

2.1.2 Fiber Volume Fraction and Strain-hardening

Fiber volume fraction refers to the percent amount of fibers that is in a given concrete mix. The addition of fibers can hinder the growth of micro cracks, suppress localization, and slightly increase the strength at which fracture will occur. Ultimately, this will slightly increase the peak load-carrying capacity and drastically increase its tensile strength. Research suggests that the best approach is to increase the fiber volume fraction as much as possible (Shao & Shah, 1997), (Li, Wu, Wang, Ogawa, & Saito, 2002), (Chao, Naaman, & Parra-Montesinos, 2006), (Maalej, Hashida, & Li, 1995). As the volume fraction increases so will the viscosity of the concrete mix, which makes it increasingly difficult to place and mix. Because of this, research advocates that when mixing concrete in bulk construction with conventional mixing techniques, it is optimal to use short fibers (25mm) with a volume fraction of less than one percent (Shao & Shah, 1997). There are also special processing techniques that can overcome the workability issues and large volume fraction of fibers. Slurry infiltrated fiber concrete (SIFCON) and slurry infiltrated mat concrete (SIMCON) are two mix examples that utilize between 5 and 20 percent fiber volume fraction successfully. Although the composites exhibited desirable strain-hardening properties as well as acceptable workability, the drawbacks of these two types of mixes are the high cost of using more fibers in the mix and its suitable applications become limited due to the special processing needs (Li, Wu, Wang, Ogawa, & Saito, 2002). A volume fraction of 5 to 20 percent is not necessarily needed to achieve strain-hardening. Strain-hardening performance can be achieved using proper selection of matrix constituents, types of fiber, and volume fraction of

fiber (Chao, Naaman, & Parra-Montesinos, 2006). Research suggests that even volume fractions as low as 0.8 percent experienced some pseudo strain-hardening behavior (Maalej, Hashida, & Li, 1995).

Consequently, composites are separated into categories in consideration of a bending test and a direct tension test. A bending test classifies a composite as either a deflection-softening material or a deflection-hardening material. If a composite experiences an increase in load capacity after first cracking it is identified as a deflection-hardening material. On the contrary, if a composite experiences a decrease in load capacity after first cracking it is identified as a deflection-softening material. Likewise, a direct tension test also classifies composites as either a strain-softening material or a strain-hardening material. If a composite experiences an increase in load capacity after first cracking it is identified as a strain-hardening material. If a composite experiences a decrease in load capacity after first cracking it is identified as a strain-softening material. A composite that exhibits both strain-hardening and deflection-hardening, has increased ductility and tensile strength (Parra-Montesinos & Chompreda, 2007).

In general, it is economical and practical to select a fiber volume fraction between 1 and 2 percent. Below this amount, the FRC may not experience strain-hardening behavior. Anything above this amount, the cost will increase and without special processing techniques, the workability will decrease.

2.1.3 Hardened Concrete Properties

2.1.3.1 Compressive Strength

Compressive strength is defined as the resistance of a material to breaking under compression. Compressive strength for fiber reinforced concrete is not only dependent on

fiber content and type but also age, water content, particle grading, chemical admixtures, and the composite fabrication process. Research shows both increases and decreases in compressive strength based on the factors above. There is increasing evidence, for most fibers, that compressive strength will initially rise with lower fiber volume fractions. As fiber volume fraction increases beyond a certain point compressive strength will then decrease. This supports the notion that the strength improvement of fibers can work against itself due to degradation (Li, A Simplified Micromechanical Model of Compressive Strength of Fiber-Reinforced Cementitious Composites, 1992).

Fibers cause a strengthening effect in two ways. First, fibers cause an increased resistance to micro crack sliding and extension. This decreases the growth rate of cracks. Secondly, due to the slowed growth of cracks, the fibers bridge any cracks that may join together with another crack to form a larger crack effectively requiring a higher strength for this crack to crack interactions to occur. Crack to crack interaction is necessary for compression failure to take place. As stated earlier, fibers have also experimentally shown that they can decrease the compressive strength of the FRC. Compressive strength is found to decrease when the volume fraction is increased beyond a given point. The reduction of strength will correlate with the void ratio. One also expects an increase in crack density. The large volume fraction of fibers will also drastically decrease the workability. (Li, A Simplified Micromechanical Model of Compressive Strength of Fiber-Reinforced Cementitious Composites, 1992).

Ultimately the increase in fiber volume fraction leads to a competing process of strength improvement due to increased resistance to micro crack sliding and a decrease in strength due to degradation (Li, A Simplified Micromechanical Model of Compressive

Strength of Fiber-Reinforced Cementitious Composites, 1992). Wu and Li studied fiber volume fraction by incorporating steel fibers into conventional concrete. The volume fractions used were 3, 6, and 8 percent. An increase of 10, 95, and 44 percent were observed for the composite ultimate strength respectively. Wu and Li concluded that while steel fibers did increase the compressive strength initially, any volume fraction larger than 6 percent will no longer cause the concrete mixture to gain compressive strength. A volume fraction of 6 percent will also significantly decrease the workability of the concrete mixture (Wu & Li, 1994). Chao et al. conducted similar research and found that a volume fraction of between 1 and 2 percent did not significantly increase or decrease the compressive strength (Chao, Naaman, & Parra-Montesinos, 2006). Shao and Shah found compressive strength increased by less than 10 percent using a volume fraction of 1.5 percent (Shao & Shah, 1997). In general, the effects of the fibers on concrete are determined by the type of fiber and its volume fraction. Mostly small increases in compressive strength were observed but as stated earlier, these results are based on different concrete matrices, fibers, and volume fractions.

2.1.3.2 Tensile Strength

Tensile strength is defined as the amount of stress a material can endure while being pulled or stretched until failure. The addition of fibers to concrete will significantly increase the tensile strength. The increased tensile strength of the concrete is due to the interaction between the fibers and cracks in the matrix. Similar to the behavior when concrete is in compression, fibers decrease crack to crack interaction. Thomas and Ramaswamy and Shao and Shah observed significant increases in post-cracking behavior as the volume fraction increased. They also observed a tensile strength increase of nearly 40 percent (Shao & Shah, 1997), (Thomas & Ramaswamy, 2007). Shende and Pander also observed a significant

increase in tensile strength, where a volume fraction of 1, 2, and 3 percent increased the tensile strength 9 to 15, 14 to 19, and 16 to 29 percent respectively (Shende & Pander, 2011). In general, increased tensile strength is the primary justification for adding fibers to a concrete mix. The type of fiber and fiber volume fraction will affect the behavior of the fiber reinforced concrete just as it did in compression.

2.1.3.3 Flexural Strength

Flexural strength, also known as the modulus of rupture or bending strength is defined as a materials ability to resist deformation due to a load. Due to the increase in tensile strength, the flexural strength of the concrete mix will also increase. When the FRC is subjected to a load causing flexure, the fibers will be placed in tension. On a micro scale, the fibers will act as reinforcement in the FRC to overcome the concrete's natural lack of tensile strength. Similar to the compressive and tensile strengths, the flexural properties will vary based on the type of fiber and the fiber volume fraction (Kim, Naaman, & El-Tawil, 2008).

2.1.3.4 Shear Strength

Shear strength is the strength of a material that resists a type of load attempting to produce a failure along a plane parallel to the direction of the force. Experimental research has established that the addition of fibers to conventional concrete increased shear strength, shear deformation capacity, energy absorption, and a structures ability to remain stiff (Canbolat, Parra-Montesinos, & Wight, 2005), (Athanasopoulou, 2010). In order to better understand the aforementioned properties, research was done on the shear resistance, strength, and interaction when fibers were added to conventional concrete. Two equations utilizing different properties have been developed to estimate the shear strength of fiber

reinforced concrete. Narayanan and Darwish developed an equation for the shear strength of FRC below:

$$v_{frc} = v_c + v_f = 2.8\frac{d}{a}\left(0.24f'_{sp} + 80\rho\frac{d}{a}\right) + 0.41\tau F_1 \; For \; a/d \geq 2.8 \quad \text{Eq. (2-1)}$$

where,

d_b = effective beam depth (mm)

a = shear span length (mm)

f'_{sp} = split cylinder strength (Mpa)

ρ = tensile reinforcement ratio

τ = fiber matrix interfacial bond

F_1 = fiber factor

"F_1" corresponds to the fiber factor which is equal to $\beta V_f \frac{l_f}{d_f}$.

β = bond factor relating to the shape and surface characteristics of the fiber

V_f = fiber volume fraction (%)

l_f = fiber length (mm)

d_f = diameter of fiber (mm)

This method formed by Narayanan and Darwish can be difficult to quantify due to its complexity and can pose limited applicability (Narayanan & Darwish, 1987). The second equation used to estimate the shear strength of fiber reinforced concrete was developed by Khuntia et al. Their research was based on multiple types of fibers gathered from several research projects. The equation assumes correlation between post cracking strength and compressive strength which is inadequate for some fibers as well as assuming $\tau = 0.68\sqrt{f'_c}$ (MPa). According to Khuntia et al., the estimated shear strength for fiber reinforced concrete is (Khuntia, Stojadinovic, & Goel, 1999):

$$v_{frc} = v_c + v_f = (0.167\alpha + 0.26F_1)\sqrt{f'_c} \quad \text{Eq. (2-2)}$$

where,

f'_c = cylinder compressive strength (Mpa)

$$\alpha = \begin{cases} 2.5\frac{a}{d} \leq 3 \; for \; \frac{a}{d} < 2.5 \\ 1 \; for \; \frac{a}{d} \geq 2.5 \end{cases}$$

A third approach to estimate the shear strength of fiber reinforced concrete was researched in 1986 by Vecchio and Collins that related the shear strength of concrete with the tensile stress formed in the cracks. This inferred that the shear input from concrete and fibers are related and could be represented as a single term (Vecchio & Collins, 1986). The two approaches previously discussed above viewed the shear strength of concrete and the shear strength of fibers independently. Research is ongoing today to better understand the shear strength of fibers.

Research has also been done on the shear resistance, strength, and interaction when fibers were added to concrete with steel reinforcement. A modified "truss model" is used to predict shear strength wherein an extra term is added for the contribution of fibers, V_f. Theoretically, V_n can now be found by adding the shear strength provided by the concrete, steel reinforcement, and fibers. This equation is simply an estimate as shear strength for those three elements individually can vary based on a number of factors (Kwak, Eberhard, Kim, & Kim, 2002).

2.1.3.5 Toughness

Toughness is defined as the ability of a material to absorb energy. Concrete toughness is ordinarily increased by using transverse reinforcement but fibers can often times imitate that property. Transverse reinforcement creates hoop tension by confining the lateral

expansion of the concrete. The lateral expansion causes deformations in the reinforcement, in turn, increasing the toughness of the concrete. When steel fibers are used, they bridge the longitudinal cracks caused by the lateral expansion of the concrete. As cracks begin to widen, fibers begin to pull out and toughness increases. The decreasing slope of the descending branch of the stress-strain curve during compression indicates an increase in toughness. The area under the curve in the stress-strain diagram ultimately represents the toughness or amount of energy absorbed by the material. Using steel fibers rather than transverse reinforcement can be beneficial because it typically has less labor cost and shorter construction time (Ou, Tsai, Liu, & Chang, 2012).

Numerous experiments have concluded that the toughness of the concrete will increase as the fiber volume fraction increases. The aspect ratio will also increase up to a certain point (Otter & Naaman, 1988), (Soroushian & Bayasi, 1991), (Ezeldin & Balaguru, 1992), (Hsu & Hsu, 1994), (Mansur, Chin, & Wee, 1999), (Nataraja, Dhang, & Gupta, 1999), (Bhargava, Sharma, & Kaushik, 2006), (Dhonde, Mo, Hsu, & Vogel, 2007), (Bencardino, Rizzuti, Spadea, & Swamy, 2008). Once a fiber volume fraction of over 2 percent was used, toughness no longer increased. It was also observed that the longer fibers outperformed the shorter fibers due to the particular aspect ratios (Ou, Tsai, Liu, & Chang, 2012).

2.1.3.6 Modulus of Elasticity

The modulus of elasticity is defined as the measure of a materials resistance to being elastically deformed when a forced is applied. Research suggests that there is generally very little correlation between adding fibers to concrete and its modulus of elasticity. Because the modulus of elasticity is determined prior to cracking, the fibers are not activated and

therefore play an insignificant role (Hannant, 2003), (Corinaldesi & Moriconi, 2011), (Ou, Tsai, Liu, & Chang, 2012).

2.1.4 Post Cracking Behavior

The addition of discontinuous fibers ultimately enhances post cracking behavior in comparison to conventional, brittle concrete. The extent of this behavior is determined by the type of fiber and fiber volume fraction. When the first crack forms in fiber reinforced concrete, the fibers become engaged. Once engaged, they begin to prevent both the widening of cracks and crack to crack interaction. The fibers can also provide residual strength to the concrete (Morton & Groves, The effect of metal wires on the fracture of a brittle-matrix composite, 1976). The forces fibers experience are due to the following: debonding of the fibers from the concrete matrix, overcoming interfacial forces which oppose the pull-out of the wires, and deforming of the fiber by other means (Outwater & Murphy, 1969), (Helfet & Harris, 1972), (Morton & Groves, The Cracking of Composites Consisting of Discontinuous Ductile Fibres in a Brittle Matrix - Effect of Fibre Orientation, 1974).

Fibers can form two types of bonds with the concrete. The first is a chemical bond which is achieved by adding a latex or epoxy resin to the cement matrix that will increase the adhesiveness of the fiber to the matrix. The second is a mechanical bond described as the bond between the fiber and the cement matrix due to a mechanical deformation in a fiber. Examples of this include crimping along the length of the fiber, hooks, or buttons on the ends (Naaman, 2003), (Willie & Naaman, 2012). By improving either the chemical or mechanical bond, the fibers can increase the amount of force required for overall FRC failure. For the concrete to fail or rupture the fiber must overcome the friction between the matrix and the

fiber (Naaman, 2003). These bonds will help maintain friction and mechanical interlocking limiting crack width and bond degradation (Chao, Naaman, & Parra-Montesinos, 2006).

There are three types of fracture modes associated with a cementitious material: brittle, quasi-brittle, and ductile. Brittle fracture is related to cement like paste which forms very small micro cracks. Quasi-brittle fracture is related to conventional concrete and most fiber reinforced concrete where many of the small micro cracks are bridged which enables the concrete to absorb some energy. Ductile fracture modes have only recently been observed. Maleej, Hashida, and Li first observed ductile fracturing using 2 percent volume fraction of polyethylene fibers in a concrete matrix. (Maalej, Hashida, & Li, 1995). As research progressed, FRC's with volume fractions between 0.5 to 1.5 percent have been used to enhance shear resistance in flexural members subjected to monotonic loads. Because of the increase in shear resistance and ductility, it changed the failure mode in many cases from brittle to ductile. Flexural members with FRC's improve shear resistance by providing tension in diagonal cracks and reducing crack width. The increase in shear resistance has been accounted for by assuming the diagonal tension resistance equal to the FRC post cracking strength. Engineered cementitious composites (ECC), commonly known as bendable concrete, have been used for seismic behavior applications. ECCs improve member ductility, shear strength, damage tolerance, and exhibit a ductile failure mode. In plastic hinge regions it also delays shear strength decay under large inelastic displacement reversals (Parra-Montesinos & Chompreda, 2007).

2.2 Rubber Concrete

2.2.1 Material Properties of Rubber and Mix Composition

Rubberized concrete contains coarse and/or fine particles of rubber. Particles of rubber are integrated into conventional concrete which contains cement, water, and aggregates in order to produce the most effective results. The amount of rubber substituted for aggregate varies depending on application. A common approach to integrating rubber into conventional concrete is done by comparing the size of the rubber being added to the size of the aggregate in the mix. The sizes of the rubber particles being added determine whether it will replace part of the fine aggregate or part the coarse aggregate. Most research has followed this common method (Eldin & Senouci, 1993), (Khatib & Bayomy, 1999), (Ghaly & Cahill(IV), 2005), (Khaloo, Dehestani, & Rahmatabadi, 2008), (Taha, El-Dieb, El-Wahab, & Abdel-Hameed, 2008), (Aiello & Leuzzi, 2010).

When replacing aggregates with rubber the most common method is to replace by volume. Therefore, the volume of aggregate removed from the conventional mix would be replaced with an equal volume of rubber particles ranging anywhere from 0 to 100 percent (Toutanji, 1996), (Taha, El-Dieb, El-Wahab, & Abdel-Hameed, 2008). When larger volumes of aggregate are replaced with rubber, workability becomes an issue as well as a large decrease in strength. As the replacement by volume percentage decreases, workability and strength will improve. Consequently, it is recommended that replacing no more than 20 percent of the aggregates volume should occur. This ensures that the properties of the rubberized concrete remain favorable (Khatib & Bayomy, 1999).

2.2.2 Fresh Concrete Properties

2.2.2.1 Unit Weight

The unit weight of rubberized concrete is less than that of conventional concrete and will decrease with increasing rubber replacement (Topçu, 1995), (Biel & Lee, 1996), (Khatib

& Bayomy, 1999), (Khaloo, Dehestani, & Rahmatabadi, 2008), (Taha, El-Dieb, El-Wahab, & Abdel-Hameed, 2008), (Zheng, Huo, & Yuan, 2008). There are two main reasons for this. First, rubber has a lower specific gravity than the aggregate it is replacing. Typically, rubber added to concrete has a specific gravity of between 1.0 and 1.2. The rubber will occupy the same volume but with less weight (Khaloo, Dehestani, & Rahmatabadi, 2008), (Taha, El-Dieb, El-Wahab, & Abdel-Hameed, 2008), (Zheng, Huo, & Yuan, 2008). Second, rubber has the capability to entrap air in between its surfaces. When air becomes entrapped between the surfaces of the rubber, it is incorporated into the mix causing a higher air content. The entrapped air takes up volume in the concrete by creating voids thus lowering the unit weight (Khatib & Bayomy, 1999), (Taha, El-Dieb, El-Wahab, & Abdel-Hameed, 2008).

2.2.2.2 Air Content

As previously stated, when rubber is added to a concrete mixture the air content increases due to the entrapped air between the surfaces on the rubber (Khatib & Bayomy, 1999), (Khaloo, Dehestani, & Rahmatabadi, 2008), (Taha, El-Dieb, El-Wahab, & Abdel-Hameed, 2008). Khaloo et al. suggest air entrapment is the result of rubber being non-polar causing it to repel water and attract air (Khaloo, Dehestani, & Rahmatabadi, 2008).

2.2.2.3 Workability

Workability is defined by Khaloo et al. as "the ease with which concrete can be mixed, transported, and placed (Khaloo, Dehestani, & Rahmatabadi, 2008)." As a result, if a given concrete mixture is deemed to have poor workability then it may not be practical. Through experimentation it is found that workability is directly dependant on the percentage of rubber in the mixture (Khatib & Bayomy, 1999), (Taha, El-Dieb, El-Wahab, & Abdel-Hameed, 2008). While both coarse and fine rubber particles can decrease workability, coarse

rubber particles tend to cause greater workability issues for any replacement level. (Taha, El-Dieb, El-Wahab, & Abdel-Hameed, 2008),(Khaloo, Dehestani, & Rahmatabadi, 2008), (Biel & Lee, 1996), (Toutanji, 1996) (Taha, El-Dieb, El-Wahab, & Abdel-Hameed, 2008). Fine rubber particles tend to have a slightly different effect on the workability. Results from experiments show that adding fine rubber particles up to 15 percent replacement levels by volume had better workability than coarse rubber (Khaloo, Dehestani, & Rahmatabadi, 2008).

2.2.3 Hardened Concrete Properties

2.2.3.1 Compressive Strength

Concrete is fundamentally utilized for its high compressive strengths, but when coarse and/or fine rubber particles replace aggregates, its compressive strength significantly decreases. Much research has been done using various replacement values of both fine and coarse rubber particles. All confirm a decrease in compressive strength. There are generally three main reasons rubber causes compressive strength to decrease in comparison to conventional concrete: 1) rubber's low modulus of elasticity, 2) high stress concentrations at the boundaries of the rubber particles, and 3) bonding issues between cement paste and rubber. Research done on the relationship between strength reduction and rubber content has led to different conclusions. Many think of it as a "systematic reduction" in that compressive strength decreases as the amount of rubber particles added increases (Khatib & Bayomy, 1999). Ghaly and Cahill IV believe the relationship to be "almost linear" while Toutanji deems the relationship to have no linear properties (Toutanji, 1996), (Ghaly & Cahill(IV), 2005).

Research on rubber particles in concrete began in 1993 when Eldin and Senouci conducted experiments using both recycled tire chips and fine crumb rubber. The tire chips ranged from 0.23 in. to 1.49 in. while the fine crumb rubber was no larger than 0.071 in. As stated earlier, the larger tire chips replace coarse aggregates and the fine crumb rubber replace fine aggregate in conventional concrete. In this particular experiment, replacement by volume never exceeded 25 percent due to the extreme drop off in compressive strength beyond this point. They observed a decrease in compressive strength up to 85 percent for replacement by tire chips and up to 65 percent for replacement by fine crumb rubber (Eldin & Senouci, 1993). Concrete's compressive strength relationship to volume replacement was further researched in 1995 by Topçu. Instead of capping replacement by volume at 25 percent, Topçu used a range of 15 to 45 percent replacement by volume. Much like Eldin and Senouci, Topçu observed significant losses in compressive strength. For replacement by coarse rubber particles, a loss of 60 to 85 percent compressive strength was observed, and for fine rubber particles a loss of 50 percent compressive strength was observed (Topçu, 1995). Taking a closer look at the results, Eldin, Senouci, and Topçu all concluded that coarse rubber causes a larger decrease in compressive strength than fine rubber did. This finding was also supported by numerous researchers (Huang, Li, Pang, & Eggers, 2004), (Taha, El-Dieb, El-Wahab, & Abdel-Hameed, 2008), (Zheng, Huo, & Yuan, 2008), and (Aiello & Leuzzi, 2010). While both sets of research performed by Eldin, Senouci, and Topçu found decreases in compressive strength, each believed it occurred for a different reason. Eldin and Senouci believed that the rubber acted as a void in the concrete unlike the fine and coarse aggregate it replaced. In conventional concrete aggregates act as a load bearing material so as rubber replacement by volume increases there become more voids and less load bearing

material in the concrete, significantly reducing the compressive strength (Eldin & Senouci, 1993).

Edge tensile stresses increase considerably in materials with a low modulus of elasticity when an opposing force is applied. The material deforms along the perpendicular axis to the load as the load is applied causing high edge stresses. Eldin et al. attributed the loss in compressive strength to the increasing stress on the boundaries of the rubber particles as load is applied. The high stress on the edges wear away the bond between the rubber and cement paste the resulting in lower strengths (Eldin & Senouci, 1993), (Topçu, 1995). The notion of large stress concentrations on the boundaries of the rubber particles was also supported by Zheng, Huo, and Yuan (Zheng, Huo, & Yuan, 2008).

Topçu believed the reduction in compressive strength was also due to the weak bond between the rubber and cement paste (Topçu, 1995). Following Topçu's conclusion, two groups of experiments were conducted to improve the bond between the rubber and cement paste. The first group focused on the pretreatment of the rubber particles. Segre and Joekes concluded that soaking the rubber aggregates in a NaOH solution would improve the bond strength (Segre & Joekes, 2000). Khaloo et al. concluded that simply washing the rubber aggregates with water would also increase the bond strength (Khaloo, Dehestani, & Rahmatabadi, 2008). Further research was done on presoaking the rubber in a NaOH solution that contradicted Segre and Joekes claims. Albano et al. found that pretreatment of washing the rubber in NaOH does not significantly change the compressive and tensile strengths in comparison to untreated rubber composites(Albano, C.; Camacho, N.; Reyes, J.; Feliu, J.L.; Hernandez, M., 2005). To settle whether pretreatment improves the bond strength further research will need to be conducted. The second solution to improving bond strength focused

on changing the type of cement used so that it chemically bonded better with the rubber. In conventional concrete Portland cement is used. Biel and Lee experimented to create a better bond between rubber and cement paste by using cement containing magnesium oxychloride. When 25 percent rubber by volume was replaced in the mix, both Portland cement rubber concrete (PCRC) and magnesium oxychloride cement rubber concrete (MOCRC) experienced a 90 percent decrease in compressive strength. The compressive strength for MOCRC was still more than two and a half times larger than that of PCRC though. Instead of a faulty bond between the rubber and cement paste, the rubber itself was failing which established that the bond strength between the rubber and cement paste had increased (Biel & Lee, 1996). In conclusion, numerous experiments were conducted and verified that replacement of rubber by volume with aggregates in concrete will reduce the compressive strength.

2.2.3.2 Tensile Strength

While concrete already has low tensile strength with respect to its compressive strength, the addition of rubber to a concrete mix only decreases the tensile strength further. Much like the compressive strength of rubberized concrete, the tensile strength decreased as the amount of rubber increased (Eldin & Senouci, 1993), (Topçu, 1995), (Khatib & Bayomy, 1999). It was also noted that the reasons for the decrease in tensile strength were the same three reasons previously stated for the decrease in compressive strength. Eldin and Senouci used various combinations of tire chips and fine crumb rubber for volume by replacement and observed up to a 50 percent decrease in tensile strength (Eldin & Senouci, 1993). Topçu conducted a similar experiment where he observed losses in tensile strength of 64 percent for coarse rubber replacement and 74 percent for fine rubber replacement. Similar to

compressive strength, the tensile strength loss for coarse rubber was more significant than that of fine rubber (Topçu, 1995).

Bond strength between the rubber particles and cement paste was an issue for tensile strength, much like it was for compressive strength. As stated earlier, Biel and Lee observed bond improvement when using magnesium oxychloride cement compared to Portland cement. This led to a higher compressive strength in MOCRC than in PCRC. The tensile strength observed in MOCRC was 14 percent greater than the PCRC further illustrating the improved bond by using magnesium oxychloride cement (Biel & Lee, 1996). Although MOCRC showed a greater tensile strength than PCRC, it still demonstrated an overall decrease in tensile strength compared to conventional concrete. All things considered, research demonstrates an overall decrease in tensile strength for rubberized concrete.

2.2.3.3 Flexural Strength

Similar to the compressive and tensile strengths, the flexural strength of concrete decreases as rubber increases in the mix. Flexural strength research for rubberized concrete began when Toutanji incorporated tire chips into concrete mixes at different replacement by volume amounts. Toutanji observed up to a 35 percent decrease in flexural strength depending on the replacement by volume amount (Toutanji, 1996). Khatib and Bayomy researched further including not only coarse rubber but fine crumb rubber as well. Using various combinations of coarse rubber and fine crumb rubber together in concrete mixes, they observed a decrease in flexural strength as rubber was increasingly added to the mix. This meant that its resistance to bending was less than that of conventional concrete (Khatib & Bayomy, 1999). Coarse rubber effects on flexural strength compared to fine crumb rubber effects on flexural strength research continued in 2010 when Aiello and Leuzzi cast two

separate specimens, each containing only one type of rubber. Using various replacements by volume amounts, the flexural strength for both members decreased. It was also observed that the coarse rubber affected the flexural strength more than the fine crumb rubber which is consistent with its effects on the compressive and tensile strength (Aiello & Leuzzi, 2010). While the overall effect on flexural strength of rubberized concrete showed significant decreases, it was not as noteworthy as the losses in the compressive and tensile strengths.

2.2.3.4 Toughness

The most useful and important attribute of rubberized concrete is increased toughness. Structures are often subject to dynamic loadings that can exert large amounts of energy on the given material comprising the structure. If the material is very tough it has the ability to absorb and dissipate large amounts of energy without failure. Eldin and Senouci examined the toughness of rubberized concrete by looking directly at the plastic energy and fracture toughness. The plastic energy can be found by examining the stress-strain diagram. When the elastic energy is subtracted from the overall energy, plastic energy remains. By displaying a large amount of plastic energy, the material is considered tough, and fracture toughness can be calculated by finding the area under the plastic portion of the stress-strain curve. Upon fracture Eldin and Senouci found that most of the total energy was in fact plastic energy and not elastic energy. Elastic energy is commonly present in large amounts when dealing with brittle materials like conventional concrete (Eldin & Senouci, 1993). Zheng, Huo, and Yuan further investigated how the addition of rubber converted the conventional concrete from a brittle material to a more ductile material (Zheng, Huo, & Yuan, 2008). Topco conducted a similar experiment and observed similar results. Topçu found that enhanced toughness with the addition of rubber elevated the energy capacity allowing more

strain at the time of the fracture. With the addition of rubber, the originally high elastic energy capacity of conventional concrete decreased as the originally low plastic energy capacity increased. As stated earlier, the increased plastic energy capacity raised the fracture toughness enabling it to exhibit higher deformation during fracture due to its ability to absorb more energy (Topçu, 1995). Toutanji took a slightly different approach a year later when Toutanji examined the load-deflection diagram. Toutanji calculated the value for toughness as the ratio between the area under the curve up to 85 percent of the total load and the area under the curve that corresponded to an estimate of the elastic behavior limit. Khaloo et al. utilized the same ratio but only up to 80 percent of the total load. Toutanji observed a toughness ratio that was larger than conventional concrete for up to 50 percent replacement by volume using tire chips which corresponds to a higher material toughness. Any amount beyond 50 percent, toughness tended to decrease due to the rapid decline in compressive strength beyond this point. The amount for replacement by volume to achieve maximum toughness was found to be 25 percent (Toutanji, 1996), (Khaloo, Dehestani, & Rahmatabadi, 2008). Huang et al. (2004), Taha et al. (2008), and Zheng et al. (2008) all conducted similar experiments after Toutanji that confirmed the increase in toughness for rubberized concrete up to 50 percent replacement by volume. In short, the addition of rubber up to 50 percent replacement by volume increases the toughness of concrete.

2.2.3.5 Modulus of Elasticity

The modulus of elasticity, which measures a materials ability to resist elastic deformation, for concrete decreases when rubber is added. It is one of the more important properties of concrete because it can drastically impact the performance of the structure. The core reason that the modulus of elasticity of concrete decreases when rubber is added is

because the modulus of rubber is less than the aggregates it is replacing (Eldin & Senouci, 1993), (Topçu, 1995), (Khaloo, Dehestani, & Rahmatabadi, 2008).

In 1999, Khatib and Bayomy oberseved the elastic modulus of two rubber concrete mixes. The mix containing coarse rubber showed a decrease in its modulus of elasticity by 28 percent. The mix containing fine rubber displayed a larger loss in its modoulus of elasticity by decreasing 53 percent. The large reduction seen in the modulus of elasticity also explains the increased ductility and flexibility of rubberized concrete (Khatib & Bayomy, 1999). Zheng et al. further studied the effect rubber has on the modulus of elasticity of a concrete mix. Zheng et al. found that the modulus of elasticity was closely related to three things: "The properties of the cement paste, the stiffness of the aggregates, and the method in which one determines the modulus." With replacement by volume amounts ranging from 15 to 45 percent, a reduction in the static modulus ranged from 14.8 to 29.9 percent for fine rubber and 27.4 to 49.9 percent for coarse rubber. Similar to the static modulus, the dynamic modulus decreased with increasing rubber replacement. A reduction in the dynamic modulus ranged from 16.5 to 25 percent (Zheng, Huo, & Yuan, 2008). In brief, both the static and dynamic modulus of elasticity showed a reduction as the rubber content increased.

2.2.4 Failure Mode

It is important to understand the entire failure process and the role the material properties play in its behavior. When rubber is a part of the concrete matrix, the rubber particles have the capacity to absorb a large amount of tensile force before failure. This capacity is larger than that of the cement paste which will cause cracks in the cement matrix before the rubber is deformed. As the cracks in the cement paste come into contact with the rubber particles, the rubber particles absorb the tensile force until the cracks become too

large and too abundant. At this point the bond between the cement paste and the rubber particles will fail. This absorbtion of energy by the rubber particles gives the concrete its added toughness and ductility. Further exploring the failure mode for rubber concrete, Eldin and Senouci looked at the type of rubber used. Edgar chips, tire chips containing steel fibers, failed gradually in compression while Preston rubber, rubber free of wires or fibers, gradually failed due to a shearing effect. A shear failure will occur if the shear stress of the rubber exceeds the shear strength of the cement. The tensile stress must also remain below its tensile strength (Eldin & Senouci, 1993).

All in all, conventional concrete is brittle and exhibits explosive behavior when it fails. Its failure tends to be extremely quick and often without warning. In contrast, concrete with rubber demonstrates a failure mode that is more gradual due to its ductile and flexible properties given to it by the replacement rubber (Eldin & Senouci, 1993), (Topçu, 1995), (Biel & Lee, 1996), (Toutanji, 1996), (Khatib & Bayomy, 1999).

2.3 Shear Walls

2.3.1 General

Shear walls, also known as structural walls, are reinforced concrete walls that resist loads acting parallel to the plane of the wall often due to earthquakes or wind. They resist both the gravity loads of the structure and the lateral loads and moments about the strong axis of the wall. In large structures, shear walls provide lateral strength, stiffness, and confine lateral drift. Due to the inability of a large structure to resist these types of loads, research has shown that they are a high performance alternative to other types of frames for regions with high seismic activity (Fintel, 1991), (Wood L. S., 1991), (Zhang & Wang, 2000).

Shear walls in structures are especially common in earthquake prone areas. The size and magnitude of an earthquake is quantified by the total amount of energy released during the entirety of the event. The energy is rapidly released through the plates into the soil and ultimately into the structures resting on the soil. Due to the complexity of seismic behavior, ongoing research constantly changes and updates code and design requirements (Earthquake Hazards Program, 2015).

While shear walls are often used in one vertical plane, many types of three dimensional assemblies exist. Configuration is dependent on application and can come in all shapes and sizes. Common shear wall configurations include barbell shaped, flanged shaped, and asymmetrical T-shaped and L-shaped sections. The configuration will ultimately affect its strength, stiffness, and ductility in response to any applied load (Paulay T. M., 1986), (Wallace & Moehle, The 3 March 1985 Chile Earthquake: Structural Requirements for Bearing Walls Buildings, 1989).

Shear walls can be divided into three groups based on their overall height-to-length ratio (h_w/l_w). Walls with a ratio of less than 1.5 are referred to as "low-rise" walls. These walls are designed either by the requirements given in ACI Code Chapter 11 or the strut-and-tie method given in ACI Code Appendix A. In low-rise walls shear action typically dominates the walls behavior. Walls with a height-to-length ratio between 1.5 and 2.0 are referred to as "mid-rise" walls. They are governed by both shear and flexure action. Walls with a ratio greater than 2.0 are referred to as "slender" or "high-rise" walls. The exact values categorizing the type of wall vary slightly depending on the source. These walls are designed by the requirements given in ACI Code Chapter 10 and 11. In slender walls, lateral loads are typically resisted by flexure action rather than shear action due to their height and can be

treated similar to a cantilever beam (Salonikios, Kappos, Tegos, & Penelis, Cyclic Load Behavior of Low-Slenderness Reinforced Concrete Walls: Design Basis and Test Results, 1999), (Zhong, Mo, & Liao, 2009). They also effectively limit lateral drift better than low-rise walls (Salonikios, Kappos, Tegos, & Penelis, Analytical Prediction of the Inelastic Response of RC Walls with Low Aspect Ratio, 2007). ACI Code Requirements for Structural Concrete govern the vast majority of the design parameters for a structural wall in both seismic and nonseismic areas. As research and testing became more advanced the values and equations for both seismic and nonseismic design were modified and updated.

General behavior and deformation capacity of shear walls is due to wall configuration, aspect ratio, wall reinforcement ratios, and the load and stress demands (Wallace, New Methodology for Seismic Design of RC Shear Walls, 1994). Research on this behavior under monotonic and reversed lateral cyclic loadings has been occurring since the 1960's. This research has provided a guideline for designing shear walls to meet strength and stiffness requirements under extreme loads. Shear walls must also be able to disperse the energy of extreme loads, especially after yielding, so that they do not suddenly fail due to shear or local instabilities (Paulay, Priestley, & Synge, 1982).

2.3.2 Design of Shear Walls

2.3.2.1 Shear Wall Foundations

The foundation beneath a shear wall must be able to transfer the moment, shear, and axial forces from the base of the wall to the supporting structure or ground. The overall performance of the foundation will profoundly affect the response of the shear wall and its effect on the structure. Consequently, the local demand on a given wall and foundation could be extremely large and critical. Because shear walls have a plethora of applications, the

foundation is designed based on the application of the wall and the behavior it wishes to exhibit. When designing an elastic foundation system for a structural wall the following steps should be taken:

1. The forces applied to the foundation are taken from the force action at the base of the wall.
2. The foundation should have strengths greater than or equal to the moments and forces applied to it from the wall.
3. The bearing area under the foundation should have negligible inelastic deformations upon the application of forces to the structure.
4. Due to yielding and energy dissipation, seismic detailing of reinforcement is not necessary.
5. Slab thickness must be in accordance with ACI Code Section 14.5.3.2 which states the foundation shall not be less than 7.5 inches thick (ACI Committee 318, 2011).

ACI Code Section 21.12 states that seismic design of foundations may require further longitudinal reinforcement that extends into the structural wall. When a lateral load, such as an earthquake, is applied to a shear wall without a significant axial load, it will cause uplift on one side of the wall between the base of the wall and the foundation. An axial load and moment is then resisted by the material under the foundation causing a varying pressure (as low as zero and as high as twice the stress) along the width of the foundation. These tensile stresses can be difficult to resist and should be avoided (Seismic Design of Reinforced Concrete and Masonry Buildings, 1992). Possible solutions to this issue are:

- Increase the radius of gyration of the footing $r = \sqrt{\frac{I}{A}}$.

- Use a pile or caisson foundations
- Divide the transferred moment by using coupled shear walls.
- Using horizontal outrigger beams, attach the base of the wall to collect the vertical loads adjacent to the columns to counteract any uplift.
- Attach the base of the wall to the ground floor, providing a horizontal force to counteract the moment at the base of the wall.
- Use a mat foundation.

When conducting research, two slabs are often cast on the top and bottom of the wall. The top slab is used to uniformly transfer load from the hydraulic actuator to the shear wall while the bottom slab acts as the wall's foundation and connection to the rest of the test structure. These slabs also provide the wall with torsional rigidity (Farrar & Baker, 1990), (Farrar & Baker, 1993).

2.3.2.2 Required Size of Wall

When designing the parameters of a shear wall it must at least meet two requirements. First, the wall must have enough stiffness to limit the lateral deflections. An estimate for the minimum stiffness a wall should have can be found by viewing the wall as a vertical cantilever with a distributed load spanning it. The walls stiffness, EI, can then be calculated based on a given deflection. Although this method is extremely simplified, it is effective in finding estimated wall stiffness. Second, it must be strong enough to resist all factored moments, shears, and axial loads acting on it. Because of the vast amount of ways to design a wall there is no widely accepted way of doing this as long as it meets the two requirements stated above. The minimum thickness for a wall is detailed via the empirical design method

in ACI Code Section 14.5.3. As stated, the rectangular cross section of a wall should be no smaller than 1/25 of the supported height or length (ACI Committee 318, 2011).

2.3.2.3 Reinforcement in Shear Walls

Reinforcement in a shear wall is comprised of two types of support systems. Distributed horizontal and vertical reinforcement are uniformly spread throughout the height and length of the wall. Concentrated vertical reinforcement is located near the edges of the wall and is tied in to the other reinforcement in the wall. The minimum amount of distributed reinforcement is detailed in ACI Code Section 14.3 if $V_u<0.5\phi V_c$. ACI Code Section 14.3.2 states that the minimum ratio of vertical reinforcement area to gross concrete area (A_g) shall be 0.0012 for deformed bars not larger than No.5. ACI Code Section 14.3.3 states that minimum ratio of horizontal reinforcement area to gross concrete area (A_g) shall be 0.0020 for deformed bars not larger than No.5. In addition, a greater amount of reinforcement may be required if $V_u>0.5\phi V_c$. ACI Code Section 11.9.9 states that if $V_u>0.5\phi V_c$ then additional horizontal shear reinforcement shall be provided to satisfy Eq. (2-16). At least two curtains of reinforcement are required if V_u exceeds $2A_{cv}\lambda\sqrt{f'_c}$. Furthermore, if the height-to-length ratio (h_w/l_w) of the shear wall is less than 0.5 then the amount of horizontal and vertical reinforcement is equal. If the height-to-length ratio (h_w/l_w) is greater than 2.5 then a minimum amount of vertical reinforcement equal to $0.0025sh_w$ is required. Because shear walls are subject to large reversals of moments under extreme loads, a larger minimum vertical reinforcement may be required in order to prevent fracture of the vertical reinforcement. The percentage of vertical steel (ρ_l) and horizontal steel (ρ_t)are detailed in equations Eq. (2-3) and Eq. (2-4):

$$\rho_l = A_{v,vert}/(hs_1) \qquad \text{Eq. (2-3)}$$

$$\rho_t = A_{v,horiz}/(hs_2) \quad \text{Eq. (2-4)}$$

where,

$A_{v,vert}$ = Area of vertical reinforcement (in^2)

$A_{v,horiz}$ = Area of horizontal reinforcement (in^2)

h = height of reinforcement (in)

s = reinforcement spacing (in)

In accordance with ACI Code Section 21.9.4.3, if h_w/l_w does not exceed 2.0 the reinforcement ratio ρ_t shall not be less than the reinforcement ratio ρ_l (ACI Committee 318, 2011).

In seismic areas boundary elements, which are extra vertical reinforcements enclosed by hoop reinforcement, may be necessary to prevent failure. Boundary elements strengthen the edges of the wall preventing buckling by resisting the reversals in stresses caused by the back and forth motion of an earthquake. The design requirement for boundary elements is stated in ACI Code Section 21.9.6. For continuous walls from the base of the structure to the top of the wall designed to have a single critical section, compression zones shall be reinforced with special boundary elements when Eq. 2-5 is satisfied.

$$c \geq \frac{l_w}{600(\frac{\delta_u}{h_w})} \quad \text{Eq. (2-5)}$$

where,

c = distance from extreme compression fiber to neutral axis (in)

l_w = length of wall (in)

δ_u = design displacement (in)

h_w = height of wall (in)

$\frac{\delta_u}{h_w}$ shall not be taken as less than .007 (ACI Committee 318, 2011).

ACI Code Section 14.3.6 details the requirements for transverse confinement ties. It states that vertical reinforcement does not need to be enclosed by transverse ties if the vertical reinforcement area ($A_{v,vert}$) is greater than 0.01 time the gross area of concrete (A_g), or where vertical reinforcement is not required as compression reinforcement. (ACI Committee 318, 2011).

2.3.2.4 Flexural, Shear, and Axial Strength of Shear Walls

The cross section of a wall is designed to satisfy the nominal flexure (Eq. (2-6)), axial (Eq. (2-7)), and shear (Eq. (2-8)) resistance modified by a strength reduction factor (ϕ).

$$\phi M_n \geq M_u \qquad \text{Eq. (2-6)}$$

$$\phi N_n \geq N_u \qquad \text{Eq. (2-7)}$$

$$\phi V_n \geq V_u \qquad \text{Eq. (2-8)}$$

The resistance capacities are set forth by the specified material strengths. ACI Code Section 9.3.2 details the strength reduction factor for flexure and axial loads and ACI Code Section 9.3.2.3 details the strength reduction factor for shear loads. ACI Code Section 9.2.1 describes the factored loads and load combinations (ACI Committee 318, 2011).

The strength reduction factor (ϕ) can be calculated using the strain (ε_t) located in the layer of steel at the depth (d_t) farthest from the extreme-compressive fiber. When c, the distance from the extreme-compressive fiber to the neutral axis, is less than $0.375d_t$ then ϕ=0.9 which is considered the tension-controlled limit for a wall. When c is greater than $.6d_t$ then ϕ=0.65 which is considered the compression controlled limit for a wall. If the distance from the extreme-compressive fiber to the neutral axis is between $0.375d_t$ and $0.6d_t$ the value of ϕ is located linearly between ϕ=0.9 and ϕ=0.65.

To find the nominal flexural strength, M_n, a procedure was developed by A. E. Cardenas et al. in 1973. The following assumptions were made using a rectangular wall section with a uniform distribution of vertical reinforcement and a factored axial load, N_u:

- All steel in the tension zone yields in tension.
- All steel in the compression zone yields in compression.
- The tension force acts at mid-depth of the tension zone.
- The total compression force acts at mid-depth of the compression zone.

Cardenas and fellow researchers were able to formulate an equation for the nominal flexural moment that closely correlated with the measured moments of the shear walls they tested. The nominal flexural moment was found to be approximately equal to (Cardenas, Hanson, Corley, & Hognestad, 1973), (Cardenas & Magura, 1973):

$$M_n = T\left(\frac{l_w}{2}\right) + N_u\left(\frac{l_w - c}{2}\right) \qquad \text{Eq. (2-9)}$$

where,

M_n = nominal flexural strength at section (kip=in)

T = tensile force (kips)

l_w = length of wall (in)

N_u = axial force (kips)

c = distance from extreme compression fiber to neutral axis (in)

Ultimate shear strength of a shear wall and its design to resist a given shear has two common approaches used by researchers. The first approach is to use the derivation of empirical expressions based on experimental data and results (Barda, Hanson, & Corley, 1977), (Aktan & Bertero, 1985), (Wood S. L., 1989), (Wood S. L., 1990). The second approach is to apply models based on structural mechanics using equilibrium and material

relationships (Collins & Mitchell, 1986), (Aoyama, 1991). Most modern building codes, such as ACI use the empirical or semi-empirical method for the ultimate shear strength of shear walls.

Design specifications for shear walls in nonseismic areas can be found in ACI Code Section 11. The design specifications for shear walls are similar to the basic beam design which can be found throughout the same section. The basic shear design equations for a reinforced concrete beam are shown in equations Eq. (2-10) through Eq. (2-12).

$$\phi V_n \geq V_u \qquad \text{Eq. (2-10)}$$

$$V_n = V_c + V_s \qquad \text{Eq. (2-11)}$$

$$V_s \geq \left(\frac{V_u}{\phi}\right) - V_c \qquad \text{Eq. (2-12)}$$

ACI Code Section 11.9.3 limits V_n for shear walls to a maximum value of:

$$10\sqrt{f'_c}hd \qquad \text{Eq. (2-13)}$$

where,

d = 0.81w

h = height of member (in)

f'_c = compressive strength of concrete (psi)

ACI Code Section 11.9.6 allows V_c to be taken as the smaller of equations Eq. (2-14) and Eq. (2-15).

$$V_c = 3.3\lambda\sqrt{f'_c}hd + (N_u d)/(4l_w) \qquad \text{Eq. (2-14)}$$

$$V_c = 0.6\lambda\sqrt{f'_c} + \frac{l_w\left(1.25\sqrt{f'_c} + \frac{2(N_u)}{l_w h}\right)}{\left(\frac{M_u}{V_u}\right) - (l_w)/2} \qquad \text{Eq. (2-15)}$$

where,

Eq. (2-14) V_c = shear force when web-shear cracking begins for low-rise walls (kips)

Eq. (2-15) V_c = shear force when flexural-shear cracking begins for low-rise walls (kips)

λ = concrete modification factor

f'_c = compressive strength of concrete (psi)

h = height of member (in)

d = distance from extreme compression fiber to centroid of longitudinal tension reinforcement (in)

M_u = moment (kip-in)

l_w = length of wall (in)

N_u = axial force (kips)

V_u = shear force (kips)

The shear strength provided by horizontal reinforcement (V_s) is (ACI Committee 318, 2011) shown in equation Eq. (2-16).

$$V_s = (A_v f_y d)/s \qquad \text{Eq. (2-16)}$$

where,

A_v = area of shear reinforcement (in^2)

f_y = yield strength (ksi)

d = distance from extreme compression fiber to centroid of longitudinal tension reinforcement (in)

s = reinforcement spacing (in)

Salonikios et al. argue that the code formula for shear strength should be based on the post-peak capacity after a given level of inelasticity. When the wall enters the inelastic range, strength degradation occurs causing a shear mechanism to form drastically affecting the strength of the wall (Salonikios, Kappos, Tegos, & Penelis, Cyclic Load Behavior of Low-

Slenderness Reinforced Concrete Walls: Failure Modes, Strength and Deformation Analysis, and Design Implications, 2000).

Design specifications for shear walls in seismic areas can be found in ACI Code Section 21. Although the nominal shear strength (V_n) and the shear strength provided by horizontal reinforcement (V_s) appear very different from ACI Code Section 11, the final values are similar. The values for nominal shear strength (V_n) and the shear strength provided by horizontal reinforcement (V_s) are shown in equations Eq. (2-17) and Eq. (2-18).

$$V_n = A_{cv}(\alpha\lambda\sqrt{f'_c} + \rho_t f_y) \quad \text{Eq. (2-17)}$$

$$V_{s,equiv} = (A_{v,horiz} f_y l_w)/s_2 \quad \text{Eq. (2-18)}$$

where,

A_{cv} = gross area of concrete section bounded by web thickness and length of section in the direction of shear force considered (in^2)

α = contribution of the concrete to shear strength. It is dependent on the height-to-length ratio.

λ = concrete modification factor

f'_c = compressive strength of concrete (psi)

ρ_t = percentage of horizontal steel

f_y = yield strength of steel (ksi)

ACI Code Section 21.9.4.4 limits V_n for seismic shear walls to a maximum value of $8\sqrt{f'_c}hd$. When h_w/l_w is greater than or equal to 2 then α=2.0. When h_w/l_w is less than or equal to 1.5 then α=3.0. Linear interpolation can be used to find the value of α if h_w/l_w is between 1.5 and 2.0 (ACI Committee 318, 2011). The α changed also based on presence of fibers in the mix composition. Chompreda and Parra found that in HPRFC low-rise walls, the

contribution to shear strength was assumed to be α=5.0 due to the "beneficial effect of arch action on the shear resistance (Chompreda & Parra-Montesinos, 2005)."Although shear walls are not specifically designed for the application of supporting an axial load, they still must support one if necessary. The critical stress for buckling of a one-way wall having a rectangular cross section is shown in equation Eq. (2-19).

$$\sigma_{cr} = \frac{\pi^2 EI}{(kl)^2}\left(\frac{1}{bh}\right) \qquad \text{Eq. (2-19)}$$

where,

σ_{cr} = critical stress for buckling (psi)

E = modulus of elasticity (N/m^2)

I = moment of inertia (lb/ft^2)

k = effective length factor for compression members

l = length of span (in)

b = width of compression face of member (in)

h = height of member (in)

The flexural stiffness of a one-way wall having a rectangular cross section is shown in equation Eq. (2-20) (ACI Committee 318, 2011).

$$EI = \frac{Ebh^3}{12} \qquad \text{Eq. (2-20)}$$

where,

E = modulus of elasticity (N/m^2)

I = moment of inertia (lb/ft^2)

b = width of compression face of member (in)

h = height of member (in)

2.3.3 Shear Wall Behavior

2.3.3.1 General

Shear wall behavior is dependent on a large number of variables. While shear walls are classified by their height-to-length ratio, research has shown that other variables, such as reinforcement, can modify the behavior and properties of walls. Advancements have aided modern seismic design which strives to create better ductility and a larger deformation capacity. To achieve thisigur, engineers now have the tools to design walls to yield in flexure prior to shear failure. Shear failure is not a desirable characteristic in seismic areas for a few reasons. First, shear strength degradation is more significant than flexural strength degradation when it is subject to cyclic lateral loadings (Biskinis, Roupakias, & Fardis, 2004). Second, when shear failure occurs, the ductility and energy dissipation capacity are significantly weakened. Research done on past earthquakes has shown that these two properties are critical to structural integrity during an earthquake (Chu, Feng, & Ye, 2012).

2.3.3.2 Behavior Prior to Yielding

As previously stated, shear failure is to be avoided in seismic areas. Taking a closer look at cyclic lateral loadings, when the first cycle of a cyclic lateral load is placed on the wall, the wall will experience tension on the loaded side and compression on the opposite end. As the load reverses, so do the forces. At the base of the wall, the strain reversals in the concrete and reinforcements become less severe approaching the middle of the wall (Pilakoutas & Elnashai, 1995). As the wall is loaded back and forth, the stiffness and integrity of the wall will slowly decrease in a linear manner causing small cracks to form (Farrar & Baker, 1990), (Farrar & Baker, 1993). Due to the imperfect closing of these small cracks, some concrete dilation is present. These small cracks will continue to occur until

flexural yielding and/or shear yielding of the reinforcement transpire due to moments exceeding the yield capacity (Pilakoutas & Elnashai, 1995). This behavior typically begins in the boundary elements.

2.3.3.3 Behavior Subsequent to Yielding

Following the onset of yielding, larger flexural and diagonal shear cracks will begin to form. These cracks cause the concrete to dilate further in both the longitudinal and lateral direction (Pilakoutas & Elnashai, 1995). The direction and size of the cracks are dependent on the tensile strength of the concrete, the steel ratio, and strength of the transverse reinforcement (Pang & Hsu, 1995). The pattern of these cracks tends to follow the grid orientation of the reinforcement, provided they are near the orientation of the principle stresses (Zhong, Mo, & Liao, 2009), (Krolicki, Maffei, & Calvi, 2011). As the wall is loaded in one direction beyond yield, permanent deformations will remain in the tension steel. When the loading is reversed, the shear is now predominantly transferred by dowel action prior to the cracks in the compression zone closing. This results in increasingly larger shear deformations in the steel and lower wall stiffness. The reduction in dowel stiffness, increased damage and size reduction of the compression zone, and loss of aggregate face to face friction will also attribute to increased shear yielding and deformation (Oesterle R. , et al., 1976), (Lefas, Kotsovos, & Ambraseys, 1990), (Biskinis, Roupakias, & Fardis, 2004), (Krolicki, Maffei, & Calvi, 2011). The deformations cause increasingly higher tensile strains, deteriorating the effective concrete strength and cause excessive concrete spalling (Stevens, Uzumeri, & Collins, 1991), (Kabeyasawa & Matsumoto, 1992), (Salonikios, Kappos, Tegos, & Penelis, Cyclic Load Behavior of Low-Slenderness Reinforced Concrete Walls: Design Basis and Test Results, 1999). Alternate yielding of the tensile reinforcement will cause a

"hinging region" to grow. The extent to which flexural yielding occurs in the reinforcement is considered the height of the plastic hinge zone (Pilakoutas & Elnashai, 1995). As the plastic hinge zone grows, the wall will lengthen in the vertical direction due to the progression of inelastic strains in the plastic hinge zone (Pilakoutas & Elnashai, 1995).

2.3.3.4 Failure

After the propagation of the larger cracks, an "ultimate crack" will form simultaneously with a large load reduction, thus commencing failure (Pang & Hsu, 1995). Failure is typically found to occur in the lower portion of the wall (Oesterle R. , et al., 1976). In general the load carrying capacity of reinforced concrete walls will be determined by the flexural yielding and behavior at the plastic hinge zones located in the boundary elements. The deformation capacity subsequent to yielding can be affected by a variety of failure modes. The most common failure modes in walls are concrete crushing of the web and the fracture of flexural reinforcement (Oesterle R. , et al., 1976), (Stevens, Uzumeri, & Collins, 1991), (Kabeyasawa & Matsumoto, 1992), (Salonikios, Kappos, Tegos, & Penelis, Cyclic Load Behavior of Low-Slenderness Reinforced Concrete Walls: Design Basis and Test Results, 1999), (Eom, Park, Kim, & Lee, 2013). The ultimate path to these failure modes are discussed hereafter.

Diagonal tension failure and diagonal compression failure are two common types of behavior that can ultimately lead to overall failure. Diagonal tension failure occurs when transverse shear reinforcement is not adequate. Due to inadequate transverse reinforcement a corner to corner diagonal tension plane forms. Yielding of a single shear link can cause all links spanning the main crack to yield as well, eventually causing a shear failure. Prevention of this failure mode can be accomplished by having adequate transverse reinforcement that

can handle a larger shear stress and produce significant flexural yielding (Paulay, Priestley, & Synge, 1982), (Pilakoutas & Elnashai, 1995), (Greifenhagen & Lestuzzi, 2005). Paulay, Priestley, and Synge found that shear applied to the top of a wall spread directly to from the top of the wall to the foundation by diagonal compression. It results from a high average shear stress coupled with excess transverse shear reinforcement. A diagonal compression failure is highly undesirable in shear walls because it is not a very ductile failure mode and causes large losses in stiffness and strength. It ultimately causes the crushing of concrete due to repeated opening and closing of cracks resulting in failure (Paulay, Priestley, & Synge, 1982), (Biskinis, Roupakias, & Fardis, 2004).

A major concern in seismic design is exceeding the shear capacity prior to developing the flexural strength of the wall. Failure in shear prior to reaching the flexural strength of the wall can result in a sliding failure. Sliding occurs following cycles of reversed lateral loadings that cause flexural yielding of the vertical reinforcement. Sliding takes place between the faces of open flexural cracks near the base of the wall that can ultimately interconnect and form a continuous horizontal shear crack. Previous loading cycles decreased the ability of the aggregate to interlock and create friction thus enabling the wall to slide (Biskinis, Roupakias, & Fardis, 2004). This action reduces the stiffness of the wall and consequently reduces the energy dissipation capacity. The sliding action can ultimately account for up to 60 percent of the displacement when approaching failure (Paulay, Priestley, & Synge, 1982) (Salonikios, Kappos, Tegos, & Penelis, Cyclic Load Behavior of Low-Slenderness Reinforced Concrete Walls: Failure Modes, Strength and Deformation Analysis, and Design Implications, 2000), (Greifenhagen & Lestuzzi, 2005). Although research has shown many techniques can be used to mitigate undesirable failure modes of shear walls, the

intrinsically brittle nature of concrete and its deficiencies are difficult to overcome. The inability of concrete under extreme load reversals to accommodate inelastic deformation of steel reinforcement is the reason bond slip, bond deterioration, concrete spalling, and ultimately bond failure can occur (Palermo & Vecchio, 2001), (Fischer & Li, 2002).

2.3.3.5 Effects of Applied Axial Load

Shear walls with a significant axial compressive load exhibit different behavior. The axial load tends to increase shear stiffness, horizontal load carrying capacity, and wall strength while decreasing ductility and energy dissipation (Oesterle R. G., Fiorato, Aristizabal-Ochoa, & Corley, 1980), (Lefas, Kotsovos, & Ambraseys, 1990), (Kabeyasawa & Matsumoto, 1992), (Zhang & Wang, 2000). The displacement of the wall is also drastically affected. Axial compression reduces both the vertical and horizontal displacement (Lefas, Kotsovos, & Ambraseys, 1990). Under extremely large axial loads subsequent to yielding, out-of-plane buckling is also possible (Zhang & Wang, 2000).

2.3.3.6 Effects of Reinforcement

It is widely agreed upon that steel reinforcement bars improve many properties and subsequently the desired behavior in shear walls. Research has been conducted on overall steel reinforcement ratios as well as the effects of transverse and longitudinal reinforcement individually. By adding steel reinforcement to a shear wall, the yield strength, ultimate strength, ductility, and energy dissipation capacity were found to increase while shear crack width decreased (Stevens, Uzumeri, & Collins, 1991), (Pang & Hsu, 1995), (Mansour & Hsu, 2005), (Chu, Feng, & Ye, 2012). It is important to note that while ductility of a shear wall increases with the initial addition of steel reinforcement, ductility will decrease as the steel ratio increases beyond the minimum required reinforcement (Pang & Hsu, 1995). Vertical

reinforcement tended to have more of an effect on the overall structure than did transverse reinforcement. Increases in horizontal reinforcement displayed little effect and sometimes a detrimental effect to shear stiffness, ductility prior to web crushing, shear strength, and deformation (Oesterle R. G., Fiorato, Aristizabal-Ochoa, & Corley, 1980). Lefas et al. observed similar strength and deformation characteristics when only half of the required horizontal reinforcement was present in a shear wall. Lefas et al. also observed that using 60 percent of the required transverse reinforcement required by the ACI Building code still caused the wall to exhibit the desired ductile behavior (Lefas, Kotsovos, & Ambraseys, 1990). It is important to note that the placement of the transverse reinforcement is what is important. Transverse reinforcement at deformation-critical locations in flexural members will result in increased ductility and capacity. It will also avoid unwanted failure modes (Pilakoutas & Elnashai, 1995), (Fischer & Li, 2002). Oersterle et al. took a closer look at the boundary elements and their effect on shear walls and concluded that by stiffening the boundary element the overall inelastic performance increased. Confinement of the reinforcement within the hinging region in the boundary element also improved the inelastic performance and increased shear capacity. Confinement can also prevent the boundary elements from deteriorating prior to web crushing (Oesterle R. , et al., 1976), (Oesterle R. G., Fiorato, Aristizabal-Ochoa, & Corley, 1980), (Chu, Feng, & Ye, 2012). As the percentage and confinement of flexural reinforcement in the boundary element increased, the hinging zone decreased (Pilakoutas & Elnashai, 1995).

Further research was conducted placing reinforcement at different angles within a shear wall. Zhong, Mo, and Liao observed that by placing diagonal reinforcement in a shear wall, it can control the undesired pinching effect in the hysteresis loops of shear walls and

increase energy dissipation (Mansour & Hsu, 2005), (Zhong, Mo, & Liao, 2009). Salonikios et al. found that through the use of bidiagonal reinforcement, shear sliding and crack propagation can be controlled (Salonikios, Kappos, Tegos, & Penelis, Cyclic Load Behavior of Low-Slenderness Reinforced Concrete Walls: Design Basis and Test Results, 1999). Diagonal reinforcement was also found to increase ductility while minimizing shear damage and slip deformation (Chu, Feng, & Ye, 2012).

2.3.3.7 Energy Dissipation

As stated earlier, energy dissipation, particularly in seismic regions, is of supreme importance for a shear wall. To assess the energy dissipation of a wall, the total amount of energy absorbed is measured by both the energy absorbed and the level of deformation. Optimally, a wall should be designed to absorb the maximum amount of energy by causing the least amount of deformation. By doing this, the hysteretic loop, discussed in the following section, remains as full as possible. Because the levels of deformations play a large role in determining the energy dissipation capacity, it can only be assumed that it is one of the main energy dissipation mechanisms. Pilakoutas and Elnashai indicated that prior to yielding, little energy was dissipated shown by a lack of deformation. After yielding occurred, the rate of dissipation rose consistently until failure. (Oesterle R. , et al., 1976), (Pilakoutas & Elnashai, 1995), (Salonikios, Kappos, Tegos, & Penelis, Cyclic Load Behavior of Low-Slenderness Reinforced Concrete Walls: Failure Modes, Strength and Deformation Analysis, and Design Implications, 2000). Damping is also an effective way to dissipate energy in a structure. Damping measures how well a structure can dissipate energy. A dampening effect can happen due to cracking, sliding friction, and slip in connections (Farrar & Baker, 1990).

2.3.3.8 Hysteretic Loop and Pinching

A hysteretic loop describes the behavioral output based on its current and past inputs. Past inputs affect the current internal state of the system and the values of future outputs. In reference to shear walls this loop is very important when looking at the behavior of the wall. The hysteretic loop can be affected in many different ways, most notably pinching. Prior to yield, no effect on the shape of the hysteretic loop is observed unless instant fracture occurs. After yielding occurs, cracking and steel deformations contribute to a pinched shape of the hysteretic loop (Mansour & Hsu, 2005). A typical hysteretic loop can be seen Figure 1.

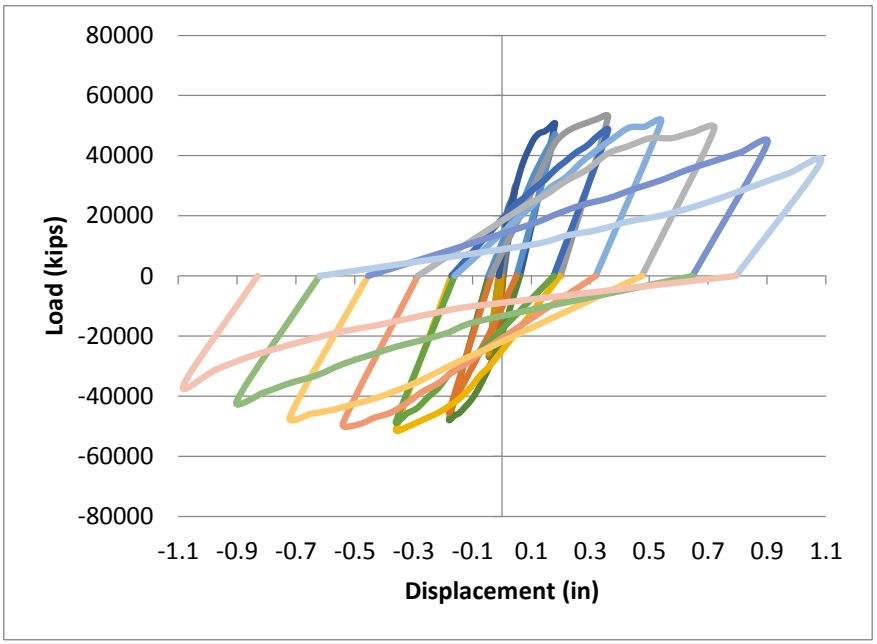

Figure 1 - Hysteretic loop with pinching

"Pinching" is an undesirable effect that can be seen in the hysteretic loop. Pinching is essentially a sharp loss in stiffness commonly seen when the loading is reversed during cyclic loading after yielding has occurred. The pinching effect can be a result of a few different behaviors. Shear sliding displacement significantly reduces the stiffness consequently causing a pinching effect. Pinching can also be caused by the deformation of reinforcing

steel, high axial loadings, and dowel action (Oesterle R. , et al., 1976), (Oesterle R. G., Fiorato, Aristizabal-Ochoa, & Corley, 1980) (Kabeyasawa & Matsumoto, 1992), (Salonikios, Kappos, Tegos, & Penelis, Cyclic Load Behavior of Low-Slenderness Reinforced Concrete Walls: Failure Modes, Strength and Deformation Analysis, and Design Implications, 2000), (Greifenhagen & Lestuzzi, 2005).

2.3.4 Fiber Reinforced Concrete Shear Implications on Shear Walls

As stated earlier, fiber reinforced concrete has advantageous effects on the properties of a member when subjected to a shear load. In structures subjected to large shear loads, behavior is fundamentally determined by the inelastic activity regions. The use of FRC is a viable option in these areas of the structure for their ability to tolerate damage and deformations as well as simplify reinforcement detailing, making FRC a prime candidate for use in shear walls (Athanasopoulou, 2010). Research even suggests that FRC subjected to shear may eliminate the need for transverse reinforcement in some situations because it provides sufficient confinement to the other reinforcement in the structure (Canbolat, Parra-Montesinos, & Wight, 2005), (Parra-Montesinos & Chompreda, 2007).

Kim and Parra applied past research of shear loads on fiber reinforced concrete in 2003 when they investigated the hysteretic response of low rise walls using FRC subject to a shear load. Using a volume fraction of 1.5 to 2 percent, the walls were placed under a reversed cyclic loading. The reinforcement used in the walls was below the required amount specified in the ACI code, and no special reinforcement was used in the boundary elements. Kim and Parra observed a stable hysteretic loop with small confined cracks and minimal damage. In addition the wall edges presented no instabilities, despite the lack of special reinforcement in the boundary elements and estimated that the fibers in the concrete mix

were responsible for 80 percent of the walls diagonal tension capacity. This research paved the way for future research to be done on the simplification of designing a shear wall (Kim & Parra-Montesinos, 2003). A study in 2006 followed Kim and Parra when Parra-Montesinos, Canbolat, and Jeyeraman studied the behavior of slender walls using FRC. After constructing two walls, one containing FRC and the other containing conventional concrete, they observed behavior characteristics similar to what Kim and Parra observed in 2003. The fibers provided a high damage tolerance and prevented instability in the boundary elements. The FRC wall experienced a flexure dominated response compared to the shear dominated response experienced by the conventional concrete wall (Parra-Montesinos, Canbolat, & Jeyeraman, 2006). In general, the application of FRC for shear walls improves stability in boundary elements, damage and deformation capacity, and can simplify reinforcement design in both the web and boundary elements.

2.4 Summary

In summary, research has shown that the addition of rubber particles in concrete increases the toughness but decreases compressive and tensile strengths. Adding fibers to concrete increases the toughness as well but it also increases the ductility, compressive strengths, and tensile strengths. Further research was done on the addition of both fibers and rubber in concrete. Adding fibers to rubber concrete increased the compressive strength, tensile strength, modulus of elasticity, and toughness.

Extensive research has been done on the design and behavior of structural shear walls. Structural shear walls require horizontal and vertical web reinforcement as well as special boundary confining reinforcement to ensure inelastic displacement and high load capacity. Additional special reinforcement is sometimes required if significant shear or

sliding demands exist. In an attempt to alleviate some of these reinforcement and design requirements, the mix composition can be altered in hopes of achieving the desired behavior of shear walls. By adding fibers and rubber to a concrete mix composition, we hope that the characteristics of both materials yield a positive effect on the walls behavior.

Prior to this research, limited research had been done on the behavior of low-rise walls containing fibers, rubber, or both. Therefore, an all-inclusive experimental research program was performed with a goal of determining the behavior and characteristics of fibers and rubber particles in concrete low-rise shear walls and shear beams.

CHAPTER 3: Methodology

3.1 Introduction

The series of tests conducted during this project were designed to study the influence of fibers and rubber in shear beams as well as the response of concrete shear walls subjected to a reverse static cyclic loading. The project included a total of 22 different mix compositions from which shear beams and shear walls were cast. Fresh concrete tests included slump, air content, and unit weight. Hardened concrete tests performed on cylinders at a standard time interval consisted of compression tests, split tensile tests, and modulus tests. The 22 shear beams were loaded in an MTS Universal Testing Machine, simply supported on two plates, and a point load was applied in the center of the beam until failure. The four wall specimens were anchored to the modular strong-block testing system in which a hydraulic actuator connected to a steel frame erected on the modular blocks simulated lateral loadings to evaluate the behavior of the walls. In the following sections, the descriptions of the materials, mixes, tests, designs, and instrumentation are provided.

3.2 Mix Properties and Design

3.2.1 Materials

The materials used in this study consisted of aggregates, cement, and water found in conventional concrete as well as rubber particles and discontinuous steel fibers. By placing these unconventional materials in concrete, the behavior and characteristics of the concrete changes. The materials used will be discussed in more detail in this section.

3.2.1.1 Aggregate

The coarse aggregate used in all of the mixtures was limestone. The limestone had a maximum size of 3/8 in. The absorption value for limestone was 1.27 percent and the bulk

specific gravity was 2.61. The values were obtained via ASTM C127 (ASTM 2012a). The fine aggregate used in all of the mixtures was sand. The absorption value for sand was 0.73 percent and the bulk specific gravity was 2.6. The values were obtained via ASTM C128 (ASTM 2012b). Figure 2 (a) and (b) show a typical sample of limestone and sand.

(a) (b)

Figure 2 - (a) Limestone and (b) Sand

3.2.1.2 Fibers

The fibers used are Nycon-SF Type 1 (Needles) High Performance Steel Fibers. The fibers are in accordance with ASTM A820 (ASTM 2011a). The fibers are 1/2 in. long, have a diameter of 0.008 in., have a specific gravity of 7.8, and a tensile strength of 285 ksi. Figure 3 shows a typical sample of steel fibers.

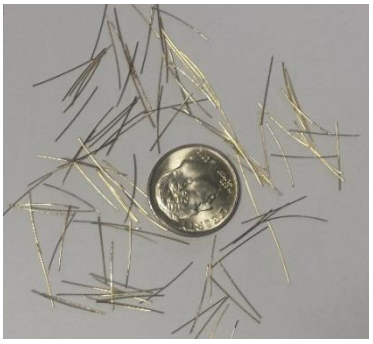

Figure 3 – Fibers

3.2.1.3 Rubber

Two different sizes of rubber were used during the project. The coarse rubber particles had a maximum size of 3/8 in., while the fine rubber particles had a maximum size of 1/10 in. The specific gravity of the rubber aggregates is 1.05. Figure 4 (a) and (b) shows a typical sample of coarse and fine rubber aggregate.

(a) (b)

Figure 4 - Rubber (a) fine and (b) coarse

3.2.1.4 Cement

The cement used was Portland Cement Type I, II produced by Holcim. The specific gravity of the cement is 3.15 and conforms to ASTM C150/C150M-15 (ASTM 2015).

3.2.1.5 Water Reducer

The water reducer used was ADVA ® 190 High-Range Water-Reducing Admixture. The water reducer was in accordance to standard ASTM C949 Type A and F (ASTM 2013a), and ASTM C1017 Type I (ASTM 2013b).

3.2.2 Mix Design

The mixes used for experimentation were taken from "Material and Flexural Properties of Fiber-Reinforced Rubber Concrete" completed at the University of Louisiana at Lafayette. The purpose was to determine the material properties of rubber concrete, fiber-

reinforced concrete, and fiber-reinforced rubber concrete and focused on determining the optimum mixture dosages for rubber and fibers as well as the two together (Helminger, 2014). Four mixes from the 22 were selected to further study their behavior in the structural shear walls. The four mixes were specifically chosen on the basis of comparable compressive strengths, dosages of the mix constituents, workability, and toughness. The first of the four mixes was selected for its superior performance in flexure and shear. This mix contained 1% fibers and 10% coarse rubber. The second mix selected was the mix containing 10% coarse rubber but no fibers so that a direct comparison could be made to the first mix. The third and fourth mixes were a plain mix and a 1% fiber mix with comparable characteristics. A nomenclature was created for the 22 mixes, shown in Table 1. Table 2 shows a summary of the mix constituents along with the predicted unit weights.

Table 1 - Nomenclature of Mixes (Helminger, 2014)

Mix #	Composition	Name
1	Plain concrete	PL1
2	Plain concrete	PL2
3	1% Fiber, No Rubber	F1
4	1% Fiber, No Rubber	F2
5	1% Fiber, 5% Coarse Rubber	F5C
6	1% Fiber, 5% Fine Rubber	F5F
7	1% Fiber, 5% Coarse + Fine Rubber	F5CF
8	1% Fiber, 10% Coarse Rubber	F10C
9	1% Fiber, 10% Fine Rubber	F10F
10	1% Fiber, 10% Coarse + Fine Rubber	F10CF
11	1% Fiber, 15% Coarse Rubber	F15C
12	1% Fiber, 15% Fine Rubber	F15F
13	1% Fiber, 15% Coarse + Fine Rubber	F15CF
14	No Fiber, 5% Coarse Rubber	5C
15	No Fiber, 5% Fine Rubber	5F
16	No Fiber, 5% Coarse + Fine Rubber	5CF
17	No Fiber, 10% Coarse Rubber	10C
18	No Fiber, 10% Fine Rubber	10F
19	No Fiber, 10% Coarse + Fine Rubber	10CF
20	No Fiber, 15% Coarse Rubber	15C
21	No Fiber, 15% Fine Rubber	15F
22	No Fiber, 15% Coarse + Fine Rubber	15CF

Table 2 - Constituents of Mixes (Helminger, 2014)

Constituents of Mixes in lbs/cuft											
Mix #	Name	Cement	Water	Sand	Limestone	Coarse Rubber	Fine Rubber	Fibers	Absorption Water	Water Reducer (oz per 100lbs cement)	Predicted Unit Weight
1	PL1	27.78	11.11	54.46	54.71	0.00	0.00	0.00	-0.83	3.0	147.22
2	PL2	27.78	11.11	54.46	54.71	0.00	0.00	0.00	0.28	1.5	148.33
3	F1	27.78	11.11	54.46	54.71	0.00	0.00	4.87	0.28	3.0	151.68
4	F2	27.78	11.11	54.46	54.71	0.00	0.00	4.87	0.32	3.0	151.73
5	F5C	27.78	11.11	54.46	49.24	2.20	0.00	4.87	-0.13	2.0	148.04
6	F5F	27.78	11.11	49.01	54.71	0.00	2.20	4.87	-0.39	2.0	147.80
7	F5CF	27.78	11.11	51.73	51.98	1.10	1.10	4.87	0.06	2.0	148.25
8	F10C	27.78	11.11	54.46	43.77	4.39	0.00	4.87	-0.02	2.0	144.91
9	F10F	27.78	11.11	43.57	54.71	0.00	4.39	4.87	-0.23	3.0	144.75
10	F10CF	27.78	11.11	49.01	49.24	2.20	2.20	4.87	0.06	2.5	145.02
11	F15C	27.78	11.11	54.46	38.30	6.59	0.00	4.87	-0.12	2.0	141.57
12	F15F	27.78	11.11	38.12	54.71	0.00	6.59	4.87	-0.33	5.0	141.44
13	F15CF	27.78	11.11	46.29	46.51	3.30	3.30	4.87	0.24	5.0	141.96
14	5C	27.78	11.11	54.46	49.24	2.20	0.00	0.00	-0.89	5.0	143.90
15	5F	27.78	11.11	49.01	54.71	0.00	2.20	0.00	-0.34	5.0	144.47
16	5CF	27.78	11.11	51.73	51.98	1.10	1.10	0.00	-0.04	4.0	144.76
17	10C	27.78	11.11	54.46	43.77	4.39	0.00	0.00	0.02	4.0	141.53
18	10F	27.78	11.11	43.57	54.71	0.00	4.39	0.00	-0.22	4.5	141.34
19	10CF	27.78	11.11	49.01	49.24	2.20	2.20	0.00	0.16	5.0	141.70
20	15C	27.78	11.11	54.46	38.30	6.59	0.00	0.00	0.05	6.0	138.29
21	15F	27.78	11.11	38.12	54.71	0.00	3.30	0.00	0.10	5.5	138.41
22	15CF	27.78	11.11	46.29	46.51	3.30	3.30	0.00	0.38	4.5	138.66

*For negative absorption water values, the amount should be taken out from the mix water.

3.2.3 Mix Procedure

The following mix procedure was followed for all mixes listed in Table 2. First, the sand and limestone were added to the empty mixer which is shown in Figure 5. The sand and limestone were mixed for two minutes. After two minutes, the cement and water were added to the mixer and proceeded to mix for an additional four minutes. After six total minutes had passed, the water reducer was added and mixed for an additional two minutes. After eight total minutes had passed, depending on the mix, either rubber or fibers were added to the mixer and mixed for an additional eight minutes. If the mixture contained both rubber and

fibers then the fibers were added after eight total minutes and the rubber was added after sixteen total minutes and then mixed for an additional four minutes.

Figure 5 - Mixer

Water reducer was added to each mix and varied based on the amount of rubber and fibers the mix contained. A desired slump of 4 in. to 6 in. was targeted for the shear beams. A desired slump of 6 in. to 8 in. was targeted for the shear walls. To achieve the desired workability for each wall mix, trial mixes were done for each of the four mixes selected for the wall specimens so that the amount of water reducer added would correspond to each mix having the desired increased workability. The results of the trial mixes were plotted and a value was chosen based on observation of the mixes and data. It should be noted that the change in water reducer amounts between the beams and walls should not affect the strengths of the mixes. The trial mix data is shown in Figure 6. Table 3 and Table 4 show the amount of water reducer for the shear beams and shear walls respectively.

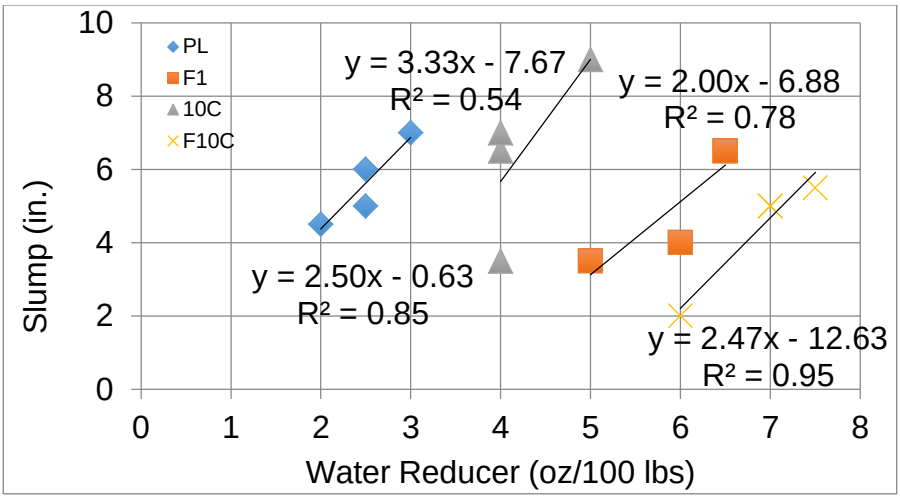

Figure 6 - Preliminary mix water reducer amounts

Table 3 - Shear beam water reducer amounts

Water Reducer (oz/100 lbs cement)	
Mix	Water Reducer (oz)
PL1	3
5C	1.5
5F	3
5CF	3
10C	2
10F	2
10CF	2
15C	2
15F	3
15CF	2.5
PL2	2
F1	5
F5C	5
F5F	5
F5CF	5
F10C	4
F10F	4
F10CF	4.5
F15C	5
F15F	6
F15CF	5.5
F2	4.5

Table 4 - Shear wall water reducer amounts

Water Reducer (oz/100 lbs cement)	
Mix	Water Reducer (oz)
PL1	3.5
F1	6.5
10C	4
F10C	7.5

3.2.4 Material Testing

3.2.4.1 Fresh Concrete Tests

3.2.4.1.1 Slump

Slump is a measurement of how workable a concrete mixture is. The slump test was performed according to ASTM C143 (ASTM 2012c). First, the slump cone was cleaned of any foreign debris and then attached to the base plate. The cone was filled by thirds of its volume. After each third of the cone was filled, the concrete was rodded 25 times. After the cone has been completely filled and rodded for the final time, excess concrete extending beyond the top of the cone was scraped off. While applying a downward force to the cone, the latches were removed. Once the latches were removed, the cone was slowly raised vertically until it was completely removed from the fresh concrete. The handle was brought to a position directly above the fresh concrete and the distance from the bottom of the handle to the top of the center of the concrete remaining on the base plate was measured. This distance was recorded as the slump value for the concrete mix. This is shown in Figure 7.

Figure 7 - Slump Test

3.2.4.1.2 Unit Weight

The unit weight of fresh concrete was obtained using a container with a volume of one-tenth of a cubic foot and a known weight. The container was filled by thirds of its volume. After each layer was placed in the container, the concrete was rodded 25 times and subsequently tapped on each side using a rubber mallet. After the final layer was placed, rodded, and tapped, the concrete extending beyond the top of the container was scraped off using a striking plate. The container was then weighed. To obtain the unit weight of the fresh concrete, the weight of the container was subtracted from the weight of the container with the fresh concrete in it and multiplied by a factor of ten. Figure 8 shows the unit weight.

Figure 8 - Unit weight

3.2.4.1.2 Air Content

The entrapped air is measured using the device show in Figure 9. Using ASTM C231/C231M the amount of air entrapped in fresh concrete was measured as a percentage by volume of concrete (ASTM 2010a). The container was filled with fresh concrete then the lid was placed on it to create an air tight seal. The process of filling, rodding, and tapping was the same process as the unit weight test. The test then begins by opening the valves on the lid and using a water dropper to drop water into the open valve until it exits the opposite valve. The water fills all of the voids between the top of the concrete and the lid. After closing the valves back, air was pumped into the cylinder. The value that the gauge points to after the air was realized into the chamber was recorded as the percentage of air entrapped in the fresh concrete.

Figure 9 - Air Content

3.2.4.2 Hardened Concrete Tests

3.2.4.2.1 Compression Tests

Compression tests were performed using the 4 in. x 8 in. cylinders in accordance with ASTM C873 (ASTM 2010b). Neoprene pads were inserted into the cylinder caps to ensure that an even load was applied to the cylinder surface. The neoprene pads were changed after every 25 tests to ensure consistency due to the deterioration of the pads. The concrete cylinders were then placed between the cylinder caps and put into the testing machine. The testing machine used was an ELE International testing machine and is pictured below in Figure 10. A constant load rate of 35 psi/sec (440 lbs/sec) was applied to the cylinder until failure. The compression test was performed on each mix for the shear walls and each mix for the shear beams.

(a) (b)

Figure 10 - (a) ELE International test machine and (b) Compression test on cylinder

3.2.4.2.2 Split Tensile Tests

Split tensile tests were performed using 4 in. x 8 in. cylinders in accordance with ASTM C496 using the same testing machine that was used for compression testing (ASTM 2011b). The 4 in. x 8 in. cylinders were placed in the steel device shown in Figure 11 between two strips of wood so that the load was distributed evenly upon the surface. A constant load rate of 2.5 psi/sec was applied to the cylinder until failure. The split tensile test was performed on each mix for the shear beams and each mix for the shear walls.

Figure 11 - Split tensile test

3.2.4.2.3 Modulus Tests

Modulus tests were performed using 4 in. x 8 in. cylinders using the same testing machine that was used for compression and split tensile testing. A compressiometer with a digital displacement output, shown in Figure 12, was placed around the cylinder and subsequently screwed to it. The cylinder was then placed in the testing machine and loaded at a rate of 35 psi/sec up to 40 percent of f'_c. The displacement was recorded at every 5000 lbs. Using the displacement and load values, the strain was calculated and plotted against the stress. The slope of this line is the modulus of elasticity.

Figure 12 - Modulus test

3.2.4.3 Reinforcing Steel

Reinforcing steel was used in all test specimens. The deformed reinforcing bars used were No. 4 and No. 5 rebar, and the deformed steel wire used was D4.5. The deformed reinforcing bars were Grade 60 steel. The deformed steel wire was obtained from Wire Products Inc. in Florida and is described as a "positive deformation pattern wire." The No.4 bars were used in all wall specimens as vertical boundary reinforcement. The No. 5 bars were used in wall specimens PL1 and F1 as vertical boundary reinforcement with No. 4 bars as well. A single No. 5 bar was also used in shear beams as flexural reinforcement. The deformed steel wire was used in all wall specimens as transverse and vertical web reinforcement. The yield strength of the No.4 and No.5 Grade 60 reinforcing steel was found to be 65.4 ksi. The yield strength of the deformed wire according to Wire Products Inc. is 75 ksi. The boundary confining reinforcement found in all of the specimens was 1/8" 1018 mild

cold rolled steel. The yield strength of the boundary confining reinforcement was 53.7 ksi (Online Metals). Further details of the reinforcement specifications are shown in Table 5.

Table 5 - Reinforcing steel specifications

Reinforcing steel	Yield Strength (ksi)	Diameter (in)	Area (in^2)	Finish
No. 4	65.4	0.500	0.200	Deformed
No. 5	65.4	0.625	0.310	Deformed
D4.5	75.0	0.239	0.045	Deformed
1/8"	53.7	0.125	0.012	Smooth

3.3 Shear Beam Test Specimens

3.3.1 General Specimen Description and Design

Twenty two shear beams were constructed and tested in the structural engineering laboratory at the University of Louisiana at Lafayette. The 22 shear beams corresponded to the mix designs found in Table 2. Each shear beam was placed in an MTS Universal Testing Machine and was simply supported by two plates. The beams were loaded using a single point load at mid-span of the beam until failure. The beams measured 4 in. wide, 8 in. high, and were 24 in. long. A single No.5 rebar was placed at a depth of 7 in. In order to examine the effects of the rubber and fibers, the beam sizes and reinforcement remained constant. The shear beam dimensions and reinforcement is shown in Figure 13. The dimensions and reinforcement of the beams were designed so that they would ultimately fail in shear.

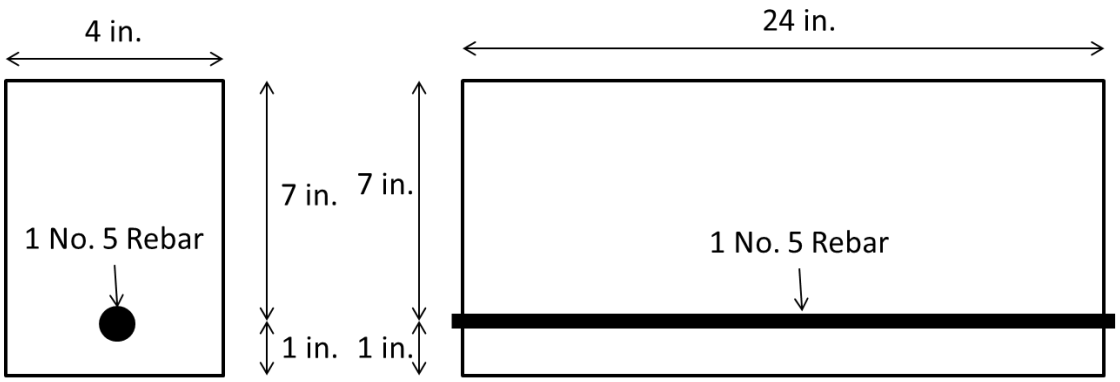

Figure 13 - Shear beam dimensions and reinforcement

3.3.2 Construction of the Specimen

The shear beams were all constructed in the structural engineering laboratory at the University of Louisiana at Lafayette. The process began by building the wooden formwork and placing each piece of No.5 rebar in the formworks (Figure 14). Each beam was cast using the 22 mixes detailed in Table 2. Concrete 4 in. x 8 in. cylinders were also prepared for all beams for hardened concrete tests in accordance with ASTM Standard C192 (ASTM 2014). After each beam was cast, wet burlap and visqueen were subsequently placed on and around the exposed concrete. The concrete cylinders were also covered. All concrete was stored in temperature controlled laboratory, and the forms were removed from all specimens after three days of moist curing. All concrete was moist cured for a total of 7 days.

Figure 14 - Wooden formwork and rebar

3.3.3 Specimen Instrumentation

Two linear potentiometers were positioned directly under the beam at mid-span on each side of the beam (Figure 15). The average displacement recorded by the two potentiometers was taken as the displacement at mid-span. The load applied by the MTS Universal Testing Machine was monitored by a force transducer in the machine and collected by a National Instruments machine where the load was recorded at a frequency of 1 Hz. The potentiometers were also wired to the National Instruments machine where the voltage was converted to a displacement at a frequency of 1 Hz.

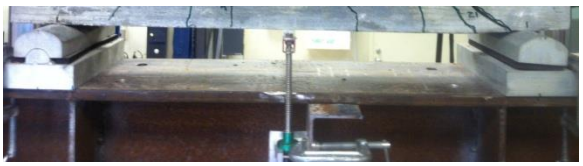

Figure 15 - Potentiometers at mid-span

3.3.4 Test Set Up and Procedure

The shear beam tests were conducted on an MTS uniaxial load frame. The frame consisted of two wide flange sections with a welded rod on the outside of one flange so that they could be gripped by the machine above and below the shear beam. Plates were

subsequently placed on the bottom wide flange section and simply supported each beam. The plates were 22 in. apart. A steel rectangle was secured to the upper wide flange and would be used to load the shear beam at mid-span. The test frame and set up are shown in Figure 16. Each beam was loaded at a load rate of .0004 in/sec until failure. As cracks appeared on the face of the shear beam, they were traced and the load was noted to view the crack progression as shown in Figure 17.

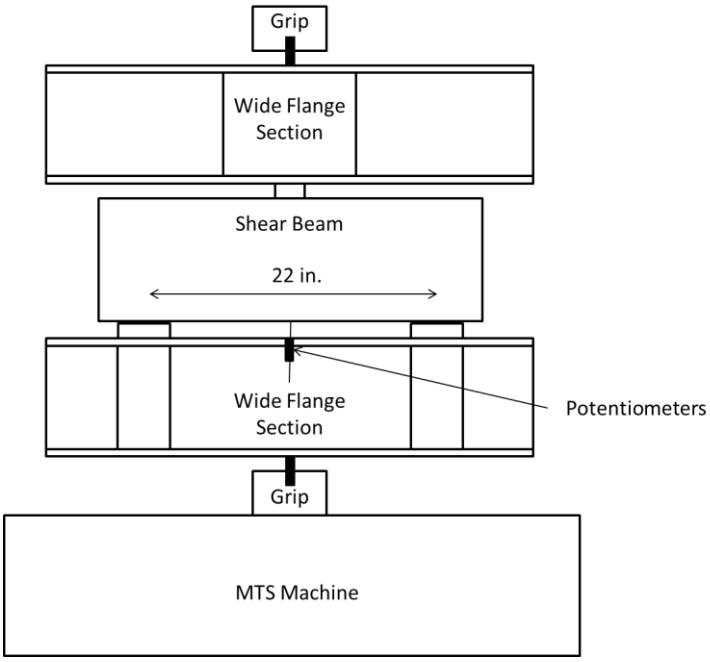

Figure 16 - Shear beam test frame set up

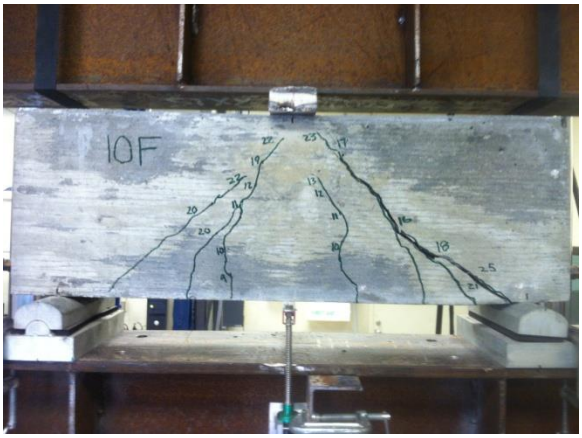

Figure 17 - Tested beam specimen

3.4 Shear Wall Test Specimens

3.4.1 General Specimen Description

Four full-scale cantilever low to mid-rise walls were constructed and tested in the structural engineering laboratory at the University of Louisiana at Lafayette. They were anchored to a modular strong-block testing system and were placed under cyclic loading using a hydraulic actuator mounted to a steel frame (Benton, 2015). The walls measured 30 in. in height, 24 in. in width, and 4 in. in depth. The five walls were each fixed to a reinforced concrete foundation measuring 72 in. long, 34 in. wide, and 18 in. deep. These foundations were anchored to the modular strong-block testing system. A 54 in. long, 14 in. wide, and 14 in. deep reinforced concrete block was cast on top of the wall so that the walls could be loaded properly. Figure 18 shows the general specimen setup.

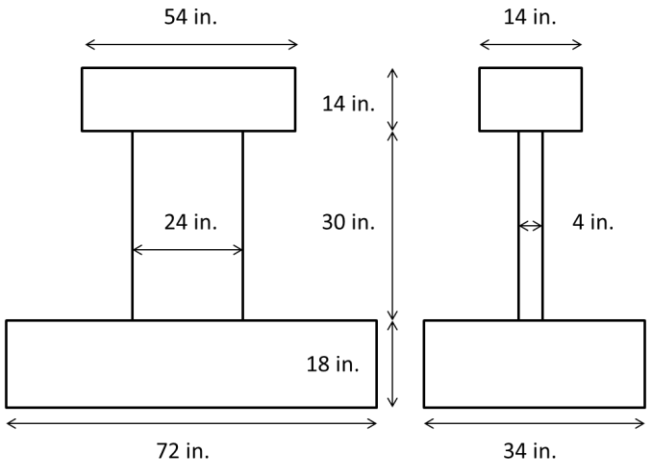

Figure 18 - General wall specimen

The bottom foundation and the top block were cast using self-consolidating concrete and the wall specimens were cast using the four selected mix designs. In order to examine the effects of the rubber and fibers, the walls size and height-to-length ratios remained constant. The mixes were selected based on their concrete strengths and fiber and rubber dosages so

that the results could be compared to each other. The design, reinforcement details, construction methods and sequence, instrumentation setup, and testing procedure loosely followed the procedure used in "Shear Strength and Drift Capacity of Reinforced Concrete and High-Performance Fiber Reinforced Concrete Low-Rise Walls Subjected to Displacement Reversals" from the University of Michigan (Athanasopoulou, 2010). It is also important to note that the size of the test specimens were governed by the crane and the capacity was governed by the test system.

3.4.2 Design of Test Specimen

The primary design of the test walls were based on the shear stress applied to the walls and their subsequent mix composition. The walls were designed using Chapter 11 and 21 of the ACI Code (ACI Committee 318, 2011). Each wall also contained vertical and horizontal reinforcement in the web as well as concentrated vertical reinforcement in the wall edges. The vertical reinforcement in the wall edges was anchored by casting them in the concrete foundation. The specifications of the reinforcement are discussed further in Section 3.4.3.

The concrete foundation and top block were designed so that they remained elastic throughout the duration of testing. The foundation was anchored to the modular strong-block testing system using post-tensioned DYWIDAG bars. The dimensions of both the foundation and top block were chosen so that the load could be safely transferred from the testing system to the wall itself. The dimensions and reinforcing details of the foundation and top block can be found in Figure 19.

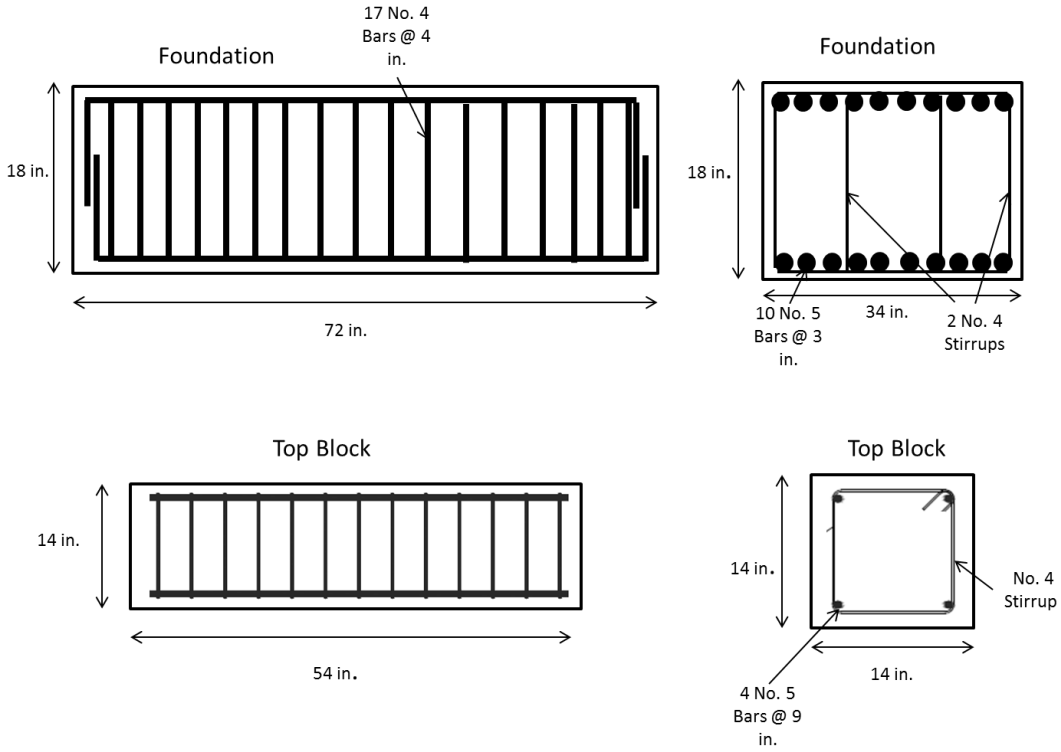

Figure 19 - Foundation and top block dimensions and reinforcement

The flexural strength of the wall, M_{max}, was found using strain compatibility. The concrete strength used for the flexural strength calculations for walls F10C and 10C was 6000 psi and the concrete strength used for the flexural strength calculations for walls PL1 and F1 was 9000 psi. The web and boundary reinforcements were also taken into account assuming their yield strengths stated in Table 5. The calculated values for flexural strength are shown in Table 6.

The maximum applied shear force for the wall, V_{max}, was found by dividing M_{max} by the shear span length, which is shown in equation Eq. (3-1). Figure 20 shows the applied loading. The calculated values for maximum applied shear are shown in Table 6.

$$V_{max} = \frac{M_{max}}{a} \qquad \text{Eq. (3-1)}$$

where,

M_{max} = Flexural strength of wall (kip-in)

a = height of wall plus the distance from the top of the wall to the mid-depth of the top block where the load was applied (in).

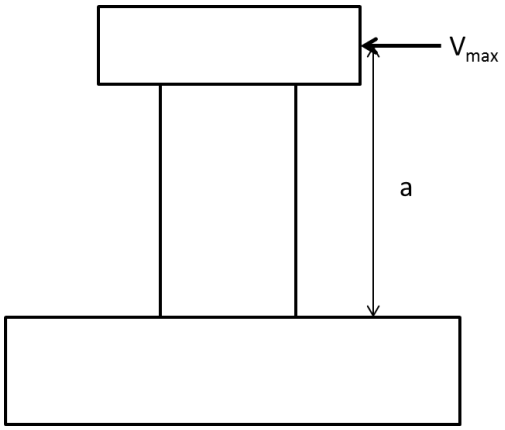

Figure 20 - Wall specimen noting height of applied load

The nominal shear strength of the wall, V_n, was calculated using equation Eq. (3-2). The calculated values for nominal shear strength are also shown in Table 6.

$$V_n = A_{cv}(\alpha\lambda\sqrt{f'_c} + \rho_t f_y) \qquad \text{Eq. (3-2)}$$

where,

A_{cv} = gross area of concrete section bounded by web thickness and length of section in the direction of shear force considered (in^2)

α = contribution of the concrete to shear strength. It is dependent on the height-to-length ratio.

λ = concrete modification factor

f'_c = compressive strength of concrete (psi)

ρ_t = percentage of horizontal steel

f_y = yield strength of steel (ksi)

Shear transfer at the base of the walls was checked using ACI Section 11.6. This section details the requirements for shear transfer between two concrete surfaces cast at separate times. This applies to both the concrete foundation and the top block. The nominal shear strength for shear transfer was found using equation Eq. (3-3).

$$V_{nb} = A_{vf} f_y \mu \qquad \text{Eq. (3-3)}$$

where,

A_{vf} = area of shear-friction reinforcement perpendicular to the shear-friction plane (in^2)

f_y = yield strength of the shear-friction reinforcement (ksi)

μ = coefficient of friction found in ACI Code Section 11.6.4.3.

The value of μ was taken to be 0.6 for all specimens to be conservative. The value for the nominal shear strength stated above was used unless it exceeded either $0.2f'_cA_c$ or $800A_c$ which is stated in ACI Code Section 11.6.5. It can be noted that all of the calculated values for shear transfer at the base of the walls exceed V_{max} meaning that no additional dowel reinforcement was required. The calculated values for shear strength at the base of the walls are shown in Table 6.

Table 6 - Wall specimen values

Name	M_{max}(k-ft)	V_{max}(kips)	V_n(kips)	V_{nb}(kips)
PL1	133	44.6	64.2	76.3
F1	168	56.2	87.4	76.3
10C	128	42.9	54.4	63.1
F10C	132	44.2	69.9	63.1

3.4.3 Reinforcing Details of Test Specimens

Based on the strengths of the walls, the longitudinal reinforcement was chosen so that the intended shear stress value could be reached before failure. The horizontal reinforcement

was chosen based on the predicted flexural strength such that it would not exceed the strength of the deformed wire making up the horizontal reinforcement. The reinforcement bar specifications for the wall specimens are shown in Table 5.

The vertical boundary reinforcement for specimens F10C and 10C consisted of 4 No. 4 Grade 60 bars placed in of two layers on both the right and left side of the wall. They were anchored to the foundation and were continuous into the top block. This created a tension reinforcement ratio, ρ, of 0.83%. The tension reinforcement ratio is found using Eq. 3-4.

$$\rho = \frac{A_s}{l_w * t_w} \qquad \text{Eq. (3-4)}$$

where,

A_s = Area of main longitudinal reinforcement in tension (in^2)

l_w = length of the wall (in)

t_w = thickness of the wall (in)

Two layers of D4.5 deformed wire were spaced at 5 in. on center as web horizontal reinforcement. The web reinforcement ratios are found using equation Eq. (3-5).

$$\rho_w = \frac{A_{sw}}{s * t_w} \qquad \text{Eq. (3-5)}$$

where,

A_{sw} = Area of web reinforcement per row

s = reinforcement spacing (in)

t_w = thickness of the wall (in)

This resulted in a vertical web reinforcement ratio of 0.45%. The horizontal web reinforcement ratio was also 0.45%. The vertical boundary reinforcement was confined using 1/8 in. round bar spaced at 4 in. This spacing was chosen so that the concrete would not be

confined in order to evaluate the difference in behavior in fiber and non-fiber reinforced concrete. The reinforcing configuration for walls F10C and 10C are given in Figure 21.

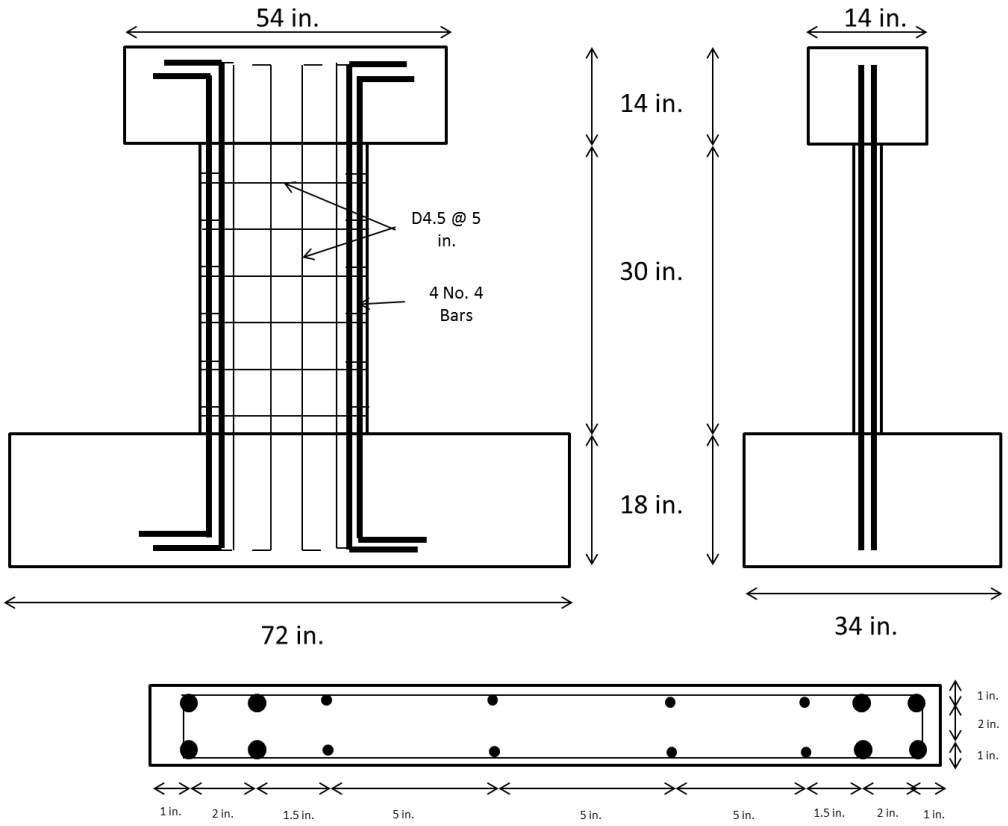

Figure 21 - Reinforcing configuration for walls F10C and 10C

The vertical boundary reinforcement for specimens PL1 and F1 consisted of 2 No. 4 Grade 60 bars and 2 No. 5 Grade 60 bars placed in two layers on both the right and left side of the wall. The No.5 bars were the outmost layer. They were anchored to the foundation and were continuous into the top block. This created a tension reinforcement ratio of 1.06%. Two layers of D4.5 deformed wire spaced at 4 in. on center were used as web horizontal reinforcement. This resulted in a vertical web reinforcement ratio of 0.56%. The horizontal web reinforcement ratio was 0.56%. The vertical boundary reinforcement was confined using 1/8" round bar also spaced at 4 in. As previously mentioned, this spacing was chosen so that the concrete would not be confined in order to evaluate the difference in behavior in

fiber and non-fiber reinforced concrete. The reinforcing configuration for walls PL1 and F1 are given in Figure 22.

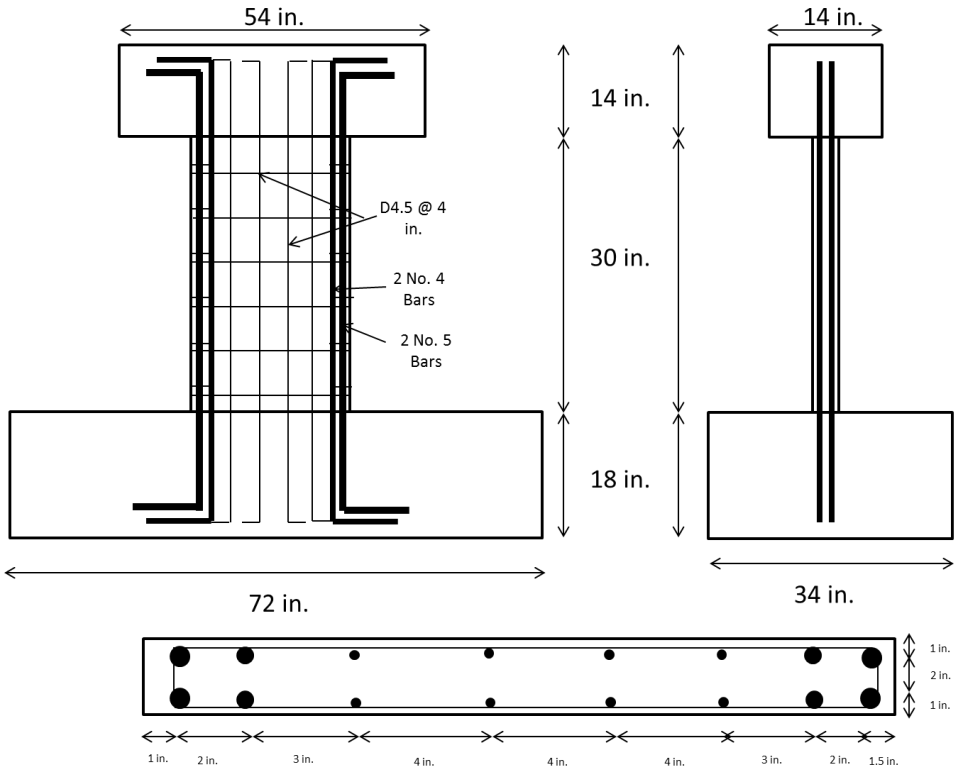

Figure 22 - Reinforcing configuration for walls PL1 and F1

3.4.4 Construction of Specimens

The foundation blocks, top blocks, and wall specimens were all constructed in the structural engineering laboratory at the University of Louisiana at Lafayette. The process began by cutting, bending, and tying the rebar for each foundation block to the correct dimensions (Figure 23).

Figure 23 - Foundation reinforcement cage

The reinforcement cage was subsequently placed in the wooden foundation block formwork (Figure 24).

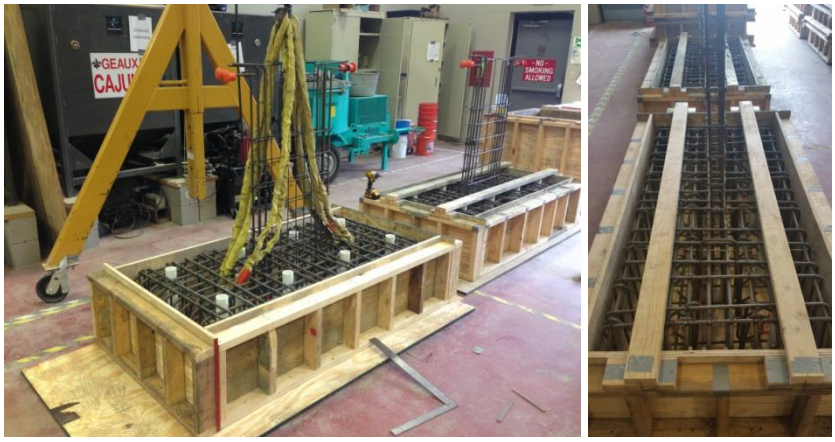

Figure 24 - Reinforcement cage in wooden formwork

Eight locations were marked for 18 in. pieces of PVC pipe with a diameter of 2 in. to be placed vertically in the foundation block. The locations of these PVC pipes were determined by the locations of the DYWIDAG bars that would anchor the specimen to the modular strong-block testing system. The locations of the PVC pipes are shown in Figure 25.

Figure 25 - PVC locations in foundations

Before the foundation block was cast, the wall's vertical reinforcement was tied to the bottom layer of the reinforcement cage in the foundation at the appropriate location. The foundation blocks were then cast using self-consolidating concrete provided by Barry Concrete (Figure 26).

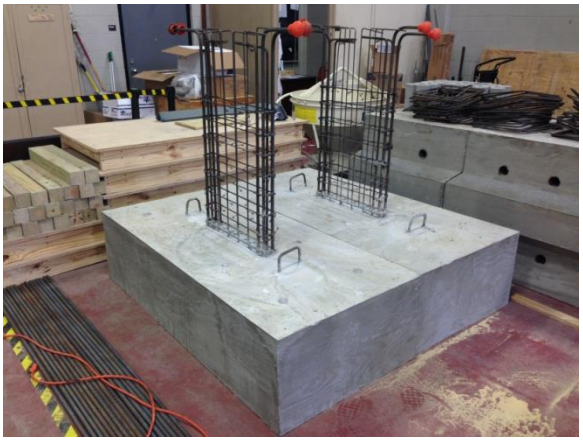

Figure 26 - Cast foundation block

Because the entire test specimen required multiple mixes, a cold joint was created between the wall and the foundation block. The concrete was left unfloated and rough in the area where the wall would be cast to create a larger coefficient of friction between the wall and foundation minimizing the probability of a sudden failure.

After the foundation block was cast, the walls horizontal reinforcement was tied to the vertical reinforcement (Figure 27).

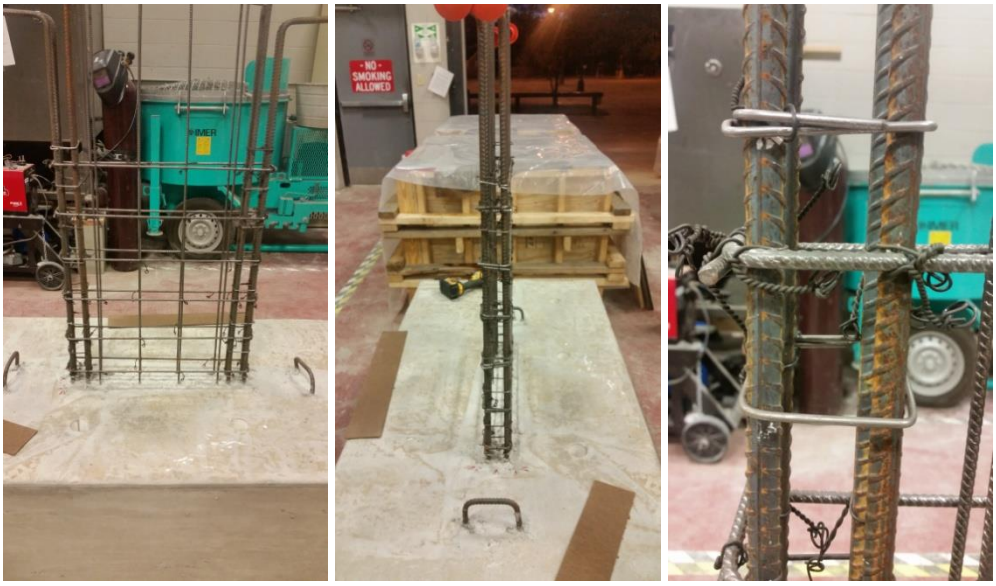

Figure 27 - Wall reinforcement

The wall's wooden formwork was then put in place around the walls reinforcement cage (Figure 28).

Figure 28 - Wall formwork

Once all of the wall reinforcement and formwork was in place the wall was cast using each of the mix designs (Figure 29).

Figure 29 - Cast wall within formwork

Lastly the formwork for the top block was placed on the wall and around the protruding wall reinforcement. The top block reinforcement was then tied into the rest of the specimen's reinforcement (Figure 30).

Figure 30 - Top block reinforcement

The top blocks were then cast using self-consolidating concrete provided by Barry Concrete. A complete test specimen is shown in Figure 31.

Figure 31 - Wall test specimen

Also included were concrete 4 in. x 8 in. cylinders for all foundations, walls, and top blocks for hardened concrete tests made in accordance with ASTM Standard C192 (ASTM 2014).

Between each casting of foundation blocks, walls, and top blocks wet burlap and visqueen were subsequently placed on and around the exposed concrete. The concrete cylinders were also covered. All concrete was stored in the temperature controlled laboratory, and the forms were removed from all specimens after three days of moist curing. All concrete was moist cured for a total of 7 days. When the testing date arrived the crane then lifted the specimen and placed it on the testing system (Figure 32).

Figure 32 - Wall specimen set up in test system

3.4.5 Specimen Instrumentation

Five linear potentiometers were positioned on a face of every wall to monitor the average shear strain and rotation of the wall (Figure 33).

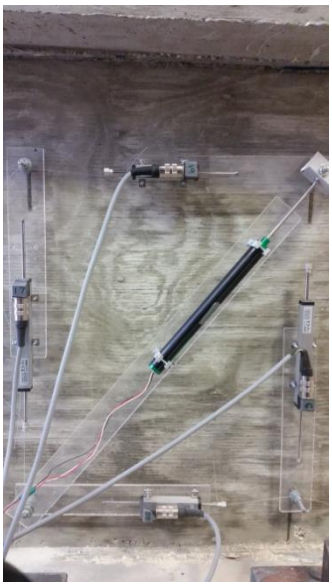

Figure 33 - Five potentiometers on wall face

Two vertical potentiometers were also placed at the wall base to measure the rotation (Figure 34).

Figure 34 - Wall edge potentiometers

A horizontal potentiometer was placed at the base of the wall and also at mid-depth of the top block to monitor sliding and drift, respectively (Figure 35).

Figure 35 - Top block lateral displacement potentiometer

Another horizontal potentiometer was placed at the base of the foundation and connected to a fixed location (modular blocks) to monitor the sliding of the entire specimen. A complete layout of all of 10 potentiometers can be found in Figure 36.

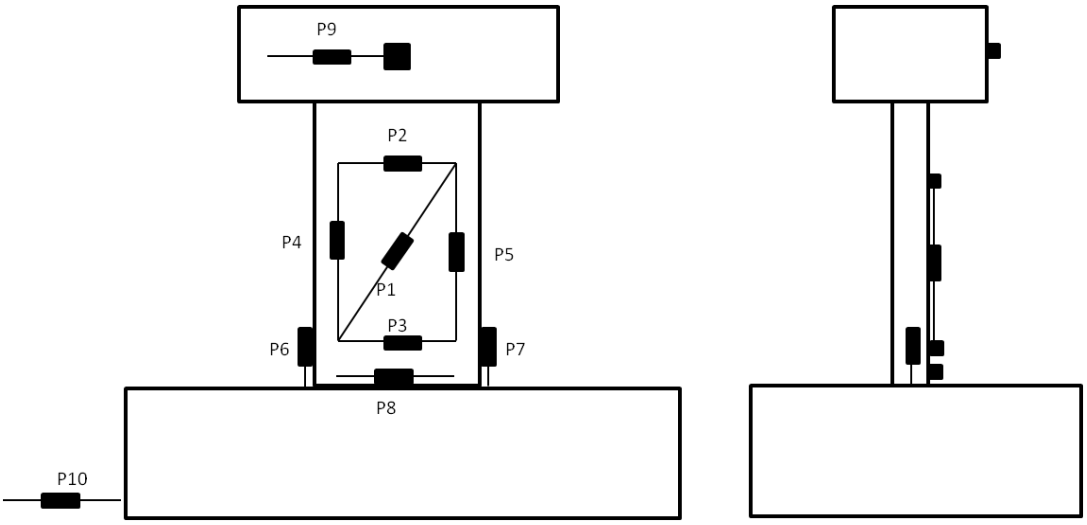

Figure 36 - Potentiometer layout

The readings from these instruments were collected using a data acquisition system. A reading from each instrument was taken at every 20% of a cycle's total drift for drift cycles 1 and 2 and at every 10% for drift cycles 3 through 10 (Figure 37).

Figure 37 - Data acquisition system

A pressure gauge was used to monitor and note the applied load of the hydraulic actuator on the specimen.

3.4.6 Test Set Up and Test Procedure

All four specimens were tested in the structural engineering lab at the University of Louisiana at Lafayette. The specimens were tested using a modular strong-block testing system with a steel frame erected on it (Figure 38).

Figure 38 - Modular block

The modular blocks were placed in a row of nine with a block to the right and left of the 5th block and post-tensioned using a specific hydraulic actuator (Figure 39).

Figure 39 - Modular block formation

The row of nine modular blocks contained six 1 in. diameter DYWIDAG bars positioned in the locations shown in Figure 40.

Figure 40 - DYWIDAG bar locations

The perpendicular row of three modular blocks also contained four 1 in. diameter DYWIDAG bars positioned in the same locations. The six bars in the row of nine blocks were tensioned to 85 kips per bar for wall specimens F1 and PL1. The six longitudinal bars were tensioned to 75 kips per bar for wall specimens F10C and 10C. The six bars in the row of three blocks were tensioned to 60 kips per bar for all of the wall specimens. After the blocks were in place and post-tensioned together, a steel frame was erected on the modular blocks so that the walls could be tested (Figure 41) (Benton, 2015).

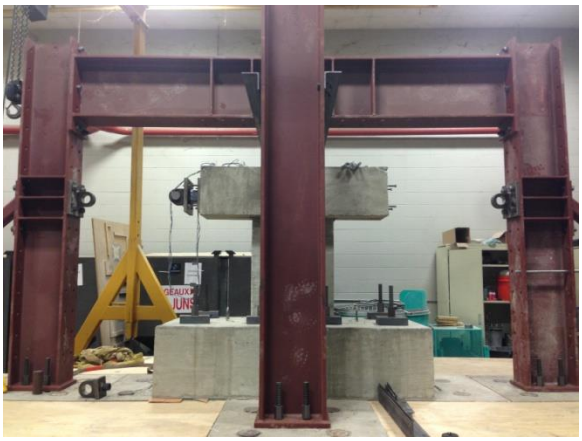

Figure 41 - Steel test frame

Before the specimen was placed on the modular blocks a sheet of plywood the size of the foundation with the holes punched out for the DYWIDAG bars was placed down. The purpose of the plywood was to increase the friction resistance to slip and to account for any inconsistencies between the specimen and test system. After the specimen was moved by the crane into position on the sheet of plywood, eight 1 in. diameter DYWIDAG bars, eight 5 in. x 8 in. x 2 in. bearing plates, and eight hex nuts anchored the foundation to the testing system. The bars were tensioned to 40 kips using a hydraulic actuator (Figure 42).

Figure 42 - Anchored foundation

The specimens were also braced to stay in plane using the pictured mechanism (Figure 43).

Figure 43 - Wall bracing

After the specimen was in place and secured, the necessary instrumentation was placed on the specimen. A specimen ready for testing is shown in Figure 44.

Figure 44 - Specimen ready for testing

When testing was set to begin, a 100-kip hydraulic actuator with a 13 in. stroke was connected at mid-depth of the top block to the steel column of the testing system. The horizontal hydraulic actuator was used to apply the lateral loading to the specimens. The mechanism to connect the hydraulic actuator to the top block during a cycle is pictured in Figure 45.

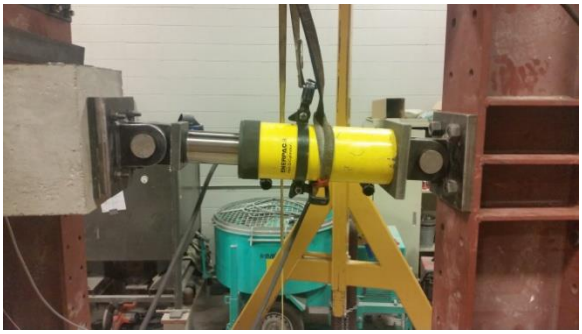

Figure 45 - Loading mechanism with hydraulic actuator

For each cycle to be completed the actuator had to be taken down and moved to the opposite side to apply a loading from each side for each cycle. The dimensions of the test frame and loading mechanism are shown in Figure 46.

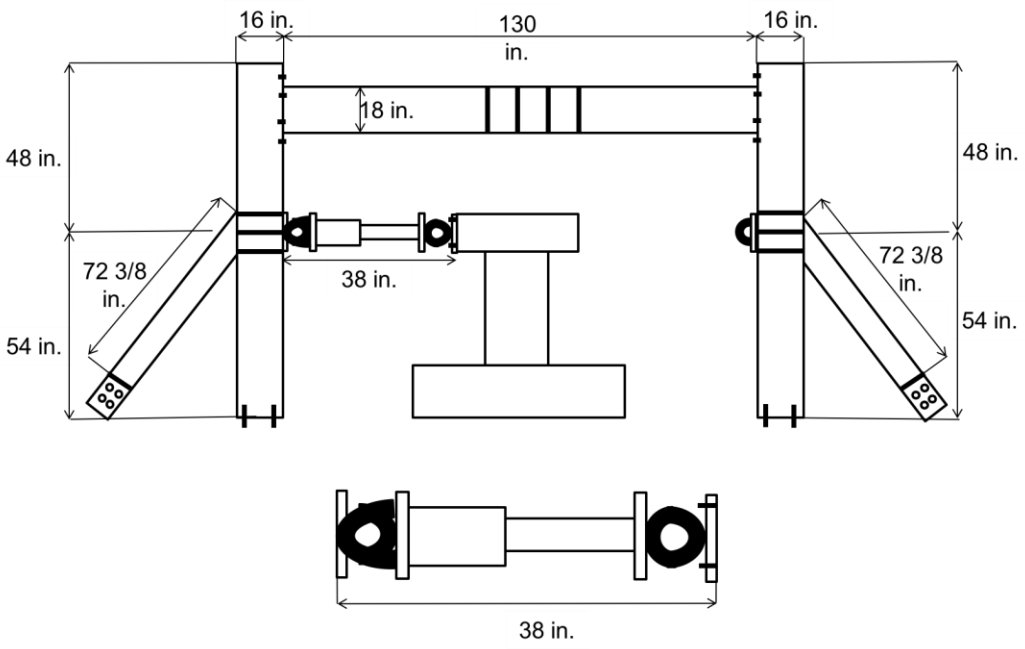

Figure 46 - Dimensions of test frame and loading mechanism

Each specimen was subjected to quasi-static reversed cyclic displacements beginning with 0.125% drift and reaching a maximum of 3%. Drift was calculated by taking the lateral displacement at mid-depth of the top block in relation to the foundation and dividing it by the initial distance between the two, 36 in. Every displacement cycle between 0.125% and 1% was applied twice to observe any decrease in strength cause by repeated cycles. A total of 10 cycles were performed on each wall. A table noting the cycle numbers and drift percentages can be seen in Table 7. It is important to note that there is no widely accepted reversed cyclic loading plan for reinforced concrete members. However, it has been reported that the loading plan can affect the behavior and ductility of the specimen (Lehmans, Moehle, & Mahin, 2004), (Matamoros & Sozen, 2003).

Table 7 - Drift cycle legend

Cycle	Drift %
1L	0.125%
1R	0.125%
2L	0.125%
2R	0.125%
3L	0.500%
3R	0.500%
4L	0.500%
4R	0.500%
5L	1.000%
5R	1.000%
6L	1.000%
6R	1.000%
7L	1.500%
7R	1.500%
8L	2.000%
8R	2.000%
9L	2.500%
9R	2.500%
10L	3.000%
10R	3.000%

CHAPTER 4: Results and Analysis

4.1 Introduction

A total of 22 shear beams and 4 shear walls were tested in the structural engineering lab at the University of Louisiana at Lafayette. The results of the shear beams are discussed in Section 4.2. The ultimate goal of the shear beams was to determine the shear strength of each mix as well as the effects fibers and rubber had on the concretes shear strengths. The results of the shear walls are discussed in Section 4.3. The loads and displacements for each shear wall were analyzed to determine their behavior and characteristics.

4.2 Shear Beams

4.2.1 Mix Properties

The fresh and hardened concrete properties were determined for each beam in a previous study. The fresh properties included slump, unit weight, and air content, while the hardened properties included compressive strength, split-tensile strength, and modulus of elasticity. Tables 8 and Figures 47-51 show the properties for each mix. The mixes highlighted in red were the mixes chosen for the shear walls.

Table 8 - Beam specimen fresh and hardened concrete properties (Helminger, 2014)

Shear Beams							
Name	**Slump (in)**	**Unit Weight (lb/ft^3)**	**Air Content**	**28 Day Compression (psi)**	**56 Day Compression (psi)**	**Tensile (psi)**	**Modulus (ksi)**
PL1	7.75	147.7	2.5%	8672	9416	657	5160
5C	6.5	143.5	2.4%	6112	6670	517	4436
5F	4.75	144.2	3.1%	7190	8144	650	4939
5CF	6.5	144.3	2.7%	7079	8121	577	5202
10C	5	140.7	2.7%	5314	5720	544	4353
10F	4	141.2	3.6%	5455	6440	522	3884
10CF	7.25	140.9	2.8%	5228	5975	520	4126
15C	5.5	136.5	2.7%	4149	4273	451	3895
15F	6	136.8	4.3%	3988	4895	433	3521
15CF	8	136.7	2.9%	4216	4636	469	3858
PL2	8.25	146.9	2.2%	8049	9106	675	5278
F1	6.5	150.1	2.4%	10193	11443	946	5872
F5C	5.75	147.2	2.2%	7121	8341	814	5037
F5F	5.5	147.4	2.6%	7973	9031	838	4994
F5CF	6	146.8	2.3%	7279	8450	765	5124
F10C	5.25	145.5	2.3%	5814	6293	474	4881
F10F	3.5	144.0	2.8%	6353	6974	611	4571
F10CF	4	145.2	2.4%	6205	6972	740	4636
F15C	6.5	141.1	1.7%	4523	5344	630	3932
F15F	6.25	142.8	2.4%	5606	6285	558	4045
F15CF	7.25	143.4	2.2%	4377	5616	596	4093
F2	6.25	151.1	2.1%	9720	10887	869	5501

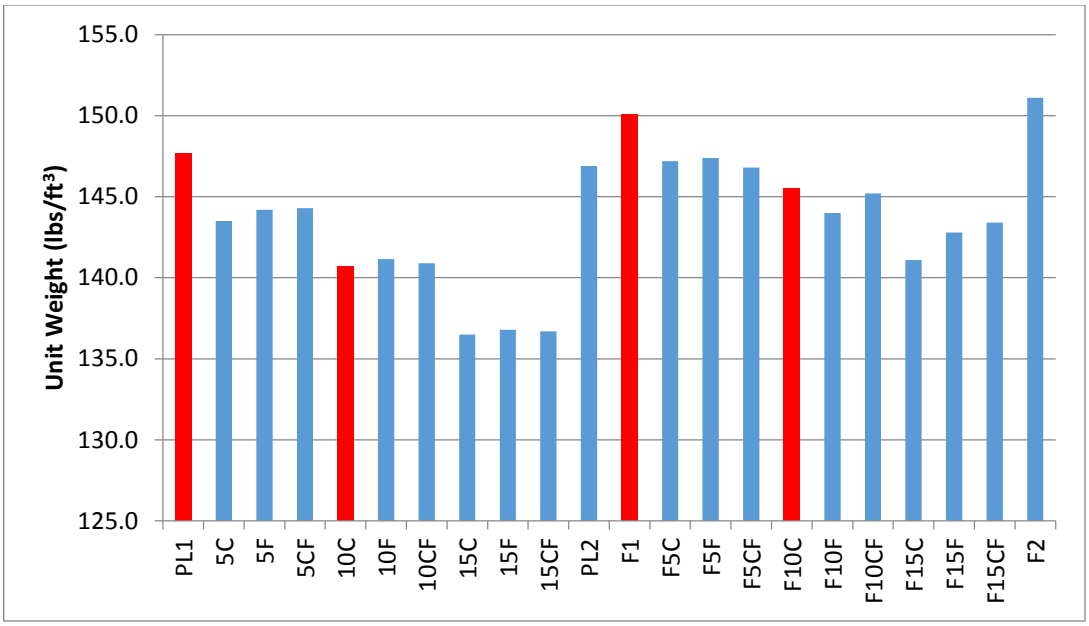

Figure 47 – Unit weights for shear beams

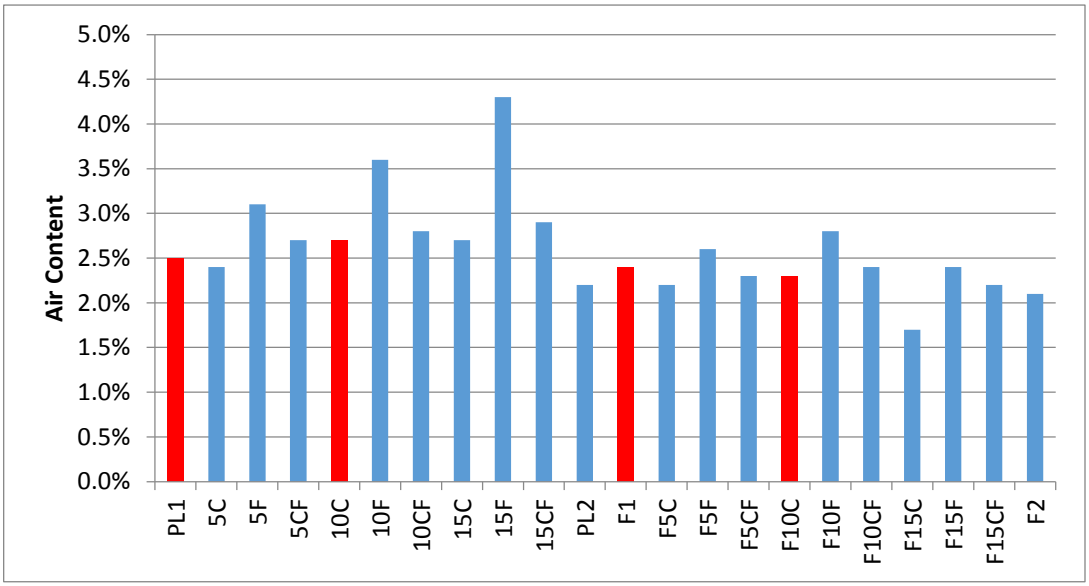

Figure 48 – Air content for shear beams

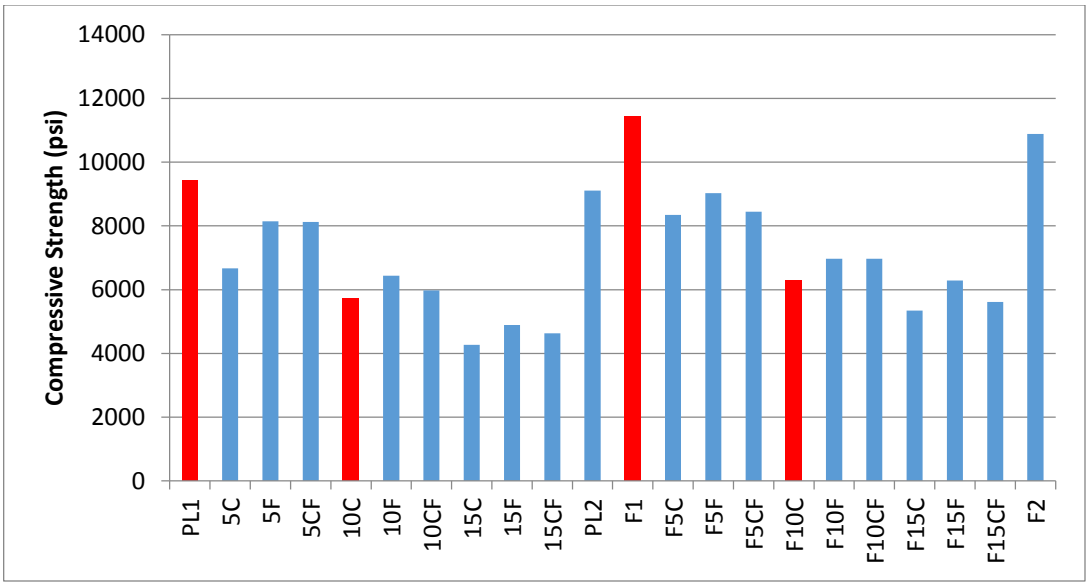

Figure 49 - Compressive strengths for shear beams

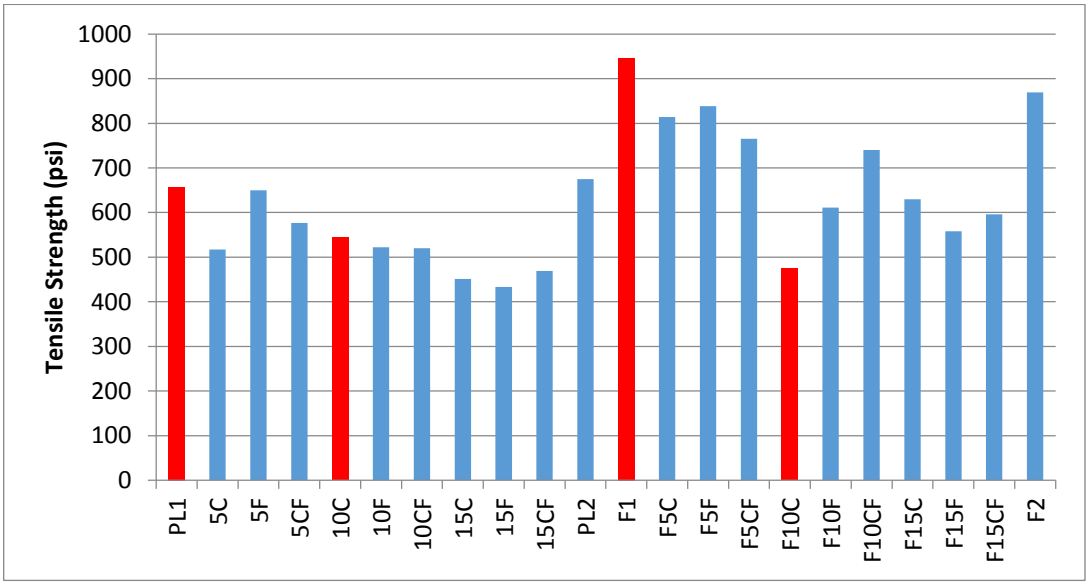

Figure 50 - Tensile strengths for shear beams

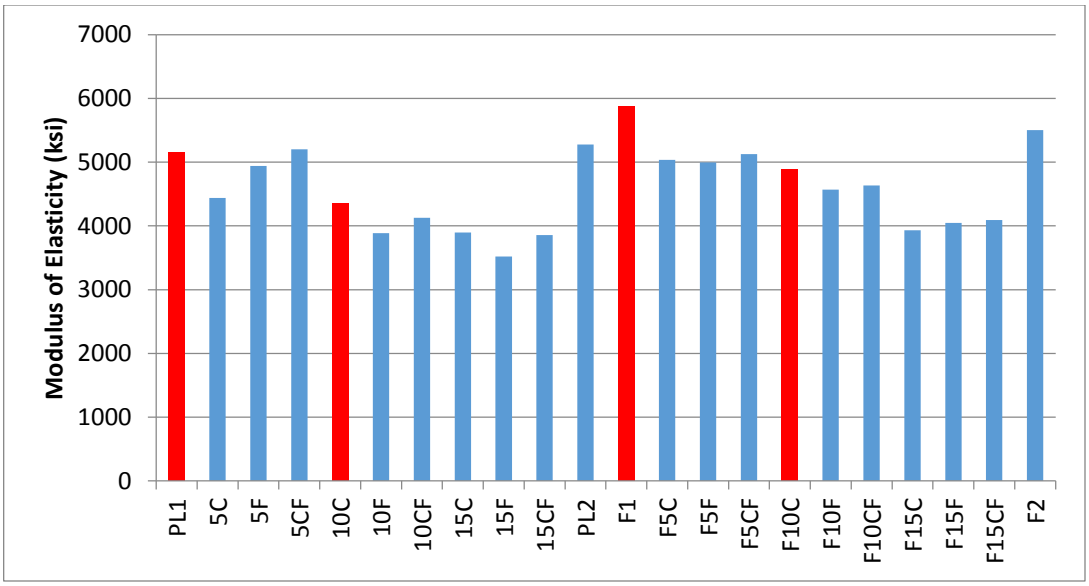

Figure 51 - Modulus of elasticities for shear beams

The goal was to achieve a slump of at least 4 inches for the beams. Due to the variety and inconsistencies in the mix compositions, the amount of superplasticizer added to each mix was different and often had to be modified during the mixing process to achieve the targeted workability. Preliminary mixes were also done to determine the initial amount of water reducer for each mix. Because fibers and rubber decrease workability as their content is increased in the mix, the amount of water reducer also increased. The unit weight for the selected mixes shows that as rubber replacement increases the unit weight will decrease. In contrast, the unit weight shows that as fibers are added to a mix without replacing any aggregates the unit weight will increase. Both of these cases are due to the weight of each material replacing a lighter material or not replacing anything at all. The air content for the selected mixes tended to increase as rubber replacement increased. This effect is not as evident when fibers are present in the mix. This may be attributed to the additional need for superplasticizer in mixes with fibers present so that the targeted workability could be achieved (Helminger, 2014).

The results show that when rubber replaces aggregate in the mix composition, the compressive strength will decrease significantly. The results also show that mixes containing fibers exhibit higher compressive strengths compared to those without fibers. With regards to tensile strength, the results show that when rubber replaces the aggregate, the tensile strength also significantly decreases. The tensile strength of mixes containing fibers saw an increase when fibers were present in the mix. Lastly the modulus of elasticity decreases when rubber replaces aggregates in the mixes. When fibers were present in the mix, the modulus of elasticity tended to increase (Helminger, 2014).

4.2.2 Shear Strength

Twenty-two shear beams were cast corresponding to the mix designs found in Table 2. The data outputs were analyzed so that the effects of the fibers and rubber could be analyzed and shear strength could be determined for each mix. The crack progression of each beam can be seen in Appendix Figures A1-A22. The load versus displacement response plots for each beam specimen can be seen in Appendix Figures B1-B22. The graphs plot the average vertical displacement recorded by the two potentiometers at mid-span versus the recorded load. Using the plots in Appendix Figures B1-B22, the observed shear strength value was recorded when a change in slope occurred denoting the first crack in shear in the concrete beam. The concrete contribution to shear strength, ψ, was found using equation Eq. (4-1). This value for each mix represented how much of a contribution the varying amounts of fibers and rubber contributed to the shear strength. These values are shown in Table 9 and Figure 52.

$$\Psi = Vc/(\sqrt{f'_c}\,(b)(d)) \qquad \text{Eq. (4-1)}$$

where,

ψ = concrete contribution to shear strength

Vc = Shear capacity of beam (lbs)

f'_c = 56 day compressive strength (in)

b = width of beam (in)

d = depth of beam (in)

Table 9 - Beam shear strength values

Name	% Rubber	% Fiber	V_C	f'_c	ψ
PL1	0%	0%	11222.5	9416	4.13
5C	5%	0%	10468.5	6670	4.58
5F	5%	0%	12159.5	8144	4.81
5CF	5%	0%	10899	8121	4.32
10C	10%	0%	12531.5	5720	5.92
10F	10%	0%	Shear/Flexure	6440	N/A
10CF	10%	0%	10291.5	5975	4.76
15C	15%	0%	10825.5	4273	5.91
15F	15%	0%	9351.5	4895	4.77
15CF	15%	0%	11310	4636	5.93
PL2	0%	0%	10743	9106	4.02
F1	0%	1%	Shear/Flexure	11443	N/A
F5C	5%	1%	Shear/Flexure	8341	N/A
F5F	5%	1%	Flexure	9031	N/A
F5CF	5%	1%	Flexure	8450	N/A
F10C	10%	1%	Shear/Flexure	6293	N/A
F10F	10%	1%	Flexure	6974	N/A
F10CF	10%	1%	Flexure	6972	N/A
F15C	15%	1%	Shear/Flexure	5344	N/A
F15F	15%	1%	Shear/Flexure	6285	N/A
F15CF	15%	1%	13365	5616	6.37
F2	0%	1%	Flexure	10887	N/A

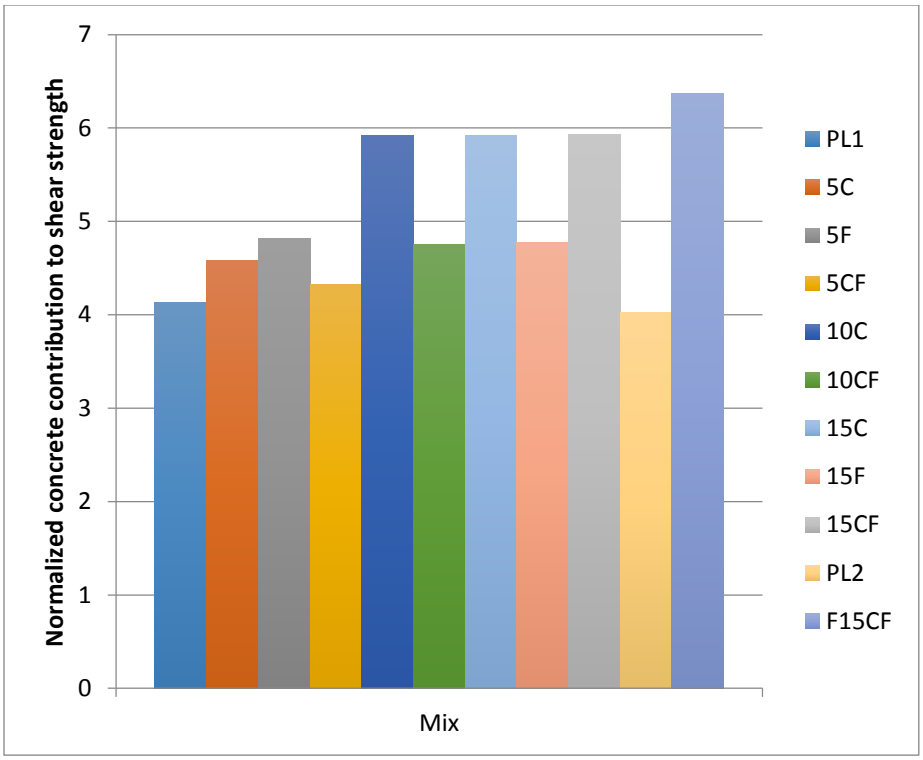

Figure 52 – Normalized concrete contribution to shear strengths for shear beams

The concrete modification factors were normalized with respect to the mix compressive strength so that they could be compared. The mix compressive strengths were taken as the 56-day strength because that was when the beams were tested. It should be noted that although all of the beams were designed to fail in shear many of the beams containing fibers ultimately failed in flexure or a combination of shear and flexure. In these beams, the shear strength increased such that the flexural failure ended up dominating the failure mode. Therefore these beams could not be analyzed for their contribution to shear strength. Figure 53 contains the percent difference in concrete contribution to shear strength for rubber concrete beams in comparison to plain concrete beams. It shows that the non-fiber mixes containing 15% rubber replacement had the most significant shear strengthening affects.

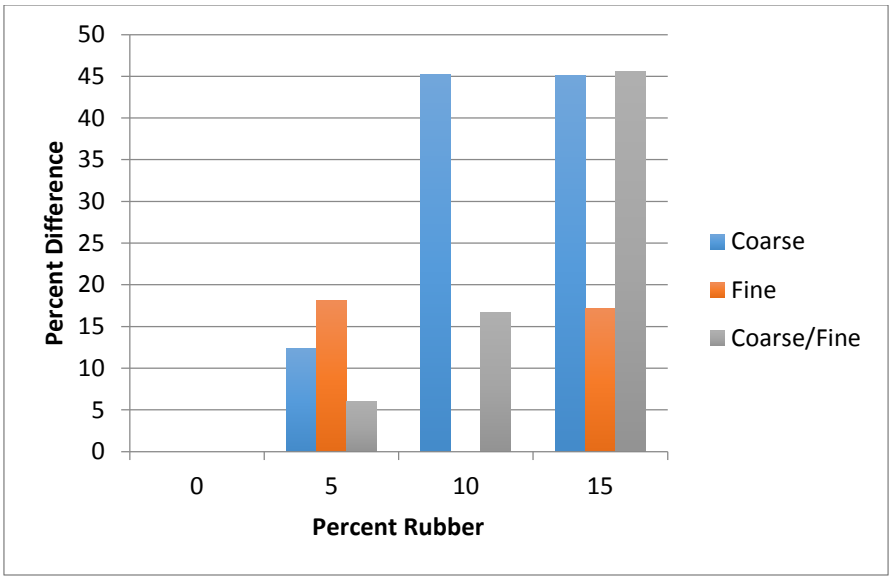

Figure 53 - Normalized concrete contribution to shear strength with no fibers versus percent rubber

The values were compared to the two plain concrete mixes. As the rubber replacement percentage increased, the percent increase in shear strength contribution increased. For coarse rubber replacement, the 10% and 15% replacement percentage showed the largest increase in contribution to shear strength. For fine rubber replacement, the 5% and 15% replacement percentage showed the largest increase contribution to shear strength. When coarse/fine rubber at a replacement percentage of 15 was used the percentage increase was more than any other mix that did not contain fibers. The mix containing 10% fine rubber was not analyzed after determining it failed due to a combination of flexure and shear.

When fibers were added the concrete behaved differently. Although the beams were all designed to fail in shear, the fibers increased the shear strength such that the flexural failure mode dominated. Only one beam containing fibers was able to be analyzed for its shear failure because of this. The beam containing 1% fiber and 15% coarse/fine rubber increased the shear strength by 56.3% compared to plain concrete. In comparison to the same

mix without fibers, the shear strength increased by 7.3%. Overall the mix with highest concrete contribution to shear strength was this mix containing 1% fibers and 15% coarse/fine rubber. The ψ of the F15CF mix was 6.37. In summary it can be determined that fibers and rubber significantly increase the shear strength of concrete for all mixes in comparison to plain concrete. The shear strength also increased when the mix containing fibers was compared to the mix with the same rubber content that did not contain fibers.

4.2.3 Beam Behavior

Using the load v. displacement plots in Appendix Figures B1-B22, some behaviors were unique to given mixes. The crack progression of each beam can be seen in Appendix Figures A1-A22. When rubber was added to mixes the shear strengths increased with respect to $\sqrt{f'_c}b_w d$. The average increases were 12.1%, 30.9%, and 35.9% for 5, 10, and 15 percent rubber, respectively. When both fibers and rubber were added to the one analyzed mix the shear strengths increased by 56.3% for 1% fibers and 15% coarse/fine rubber. Mixes containing rubber tended to fail at lower loads than mixes without rubber. After the beam cracked, the rubber mixes could not sustain a significant load for an extended period of time due to the low stiffness of rubber resulting in a low displacement at failure and a low post crack shear strength. Immediate failure after the development of the first shear crack was unexpected. The mixes containing fibers increased the shear strength such that the beam was controlled by a flexural failure and could not be analyzed for its exact concrete contribution to shear strength. When the beams cracked, the fibers exhibited strain hardening behavior. These fiber beams were able to support significant loads for much longer than mixes only containing rubber and the displacement at failure was much larger.

4.3 Shear Walls

4.3.1 Definitions

Shear stress is defined as the lateral load divided by the cross sectional area of the wall, shown by equation Eq. (4-2). The shear stresses are normalized with respect to the square root of the concrete strength throughout. This allows for direct head-to-head comparisons to the predicted values found in ACI.

$$v = \frac{F}{l_w * t_w} \qquad \text{Eq. (4-2)}$$

where,

v = average shear stress (psi)

F = applied lateral load (kips)

l_w = length of wall (in)

t_w = thickness of wall (in)

The drift of each wall was determined by evaluating the lateral displacement with respect to the shear span. The shear span length is the distance from the height of the applied load to the base of the wall. The shear span length was illustrated in Figure 20. Equation Eq. (4-3) was used to calculate the drift.

$$\delta = \frac{\Delta}{a} \qquad \text{Eq. (4-3)}$$

where,

δ = drift

Δ = lateral displacement (in)

a = shear span length (in)

Shear strain, γ, in the wall can be obtained using a strain rosette formed by potentiometers P1 to P5. Engineering shear strain is defined as the change in angle of a

shape. The wall rectangle is made by the four points in which potentiometers were connected to the face of the wall. This rectangle measures 20 in. tall and 16.5 in. wide. The diagonal length created by this rectangle is 25.928 in. A diagram further illustrating these variables can be found in Figure 54. The law of cosines was used to find the two angles noted in Figure 54 and they were subsequently subtracted from the original angle of 90 degrees to find the shear strain. This is shown in Eq. (4-4). It should be noted that the measured shear strain is overestimated because of the flexural deformations in the wall.

$$\Upsilon = 90° - \theta_1 - \theta_2 \qquad \text{Eq. (4-4)}$$

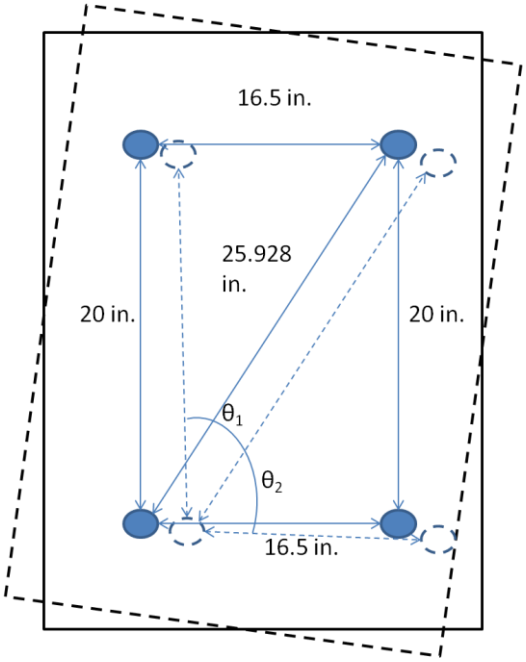

Figure 54 - Shear strain diagram

4.3.2 Mix Properties

The fresh and hardened concrete properties were determined for each wall. The fresh properties included slump, unit weight, and air content, while the hardened properties included compressive strength, split-tensile strength, and modulus of elasticity. Table 10 and Figures 55-59 show the properties for each mix.

Table 10 - Wall specimen fresh and hardened concrete properties

Name	Slump (in)	Unit Weight (lb/ft^3)	Air Content	28 Day Compression (psi)	Tensile (psi)	Modulus (ksi)
PL1	10	146.1	2.0%	6890	667	5190
F1	7.75	151.4	1.4%	9660	1059	6290
10C	9.75	140.7	2.1%	5870	589	4890
F10C	8.75	146.7	0.4%	6120	835	4820

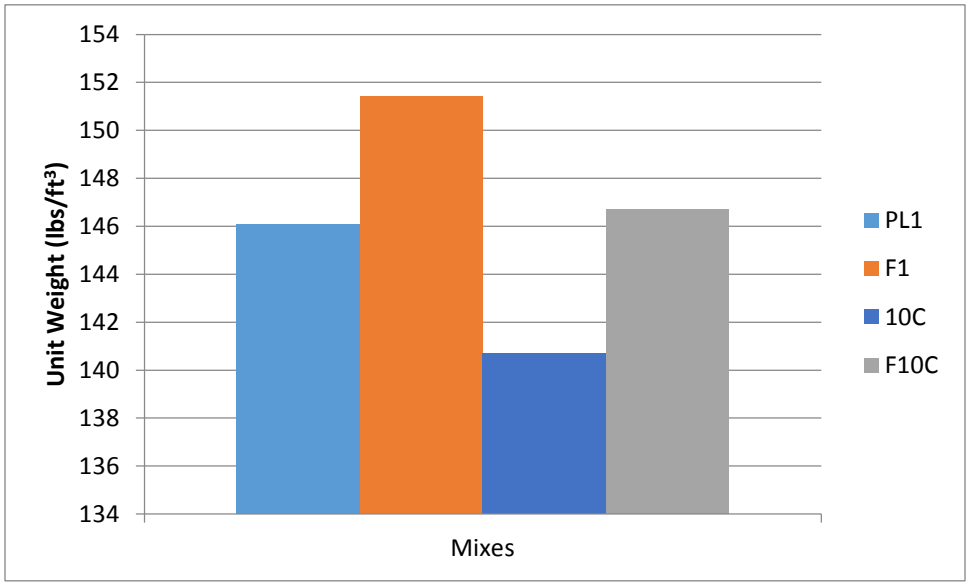

Figure 55 – Unit weights for shear walls

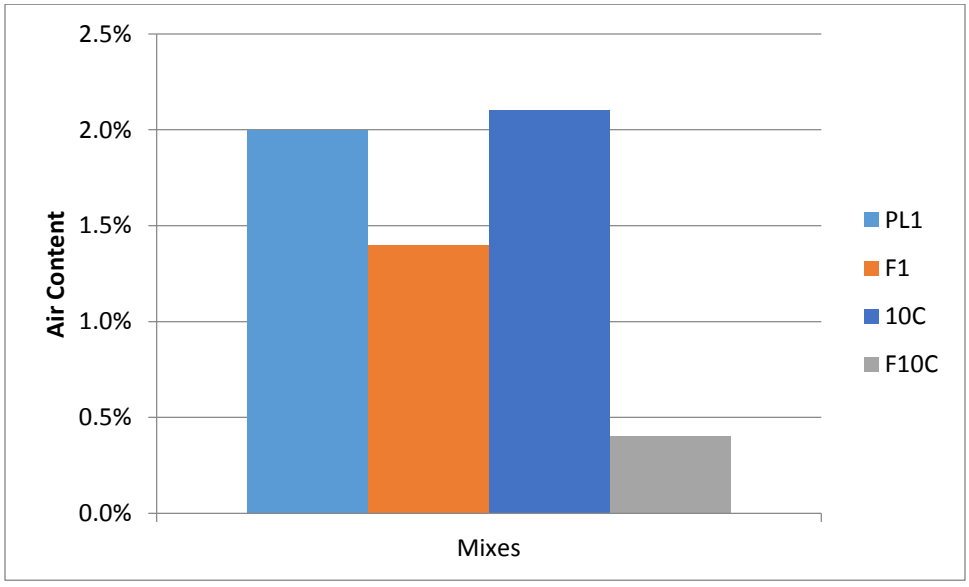

Figure 56 – Air content for shear walls

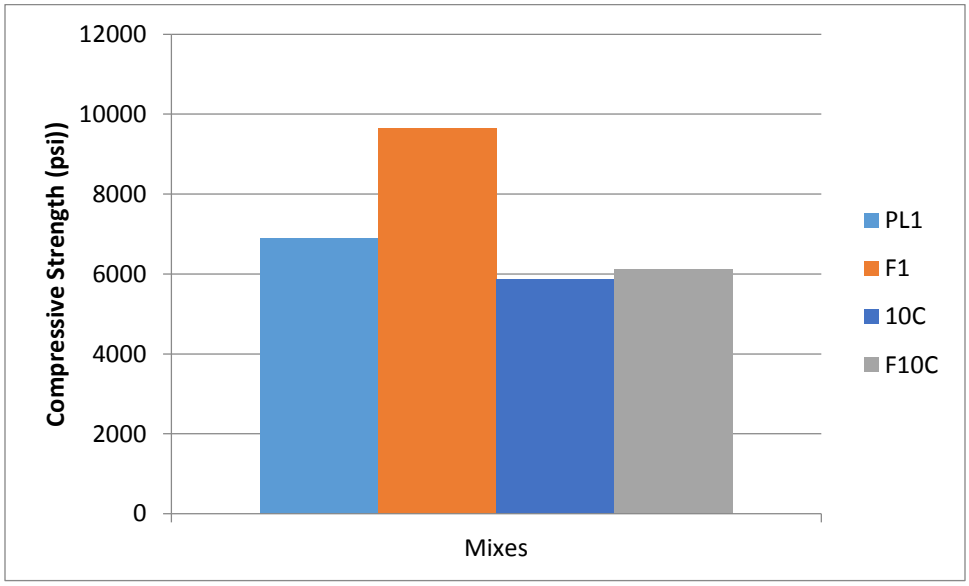

Figure 57 – Compressive strengths for shear walls

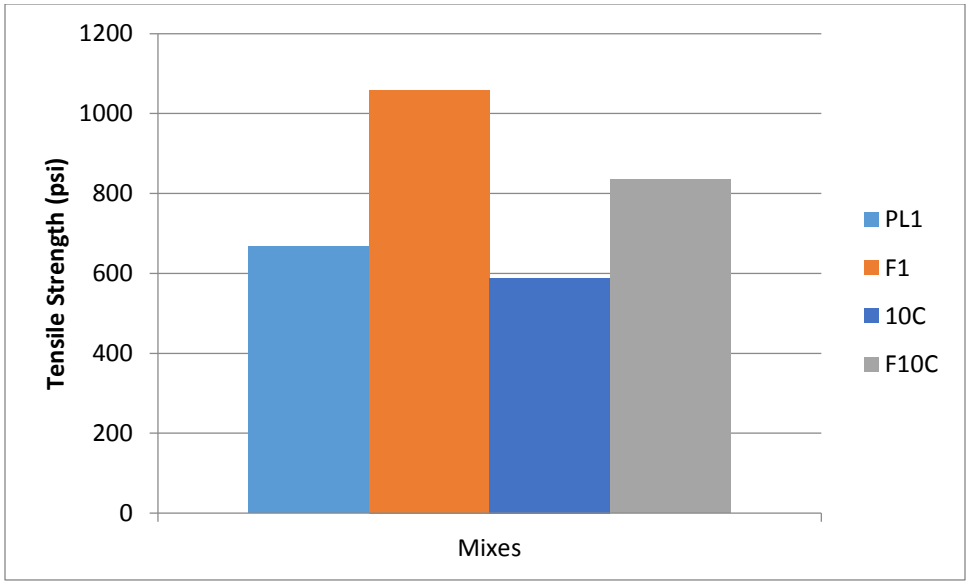

Figure 58 – Tensile strengths for shear walls

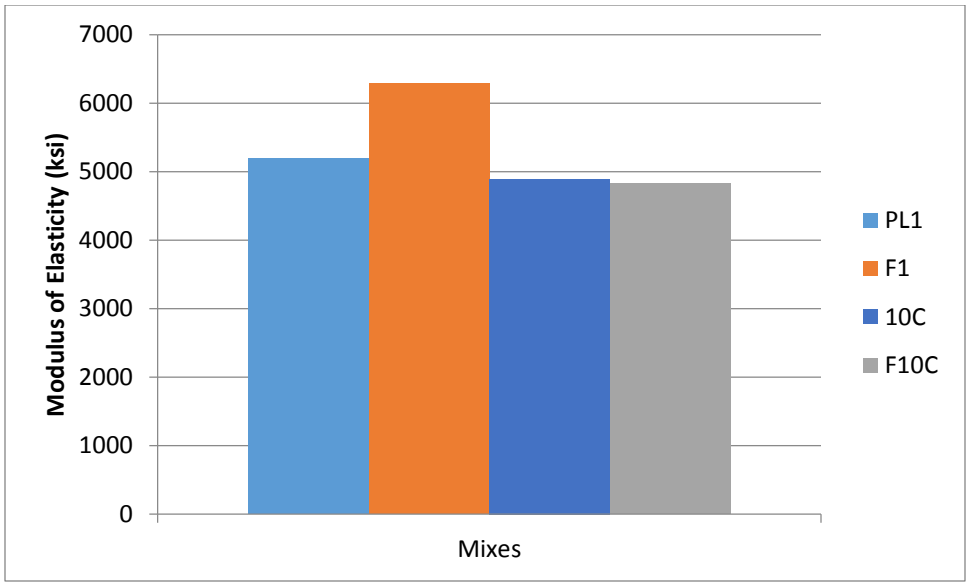

Figure 59 – Modulus of elasticities for shear walls

The goal was to achieve a slump of at least 6 inches for the walls. Preliminary mixes were also done to determine the initial amount of water reducer for each mix and water reducer was sometimes modified during the mixing process to achieve the targeted workability. The fresh concrete properties for the walls were affected in the same manner as the shear beams for both fibers and rubber.

The results show that when rubber replaces aggregate in the mix composition, the compressive strength will decrease significantly. The results also show that mixes containing fibers exhibit higher compressive strengths compared to those without fibers. With regards to tensile strength, the results show that when rubber replaces the aggregate, the tensile strength also significantly decreases. The tensile strength of mixes containing fibers saw an increase when fibers were present in the mix. Lastly the modulus of elasticity decreases when rubber replaces aggregates in the mixes. When fibers were present in the mix, the modulus of elasticity tended to increase but only when rubber was not present.

4.3.3 Lateral Load Versus Displacement Response

The lateral load versus displacement response plots for each wall specimen can be seen in Figures 60-63. The graphs plot the applied load versus drift. It is important to note that the descending portion of the line in each cycle is drawn linear because the data points during unloading were only recorded for when the load was last applied and zero. Included in the plots are two positive and negative horizontal lines representing the value of the calculated nominal shear strength, V_n, and the probable shear demand of the wall, V_{max}, for each wall specimen. The nominal shear strength and probable shear demand of the wall were calculated as it was described in Section 3.4.2 and can be found in Table 6. All calculations were done using the yield strengths found in Table 5 as well as the concrete cylinder compressive strengths from the test day found in Table 10.

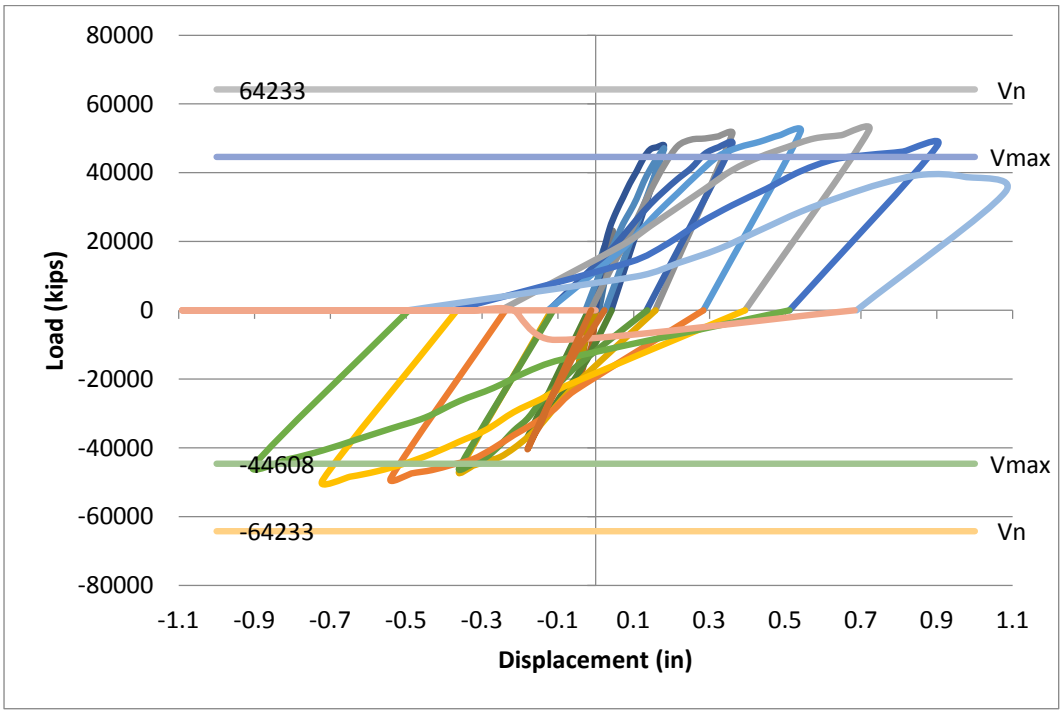

Figure 60 - Wall specimen PL1 lateral load versus displacement response

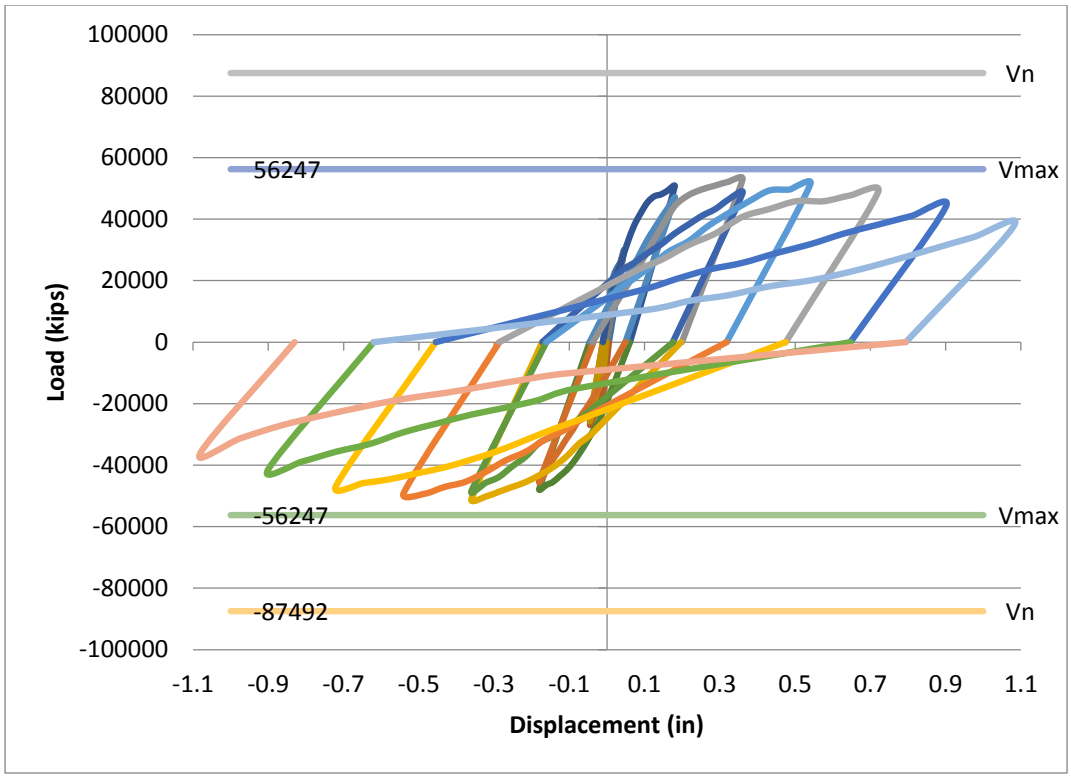

Figure 61 - Wall specimen F1 lateral load versus displacement response

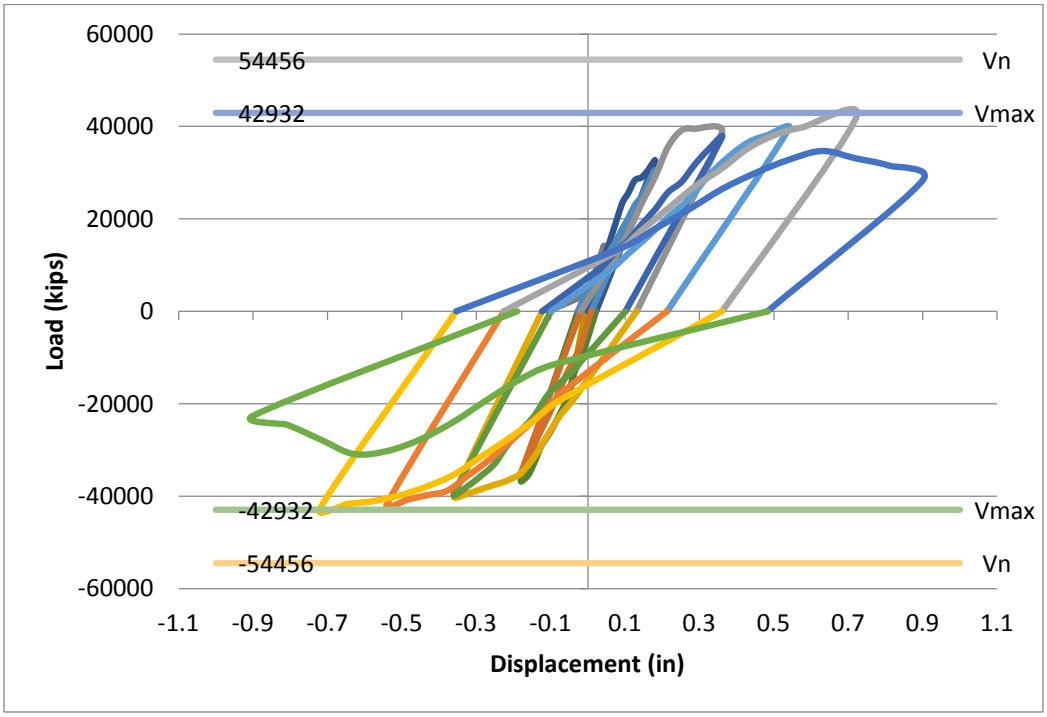

Figure 62 - Wall specimen 10C lateral load versus displacement response

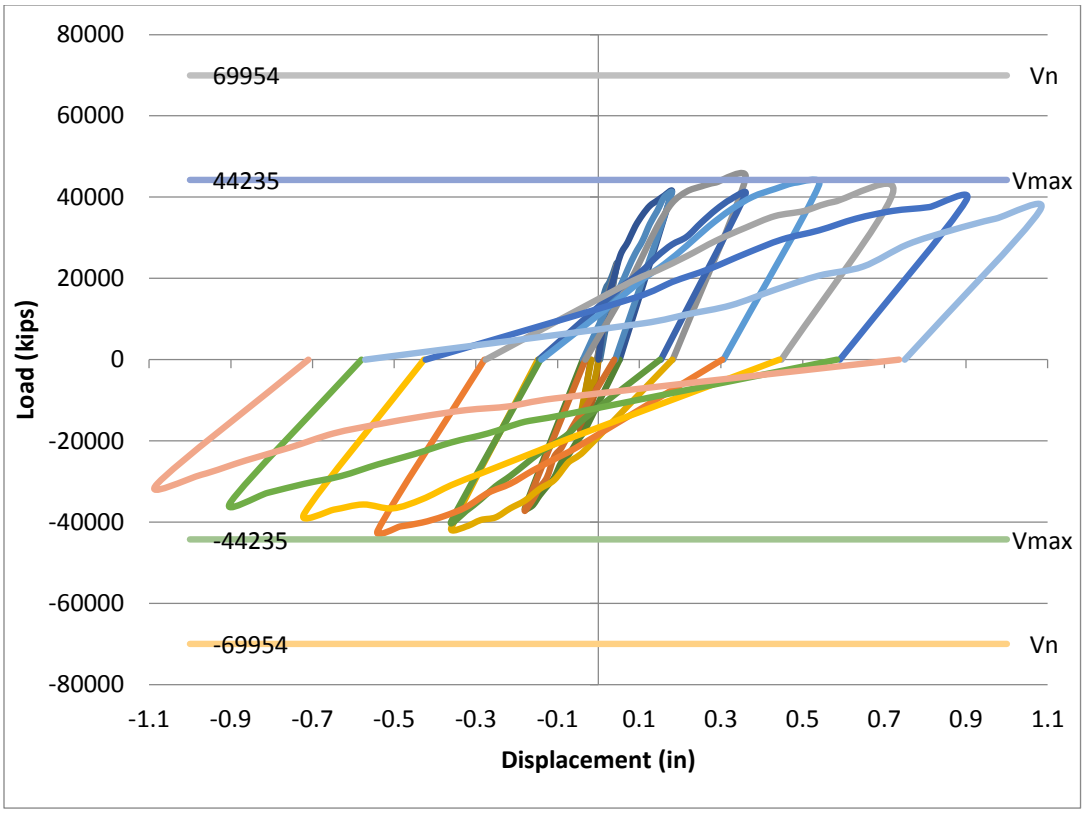

Figure 63 - Wall specimen F10C lateral load versus displacement response

Viewing the Figures 60-63, it can be noted that the predicted shear loads causing failure to the test specimens were close to the actual failure load each wall experienced. The predicted shear strengths of the walls were on average 2.7% higher the actual failure load. The comparison between actual and predicted load can be found in Table 11 and Figure 64.

Table 11 - Actual versus predicted load

Wall	Predict Load (kips)	Actual Load (kips)	Percent Difference
PL1	44.6	52.2	17.0%
F1	56.2	52.8	-6.1%
10C	42.9	42.6	-0.8%
F10C	44.2	44.6	0.8%
		Total	2.7%

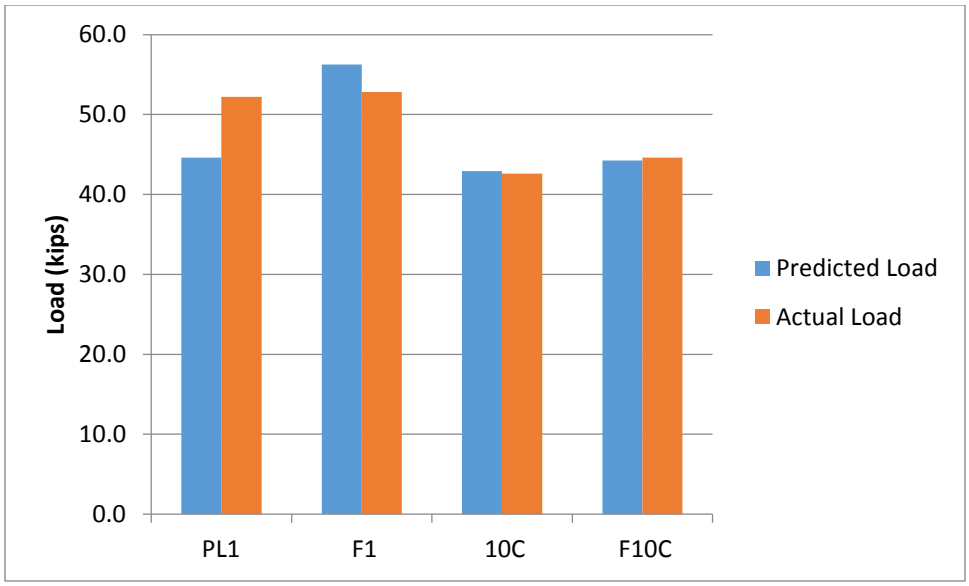

Figure 64 – Predicted load versus actual load for shear walls

It should be noted that the predicted load for wall specimen PL1 had the highest difference due to the reinforcement chosen. The expected compressive strength of the PL1 mix was 9261 psi. so more significant reinforcement was used. All test specimens were designed so that the predicted load capacity would be met before the nominal shear strength was reached. This ensured that a diagonal tension or compression failure would not occur although during the testing of the 10C wall specimen it failed due to a diagonal tension failure. The other three wall specimens failed in shear prior to reaching the flexural strength of the wall. The result of this was a sliding shear failure which occurs following reversed cyclic loadings causing flexural yielding of the vertical reinforcement decreasing the ability of the aggregate interlock and friction. When shear sliding begins it reduces the stiffness of the wall and energy dissipation. The load versus displacement plots also demonstrate pinching in the hysteresis loop for the majority of the testing of each wall except for test specimen 10C which experienced sudden failure due to a diagonal tension failure. Pinching is evident in the other three walls but is most apparent in the walls containing fibers because the fibers bridge

the cracks preventing them from widening and causing immediate failure. This is due to the large shear effect on low-rise specimens causing stiffness reduction in the walls for each cycle.

For test specimen PL1, yielding of the longitudinal boundary reinforcement beginning at the base appears to begin at 0.5% drift when pushing in both the positive and negative direction. The wall began to experience small deformations when the longitudinal boundary reinforcement yielded at these drifts. The deformations caused small residual initial displacements at the base of the wall for each subsequent cycle which ultimately factored into the recorded displacement at the top of the wall. A peak load of 52.2 kips in the positive direction and 49.3 kips in the negative direction occurred at a displacement of 0.720 in. The PL1 wall specimen was able to adequately sustain its loading (greater than 80% of peak load) up to a displacement of 0.9 in. in both the positive direction and negative direction. At this point it can be noted that the sliding displacement had contributed to 32.2% of the final displacement at failure. The percent contribution of sliding to final displacement at failure was calculated by dividing the displacement at failure by the sliding displacement at failure. This meant that at the conclusion of the test, the lateral displacement caused by the loading was significantly less than what was perceived.

For test specimen F1, yielding of the longitudinal boundary reinforcement beginning at the base appears to begin at 0.5% drift when pushing in both the positive and negative direction. The wall began to experience small deformations when the longitudinal boundary reinforcement yielded at these drifts. The deformations caused small residual initial displacements at the base of the wall for each subsequent cycle which ultimately factored into the recorded displacement at the top of the wall. A peak load of 52.8 kips in the positive

direction and 50.9 kips in the negative direction occurred at a displacement of 0.360 in. The F1 wall specimen was able to adequately sustain its loading (greater than 80% of peak load) up to a displacement of 0.9 in. in the positive direction and 0.72 in. in the negative direction. At this point it can be noted that the sliding failure had contributed to 36.6% of the final displacement at failure.

For test specimen 10C, yielding of the longitudinal boundary reinforcement beginning at the base appears to begin at 1% drift when pushing in both the positive and negative direction. The wall experienced further yielding of the boundary elements until failing at a displacement of 0.72 in. due to a diagonal tension failure. This type of failure caused an immediate reduction in the walls capacity, causing it to no longer adequately sustain its loading in both directions. The failure also caused an immediate reduction in stiffness. Because no significant sliding occurred, the lateral displacement output at the top of the wall could almost completely be contributed to the lateral loading. A peak load of 42.6 kips in the positive direction and 41.7 kips in the negative direction occurred at a displacement of 0.720 in. The 10C wall specimen was only able to adequately sustain its loading (greater than 80% of peak load) up to the same displacement it experienced peak load because of its sudden failure. This sudden failure was also observed in the shear beams that contained rubber.

For test specimen F10C, yielding of the longitudinal boundary reinforcement beginning at the base appears to begin at 0.5% drift when pushing in both the positive and negative direction. The wall began to experience small deformations when the longitudinal boundary reinforcement yielded at these drifts. The deformations caused small residual initial displacements at the base of the wall for each subsequent cycle which ultimately factored

into the recorded displacement at the top of the wall. A peak load of 44.6 kips at a displacement of 0.36 in. in the positive direction and 42.0 kips occurred at a displacement of 0.54 in. in the negative direction. The F10C wall specimen was able to adequately sustain its loading (greater than 80% of peak load) up to a displacement of 1.08 in. in the positive direction and 0.72 in. in the negative direction. At this point it can be noted that the sliding failure had contributed to 32.5% of the final displacement at failure.

4.3.4 Lateral Load Versus Drift Envelope

The load versus drift envelope plots for each wall specimen can be seen in Figures 65-68. Figure 69 shows the load versus drift envelope for all wall specimens. The plots illustrate a data point from each cycle representing the maximum drift and load during that cycle. Due to cycles 1 and 2, 3 and 4, and 5 and 6 repeating the same drift percentage, the first cycle for a given drift and the subsequent repeated cycle for the same drift are plotted separately. By plotting the repeated cycles separately, deformations causing capacity and stiffness loss can be observed. The values for the maximum load and drift percentage for all wall specimens can be seen in Tables 12-15. A plot illustrating the normalized shear stress envelope can be seen in Figure 70. The normalized shear stresses were found by dividing the load by the square root of each mixes compressive strength times the width and length of the wall.

Table 12 - Wall specimen PL1 maximum load and drift percentage

Cycle	Load (kips)	Drift %
0	0	0
1L	22.0	0.125%
1R	-18.8	-0.125%
2L	22.9	0.125%
2R	-15.6	-0.125%
3L	47.7	0.500%
3R	-36.9	-0.500%
4L	46.7	0.500%
4R	-40.4	-0.500%
5L	51.2	1.000%
5R	-46.7	-1.000%
6L	48.3	1.000%
6R	-45.8	-1.000%
7L	51.9	1.500%
7R	-48.7	-1.500%
8L	52.2	2.000%
8R	-49.3	-2.000%
9L	47.7	2.500%
9R	-44.9	-2.500%
10L	34.4	3.000%
10R	0.0	-3.000%

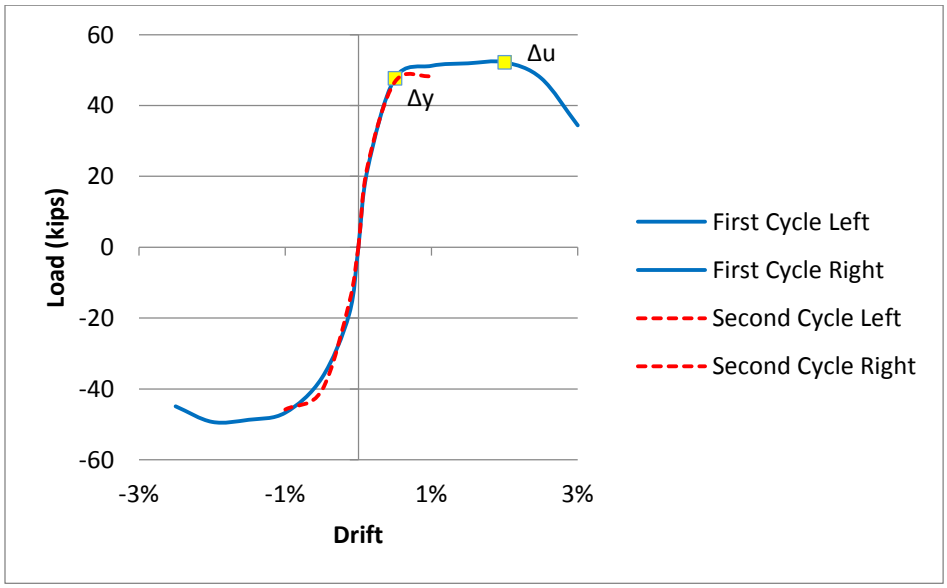

Figure 65 - Wall specimen PL1 lateral load versus drift envelope

Table 13 - Wall specimen F1 maximum load and drift percentage

Cycle	Load (kips)	Drift %
0	0	0
1L	29.6	0.125%
1R	-26.7	-0.125%
2L	29.3	0.125%
2R	-25.1	-0.125%
3L	50.6	0.500%
3R	-47.7	-0.500%
4L	46.8	0.500%
4R	-45.2	-0.500%
5L	52.8	1.000%
5R	-50.9	-1.000%
6L	48.4	1.000%
6R	-48.4	-1.000%
7L	51.2	1.500%
7R	-49.0	-1.500%
8L	48.7	2.000%
8R	-46.8	-2.000%
9L	43.9	2.500%
9R	-41.4	-2.500%
10L	37.6	3.000%
10R	-36.0	-3.000%

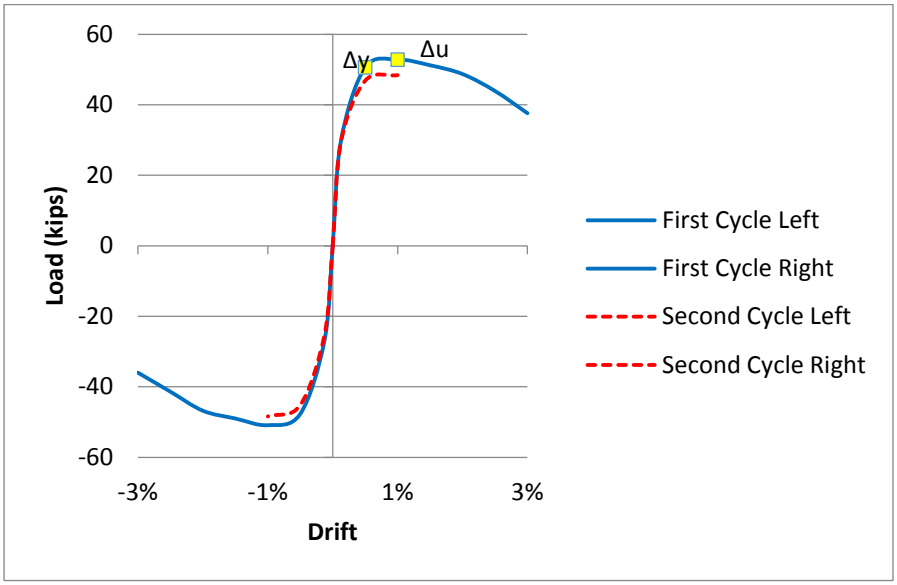

Figure 66 - Wall specimen F1 lateral load versus drift envelope

Table 14 - Wall specimen 10C maximum load and drift percentage

Cycle	Load (kips)	Drift %
0	0	0
1L	17.2	0.125%
1R	-19.4	-0.125%
2L	14.0	0.125%
2R	-16.2	-0.125%
3L	32.5	0.500%
3R	-36.6	-0.500%
4L	30.6	0.500%
4R	-35.0	-0.500%
5L	38.5	1.000%
5R	-39.8	-1.000%
6L	37.6	1.000%
6R	-39.5	-1.000%
7L	39.5	1.500%
7R	-41.7	-1.500%
8L	41.7	2.000%
8R	-42.6	-2.000%
9L	28.3	2.500%
9R	-22.6	-2.500%
10L		3.000%
10R		-3.000%

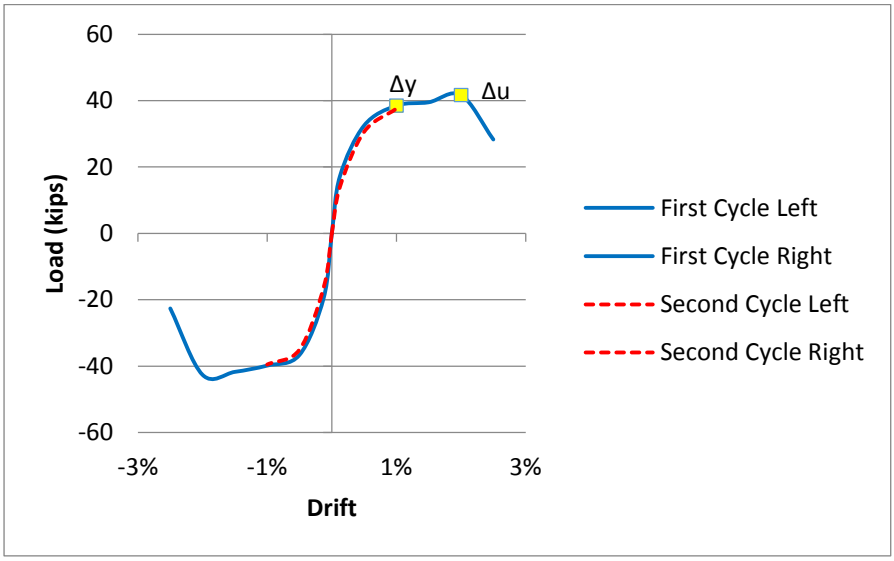

Figure 67 - Wall specimen 10C lateral load versus drift envelope

Table 15 - Wall specimen F10C maximum load and drift percentage

Cycle	Load (kips)	Drift %
0	0	0
1L	23.6	0.125%
1R	-17.2	-0.125%
2L	23.2	0.125%
2R	-14.3	-0.125%
3L	41.4	0.500%
3R	-36.6	-0.500%
4L	41.1	0.500%
4R	-36.9	-0.500%
5L	44.6	1.000%
5R	-41.4	-1.000%
6L	40.7	1.000%
6R	-39.8	-1.000%
7L	43.0	1.500%
7R	-42.0	-1.500%
8L	40.7	2.000%
8R	-37.9	-2.000%
9L	39.1	2.500%
9R	-35.0	-2.500%
10L	36.6	3.000%
10R	-30.6	-3.000%

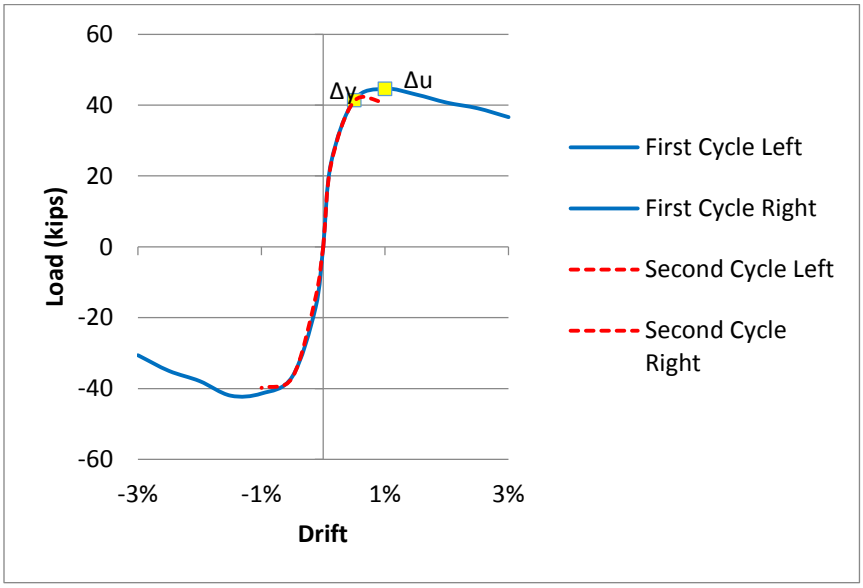

Figure 68 - Wall specimen F10C lateral load versus drift envelope

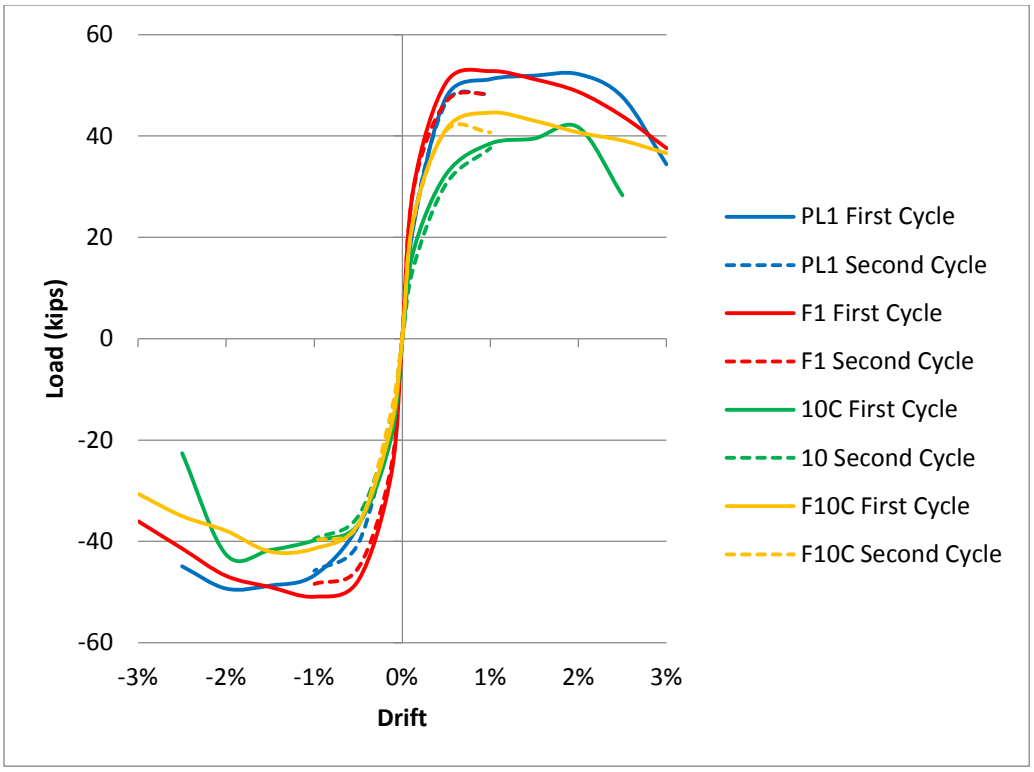

Figure 69 - All wall specimens lateral load versus drift envelope

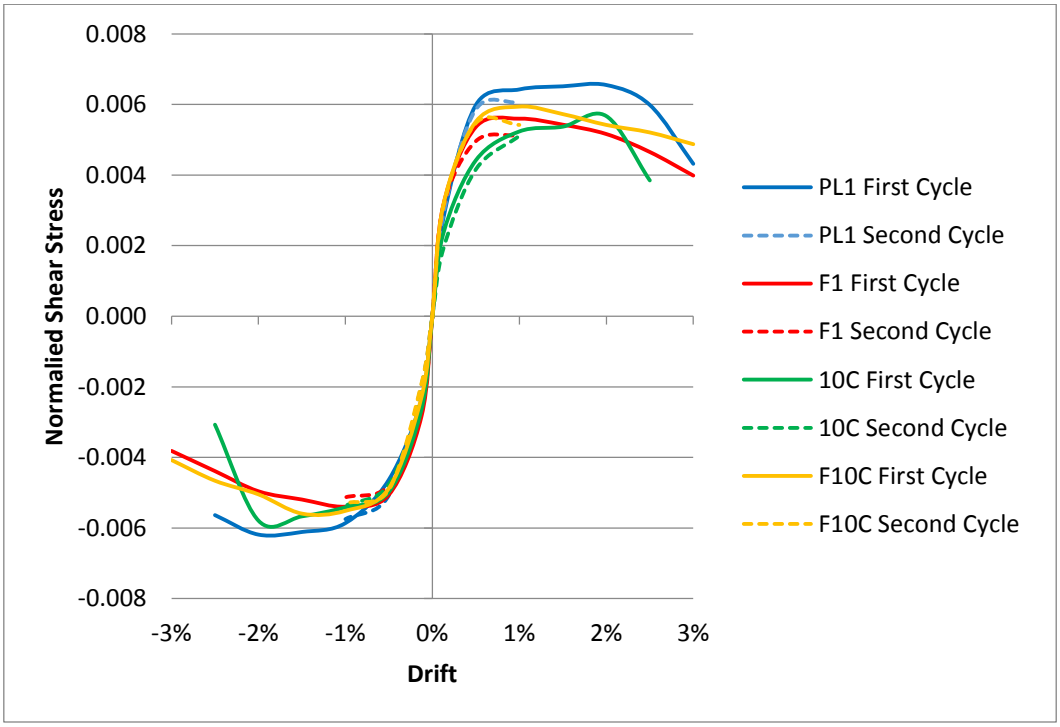

Figure 70 - All wall specimens normalized shear stress envelope

All of the specimens showed similar load versus drift envelopes in the stages approaching failure. When the sliding failures occur for test specimens PL1, F1, and F10C the load outputs remain steady or decrease slightly over a few cycles. When test specimen 10C fails due to a diagonal tension failure the load capacity immediately decreases as shown in Figure 67. This behavior also occurred in the beams with rubber present and no fibers. It can also be noted from the figures that when the second cycle occurs it never exceeds the load at that drift of the first cycle due to deformations and stiffness loss caused by the first cycle. The only time the second cycle carries a larger load than the first is in specimen PL1. This is because the boundary reinforcement did not yield in the negative direction until after the reinforcement had yielded in the positive direction. Looking at Figure 70, it can be noted that the normalized shear stresses were the largest in the plain mix. The addition of both fibers and rubber decreased shear stresses

4.3.5 Shear Strain

The shear strains for each wall specimen were calculated using Section 4.3.1.3. The average shear strains and normalized average shear strains at each drift percentage for all of the wall specimens are plotted in Figure 71 and 72. The average shear strains were normalized with respect to the wall's compressive strength. Similar shear strains were experienced prior to 1% drift. After 1% drift, wall specimen PL1 remained linear until failure and the shear strain increased at a higher rate than the rest of the walls. Specimens F1, 10C, and F10C all experienced similar shear strains throughout the duration of testing. Ultimately, the shear strain values explain the change in the shape of the wall. Wall specimen PL1 experience the most change in shape while the other three walls experienced relatively the same changes in shape.

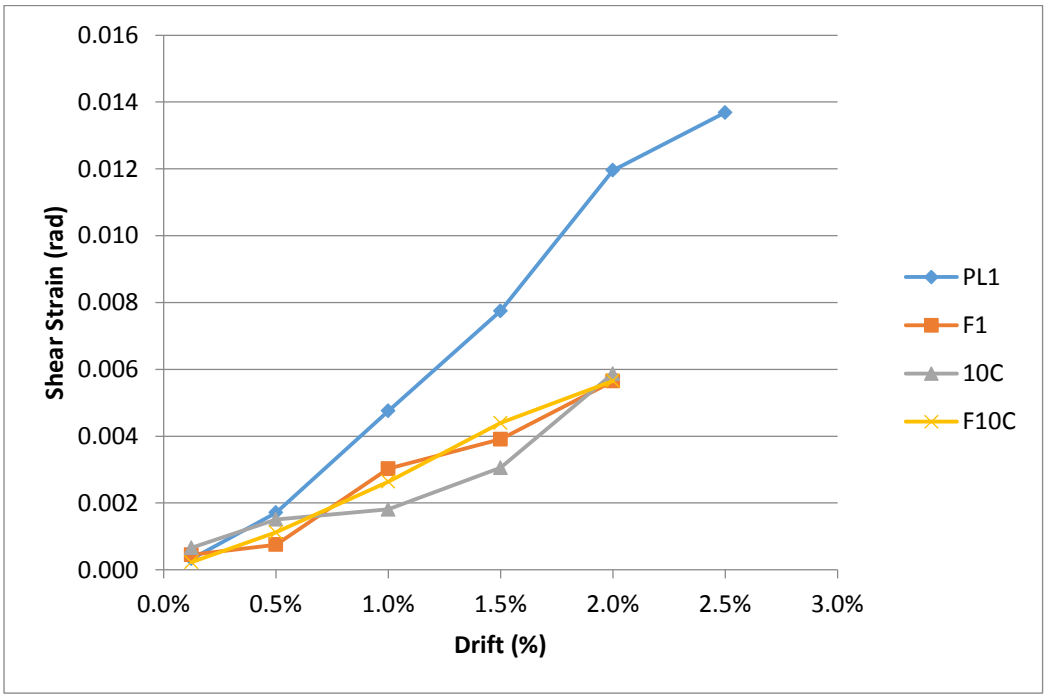

Figure 71 - Average shear strains of all wall specimens

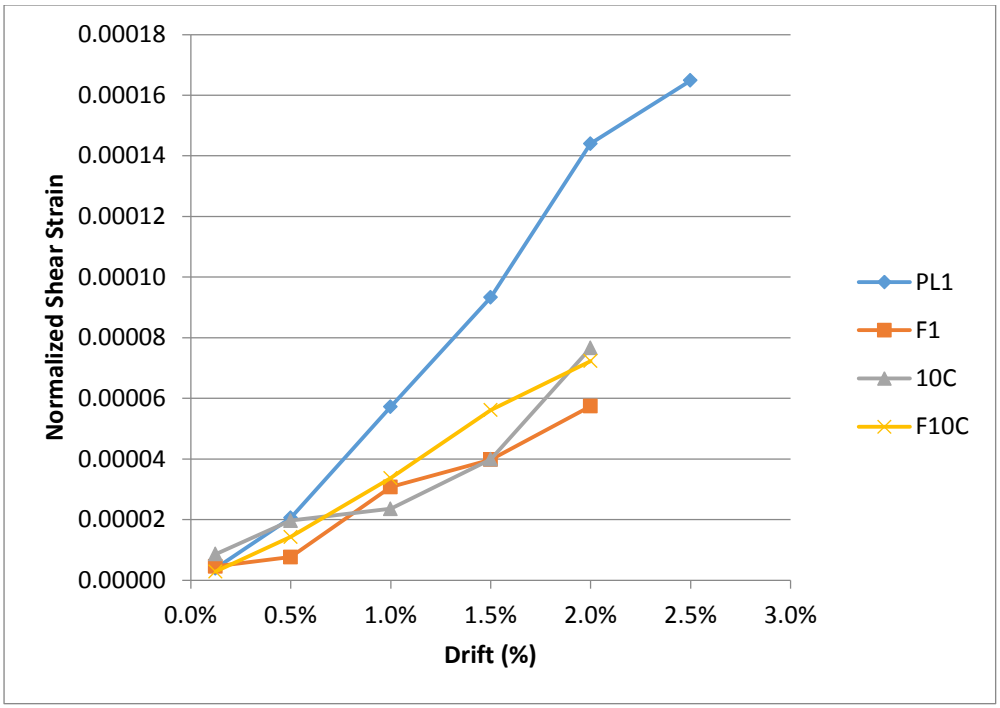

Figure 72 – Normalized average shear strains of all wall specimens

4.3.6 Sliding Shear Response

The sliding that occurred at the base of the wall and foundation intersection was collected by potentiometer P8. The plots of the lateral loads versus horizontal sliding displacement can be found in Figures 73-76. The plots of the average sliding displacement and normalized average sliding displacement versus drift can be found in Figures 77 and 78. The average sliding displacements were normalized with respect to the wall's compressive strength. Test specimens PL1, F1, and F10C all experienced significant sliding behavior during their testing. In all specimens slip began to occur first in the positive direction. Yielding deformations in the boundary reinforcement, which began to occur at 0.5%, accounted for the minor initial slip displacement values during each subsequent cycle. As each cycle occurred, more and more deformations formed thus increasing the initial residual slip displacement. Significant slip was taken as a slip displacement of greater than .05 in

(Athanasopoulou, 2010). Significant slip first occurred at 1.5% for specimen PL1, 1.0% for specimen F1, and 1.5% for specimen F10C. By the time PL1, F1, and F10C had been considered failures, slip displacement had contributed to the overall lateral displacement by 32.2%, 36.6%, and 32.5% respectively. Each plot, up until failure, is similar in shape and symmetry. This is due to the deformations caused by similar loads at similar drifts for each loading direction. PL1, F1, and F10C also all exhibited pinching which is shown again in the hysteresis loops for the load versus slip plots. It is also important to note that the rate at which sliding occurred and contributed to the overall wall displacement increased steadily for all three walls that experienced sliding.

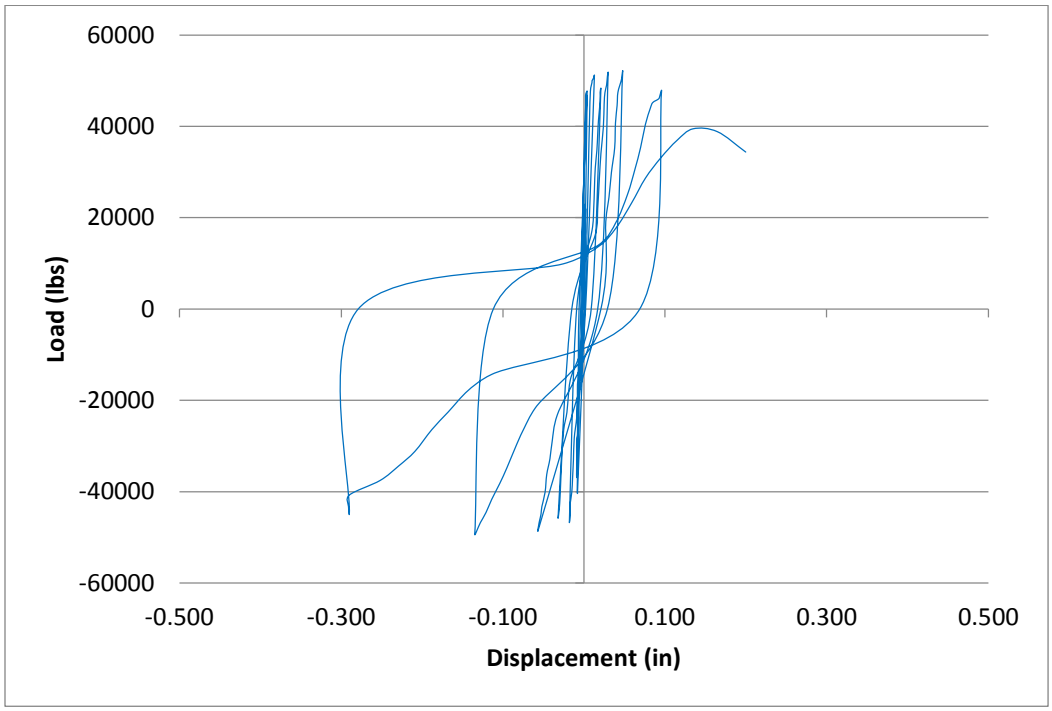

Figure 73 - Wall specimen PL1 sliding shear

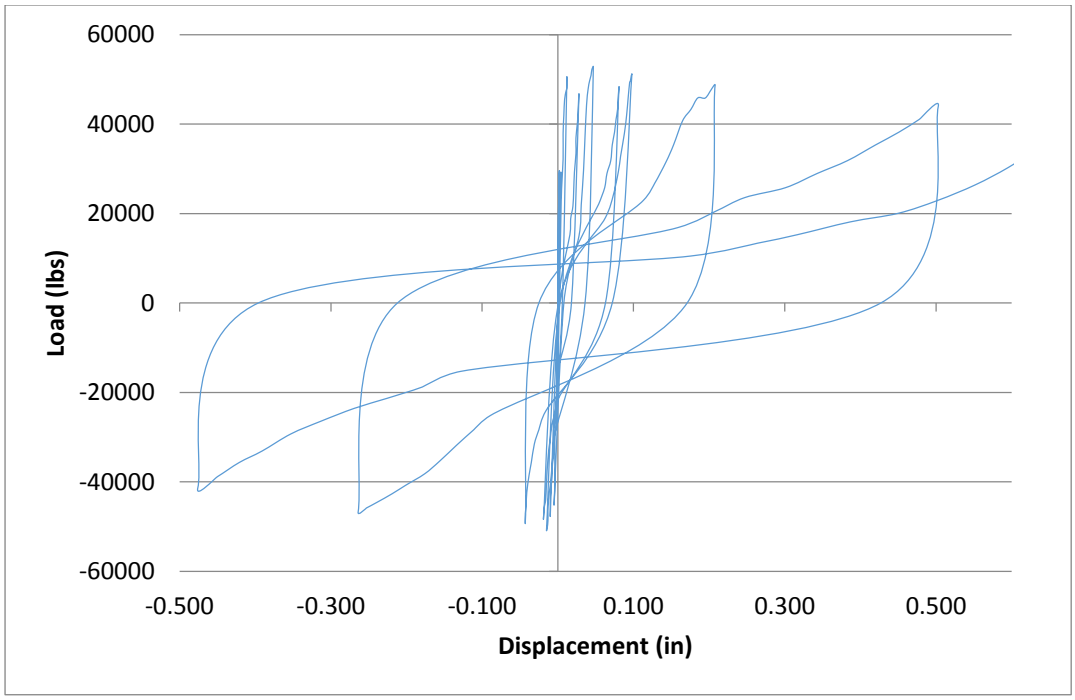

Figure 74 - Wall specimen F1 sliding shear

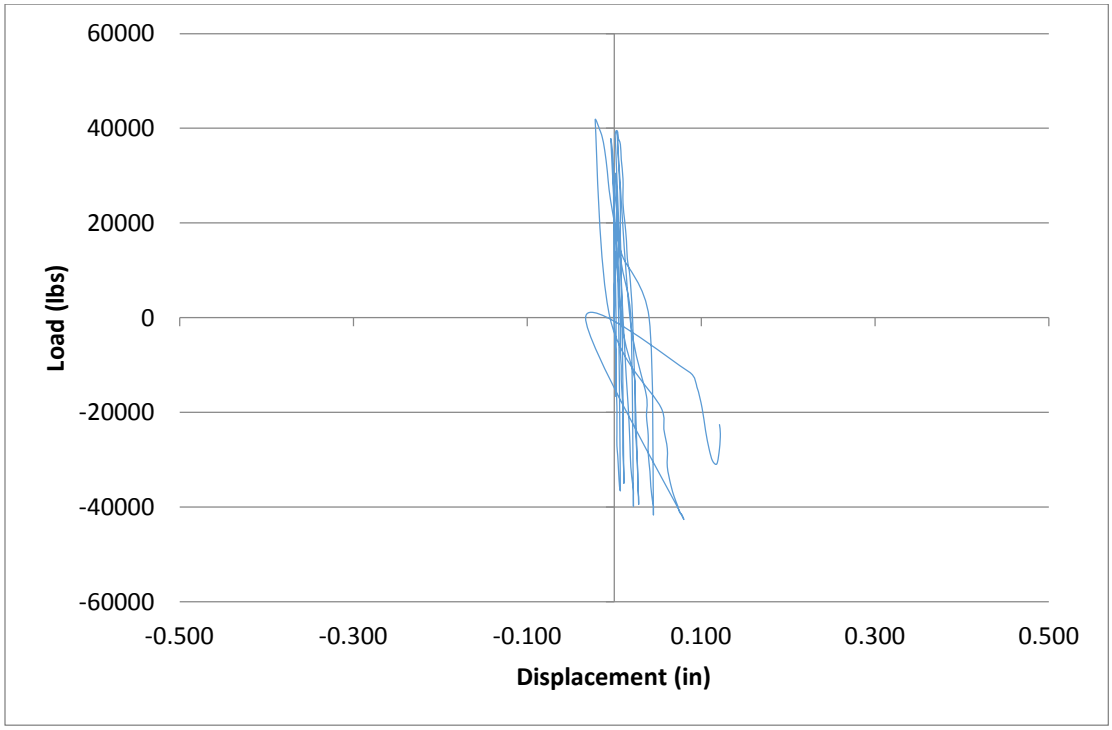

Figure 75 - Wall specimen 10C sliding shear

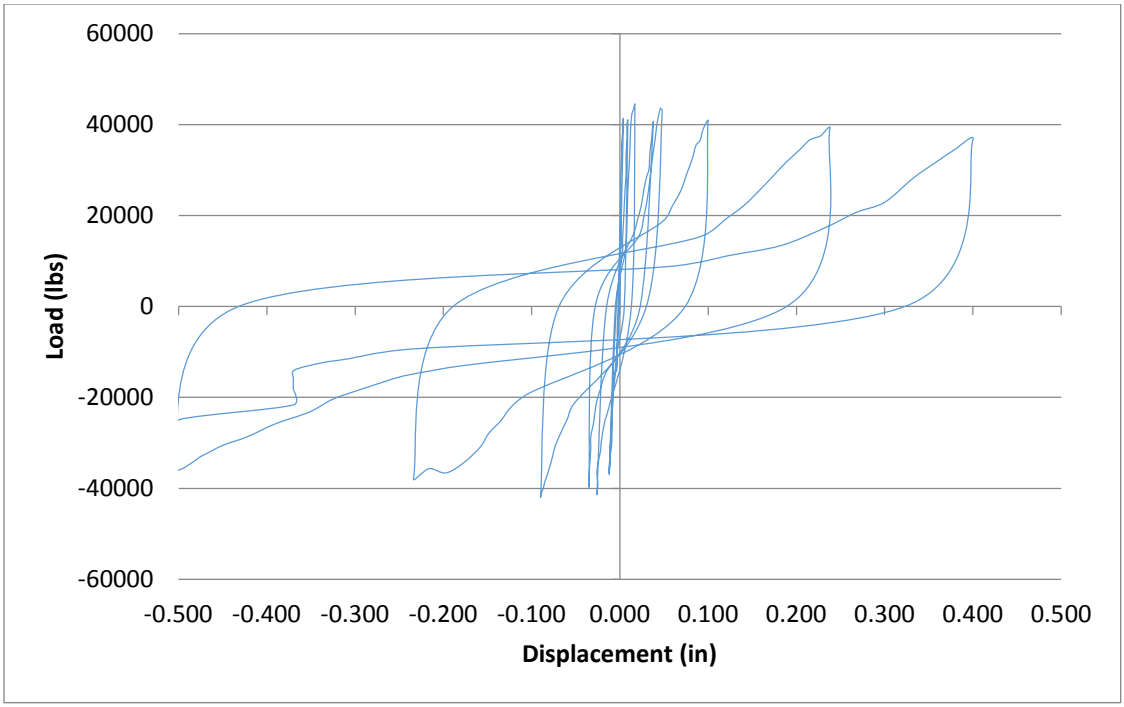

Figure 76 - Wall specimen F10C sliding shear

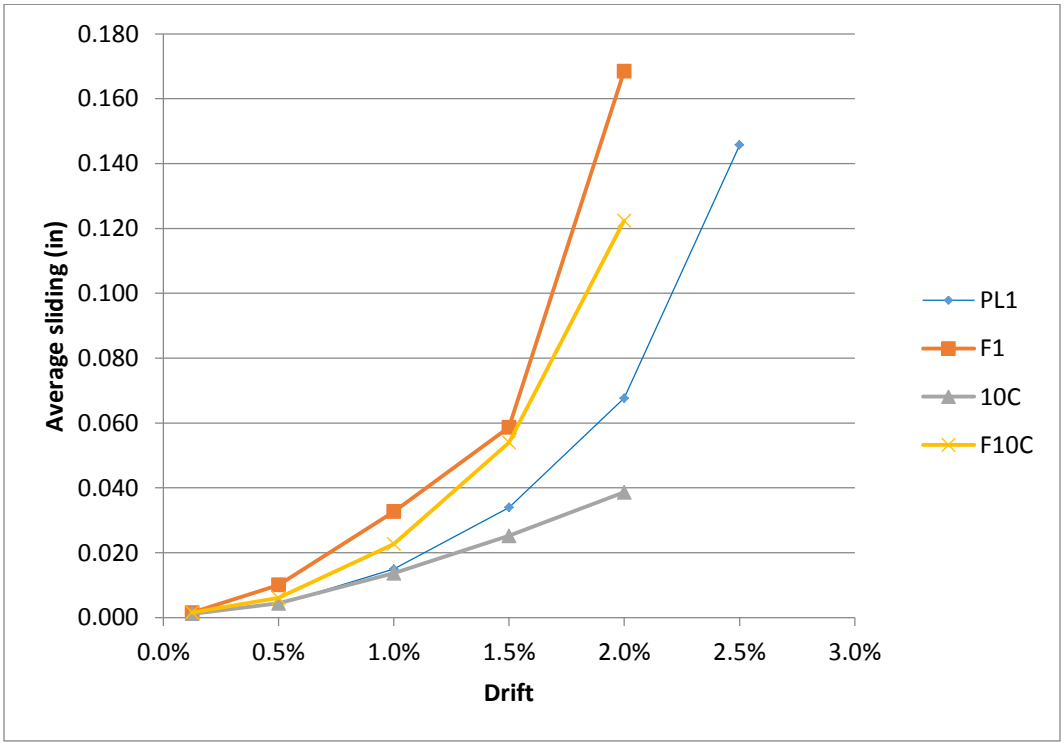

Figure 77 - All wall specimens average sliding shear

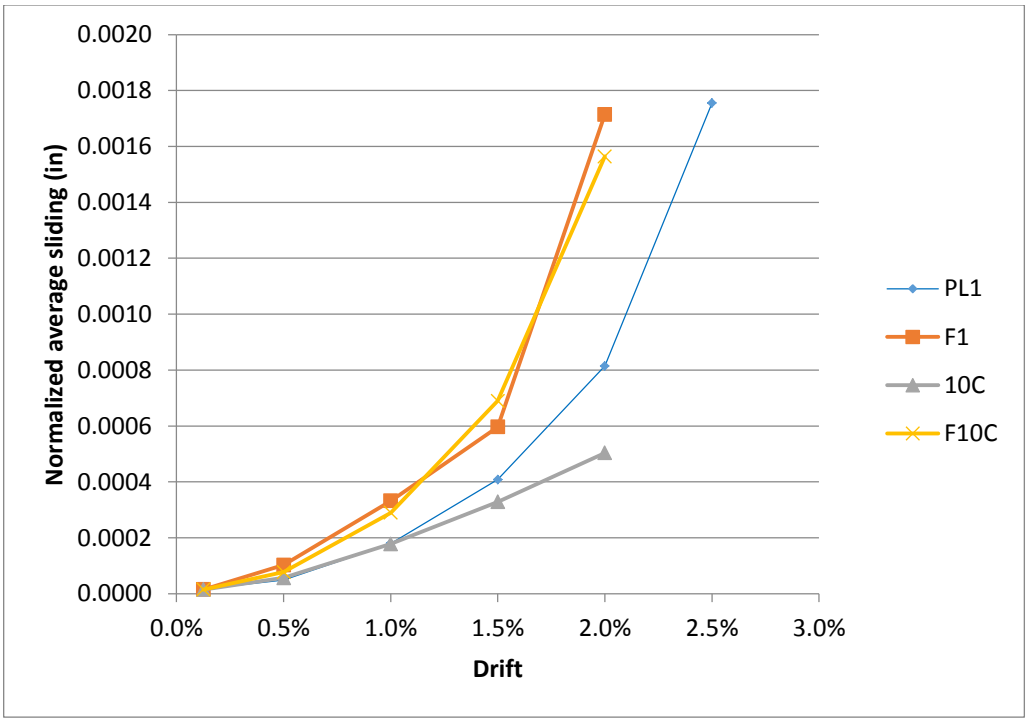

Figure 78 - All wall specimens normalized average sliding shear

4.3.7 Wall Dilations

The wall dilations that occurred at the bottom and top of the face of the wall were collected by potentiometers P4 and P5. Potentiometer P4 was placed 3.75 in. from the base of the wall, and potentiometer P5 was placed 23.75 in. from the base of the wall. The wall dilations were subsequently taken from these two heights on the walls. The top and bottom wall dilations described how much the wall expanded and contracted at each given height. The dilations were mostly dependent on the size and amount of cracks. The plots of the lateral loads versus the dilations of each wall at each height can be found in Figures 79-82. The average dilations and normalized average dilations can be found in Figures 83 and 84. The dilations were normalized with respect to the wall's compressive strength.

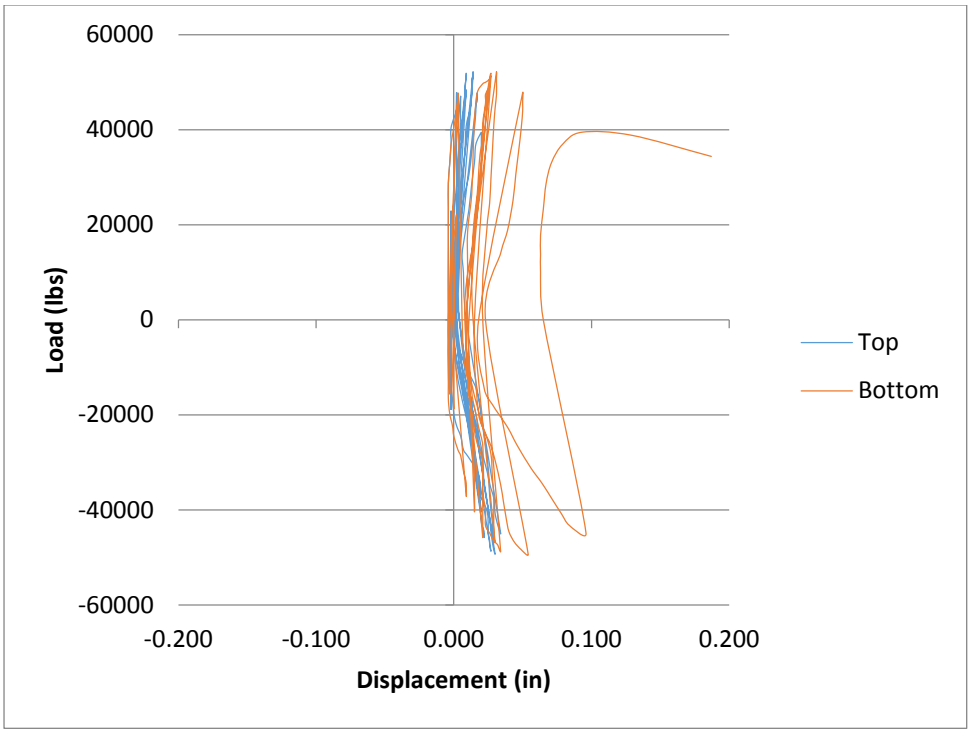

Figure 79 - Wall specimen PL1 Wall Dilations

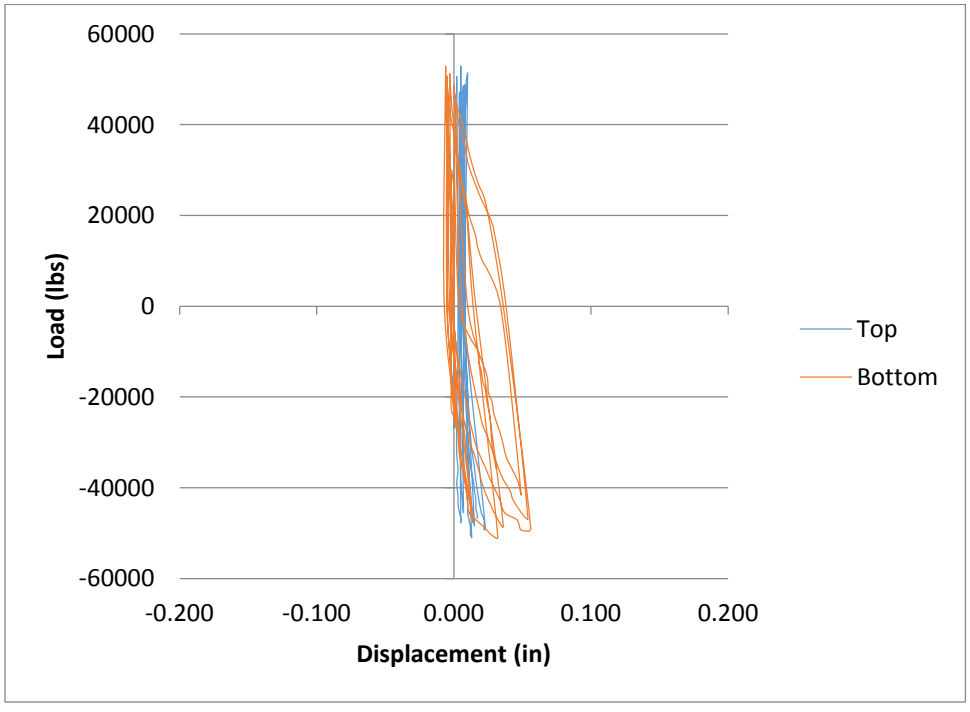

Figure 80 - Wall specimen F1 Wall Dilations

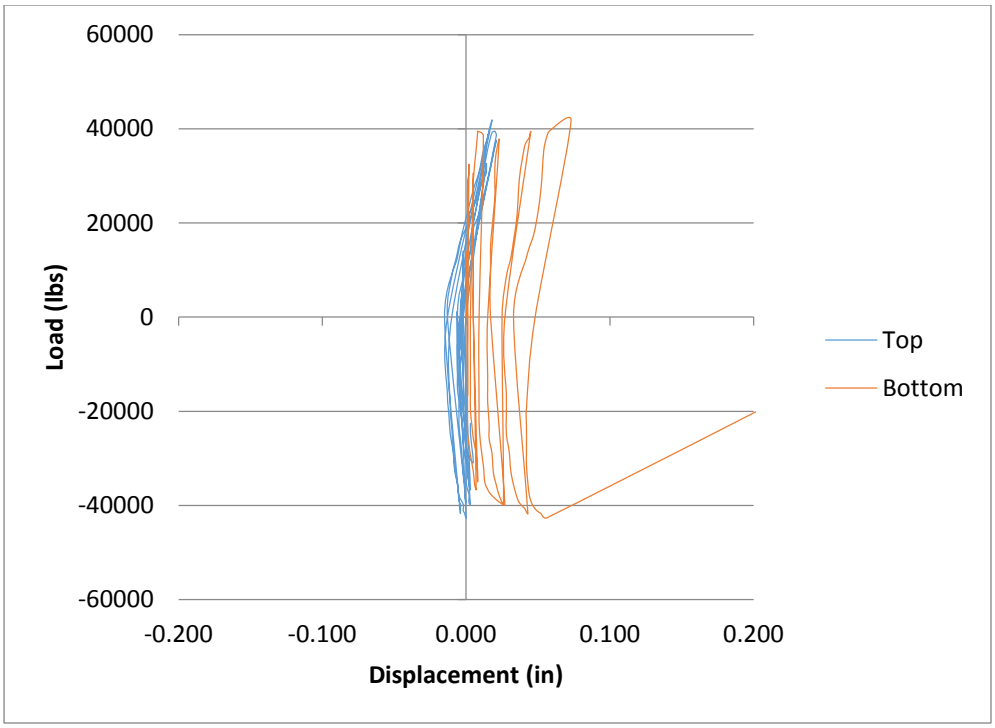

Figure 81 - Wall specimen 10C Wall Dilations

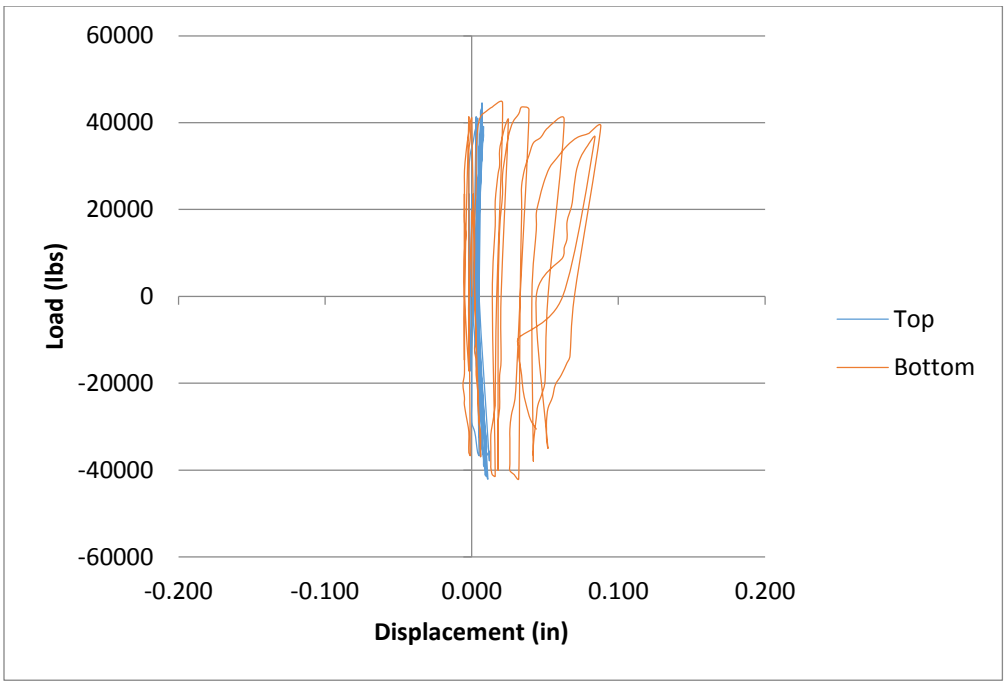

Figure 82 - Wall specimen F10C Wall Dilations

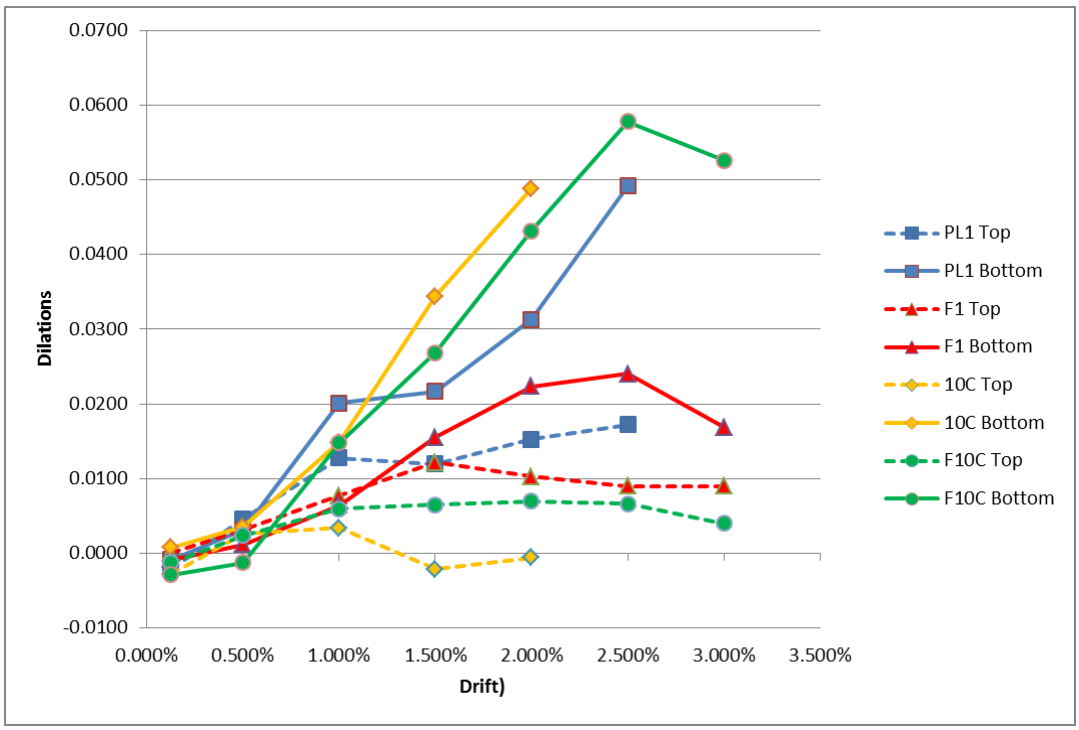

Figure 83 - All wall specimens average wall dilations

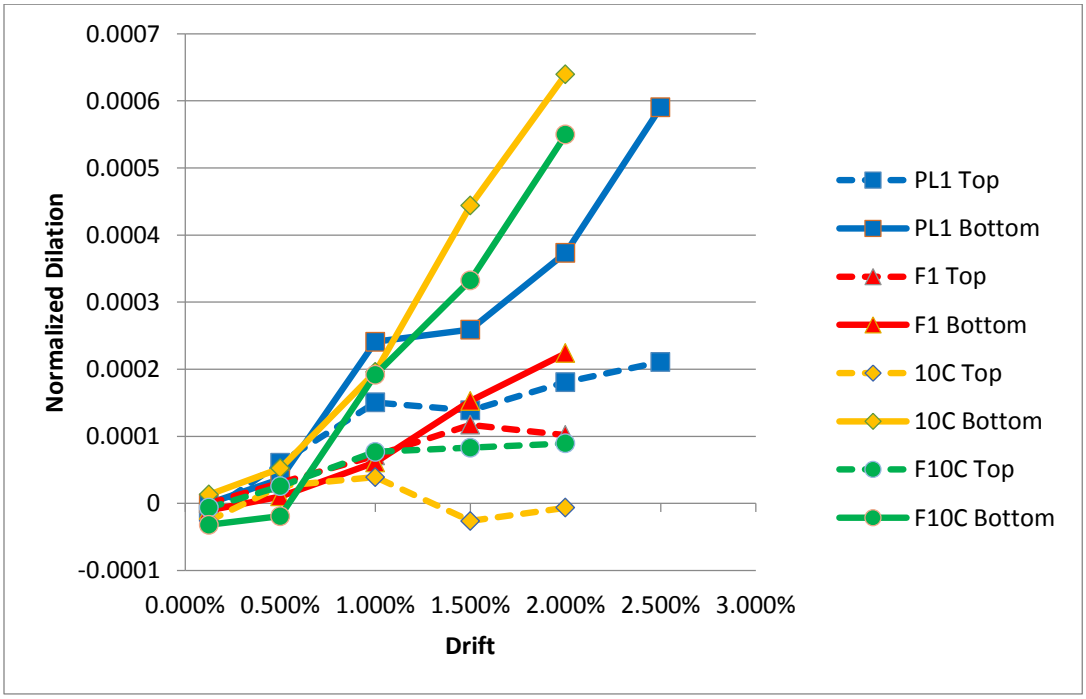

Figure 84 - All wall specimens normalized average wall dilations

The dilations in the bottom of the wall were significantly larger than the top of the wall. This is consistent with the damage progression of each wall where the majority of the damage and cracks occurred towards the bottom of the wall. This allowed for larger dilations in the bottom of the wall for each cycle. The dilations in the bottom of the wall were on average three and a half times larger than the top of the wall during the cycle in which the wall failed. It can also be noted for wall specimen F10C that the cracks causing the dilations tended to remain the same in between cycles. This means that the crack widths did not close when the load was reversed and only grew larger with each subsequent cycle. When the load was dissipated in between cycles for wall specimens PL1 and 10C the cracks closing caused an inward pinch in the plot when the lateral load was zero. This may be due to the fibers bridging the cracks. When the fibers bridge the cracks it provides a resistance to the crack closing when the load is disengaged. Although the micro-cracks found in the walls with fibers were small, these cracks were unable to close back in between cycles. There were also significantly more cracks found on the fiber walls. Overall the walls containing rubber increased dilations and the walls containing fibers decreased dilations. Each wall ultimately exhibited expected dilations in accordance to the damage and cracks observed for each test specimen.

4.3.8 Rotations

The flexural rotation at the base of the walls can be obtained using the data measured by potentiometers P6 and P7 on the sides of the walls. The lateral load versus concentrated rotations at the base of the walls plots are shown in Figures 85-88. Figure 89 and 90 plots all of the walls average rotations and normalized average rotations at each drift cycle. The average rotations were normalized with respect to the wall's compressive strength. It can be

noted looking at the damage progression for a given lateral load that the concentrated rotation correlates with the amount and size of the cracks located on the tension face of the wall. In the cycles preceding failure where concrete crushing and spalling occurs at the boundary elements, the potentiometer readings became inconsistent due to the bond between the potentiometer and wall being compromised. Data that was believed to have been compromised due to this was subsequently omitted. Rotations for all wall specimens were linear as the drift increased. The rotation for each wall specimen increased as would be expected for each drift cycle. Prior to yielding, wall specimen F1 experienced a slightly larger base rotation. Wall specimen F1 had also recorded the highest rotations at failure. Looking at the normalized rotations it can be noted that the PL1 wall had slightly larger rotations throughout the test. In general, walls that contained fibers tended to experience larger rotations prior to yielding in comparison to walls with the same reinforcement and no rubber. This is consistent with walls containing fibers losing the most stiffness in the early drift cycles. Wall specimens containing rubber experienced the smallest overall rotations.

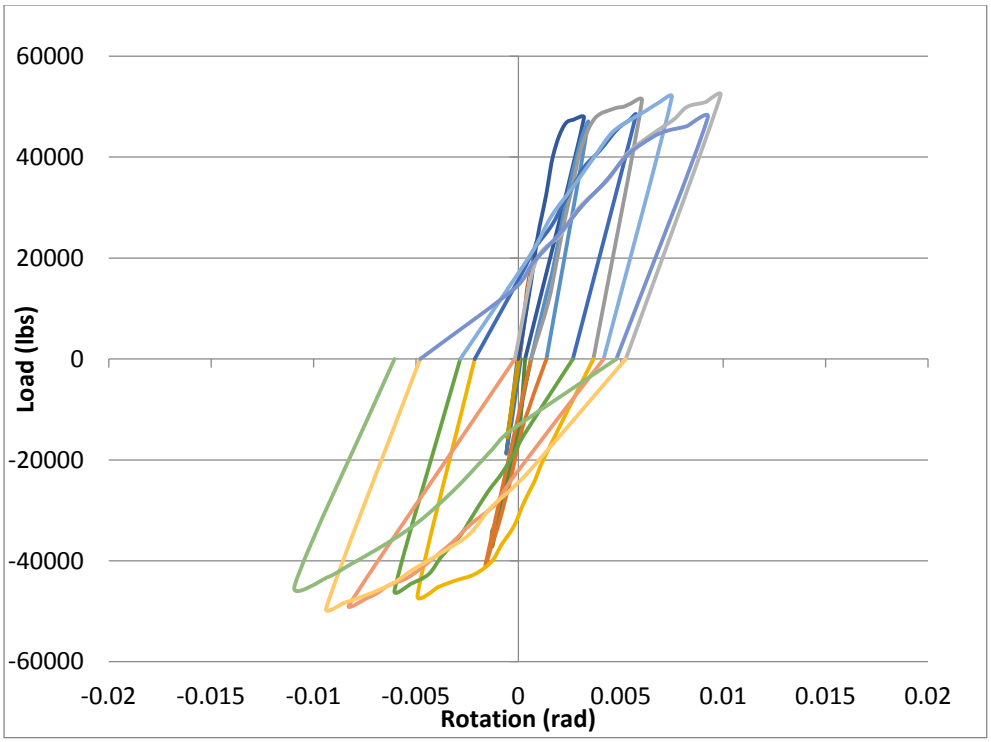

Figure 85 - Wall specimen PL1 rotations

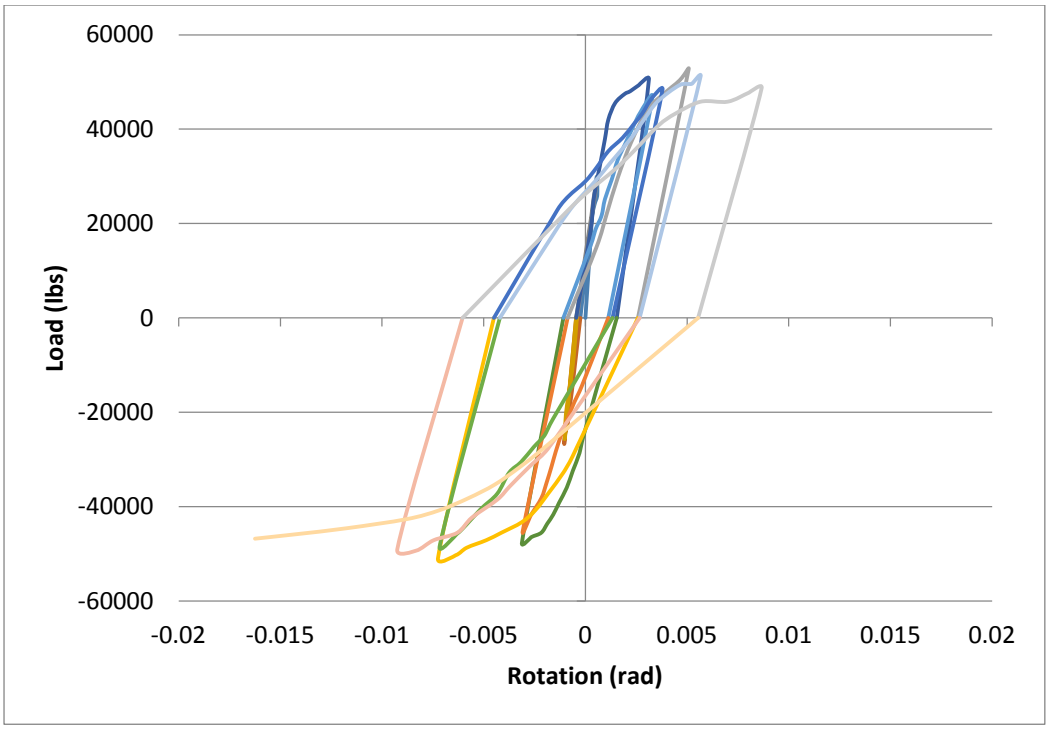

Figure 86 - Wall specimen F1 rotations

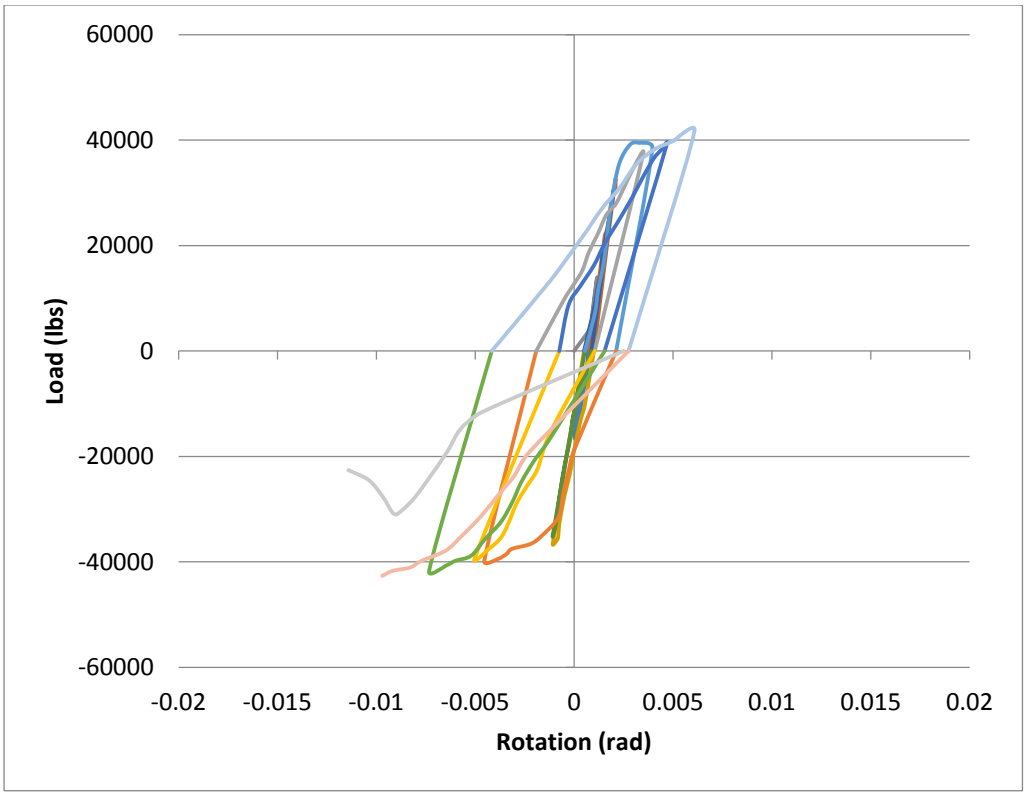

Figure 87 - Wall specimen 10C rotations

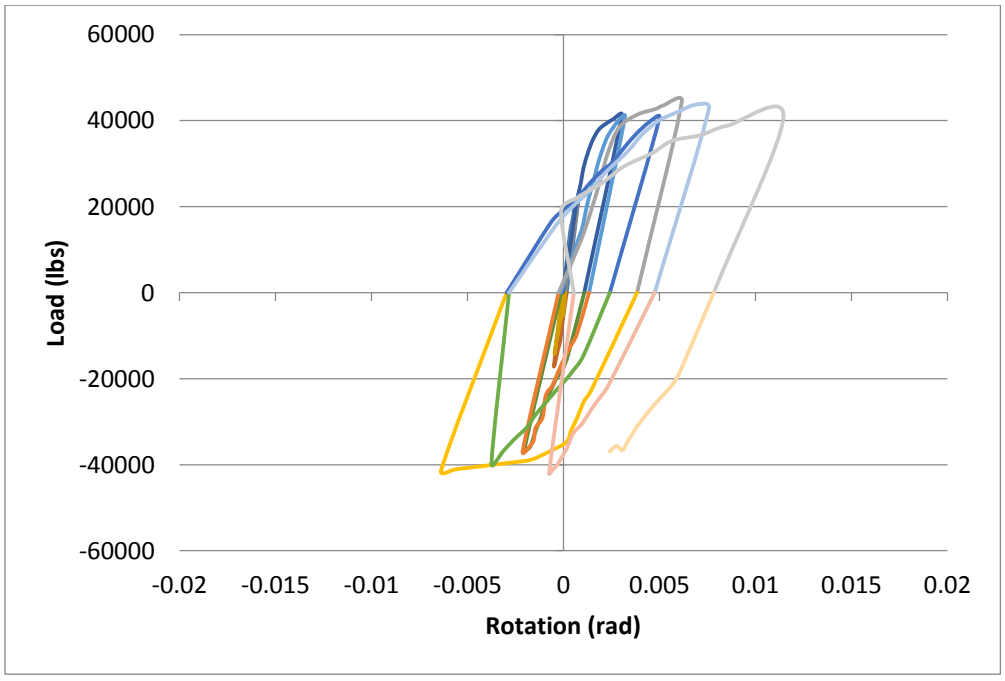

Figure 88 - Wall specimen F10C rotations

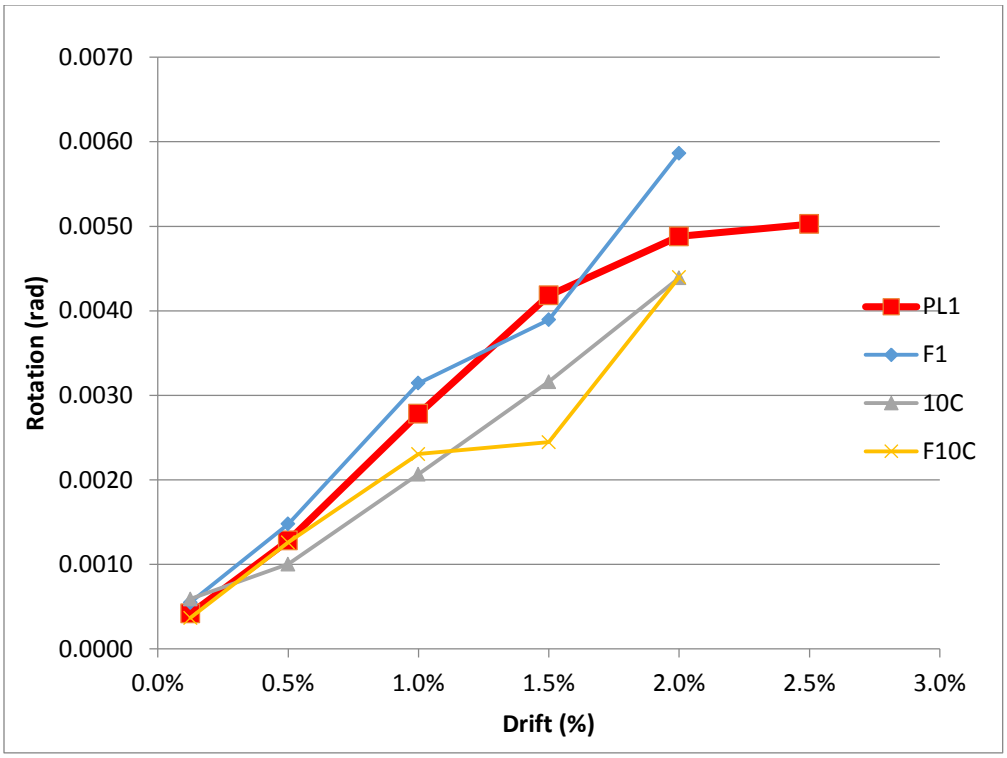

Figure 89 – Average rotation versus drift for all walls

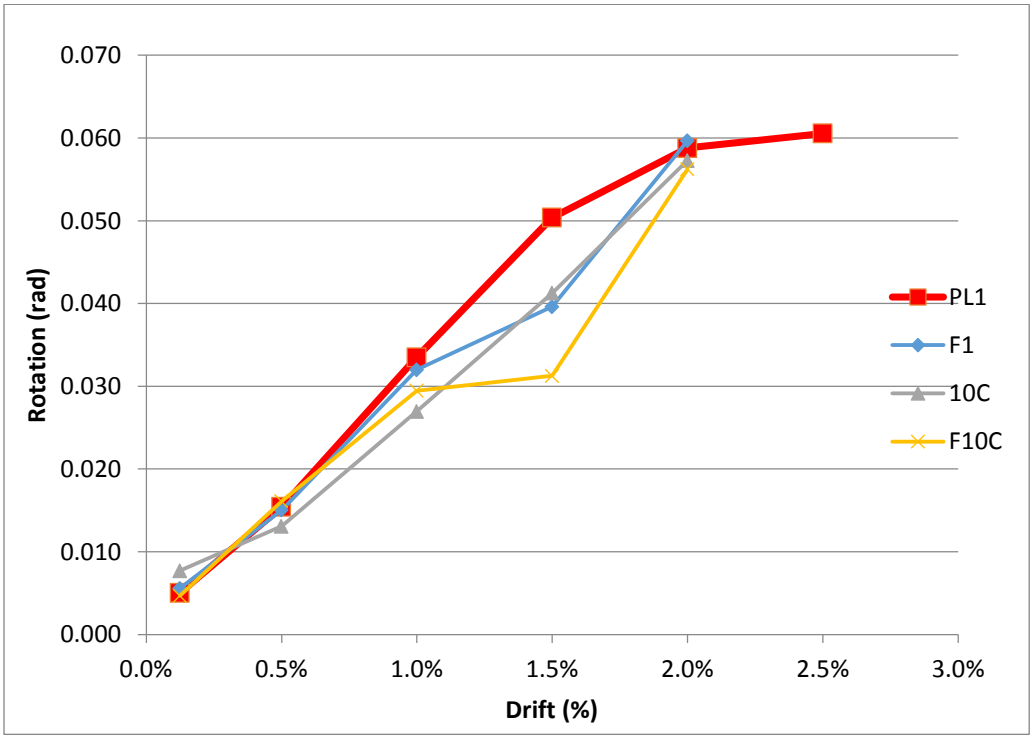

Figure 90 – Normalized average rotation versus drift for all walls

4.3.9 Stiffness Retention Capacity

The stiffness values of each wall specimen at a given cycle are the maximum load at that cycle divided by the displacement. The peak stiffness value for each wall specimen and the average stiffness for the first drift cycle can be found in Table 16 and Figure 91. A comparison of the stiffness values at each drift cycle to the original drift cycles average stiffness shows the percent loss in stiffness at each cycle. It can be noted that the stiffness of each wall decreased with an increase in drift but the rate at which the stiffness decreased was slightly different for each wall specimen. Plots illustrating the stiffness values with respect to the max stiffness for each wall versus drift for each cycle can be found in Figures 92-95. A plot comparing the average stiffness values with respect to the average first drift stiffness for each wall versus drift can be found in Figure 96. Two plots charted the average stiffness and normalized average stiffness versus drift in Figures 97 and 98.

Table 16 - Peak and Average First Drift Stiffness

Wall	Peak Stiffness (kip/in)	Average First Drift Stiffness (kip/in)
PL1	509	441
F1	658	615
10C	431	371
F10C	524	435

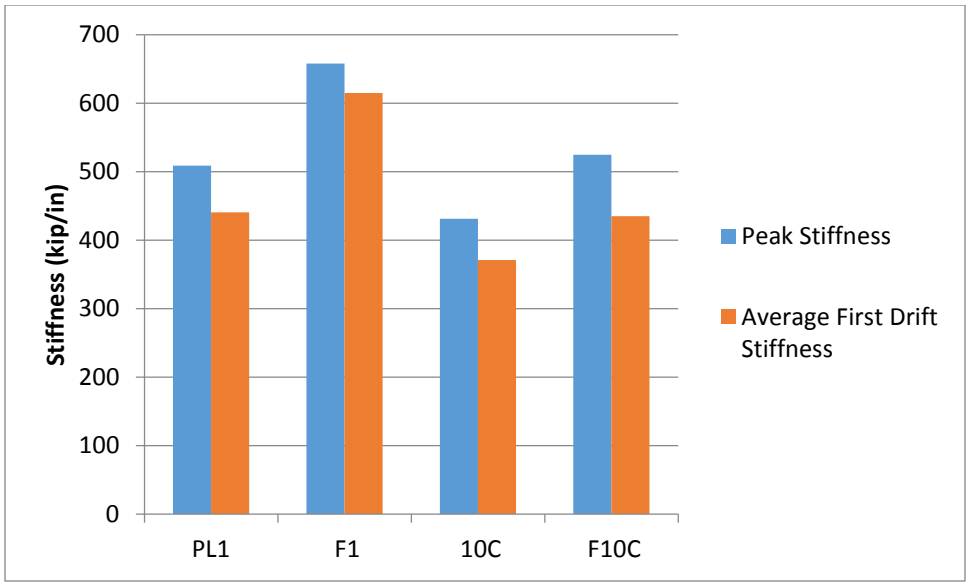

Figure 91 - Peak stiffness and average first drift stiffness for wall specimens

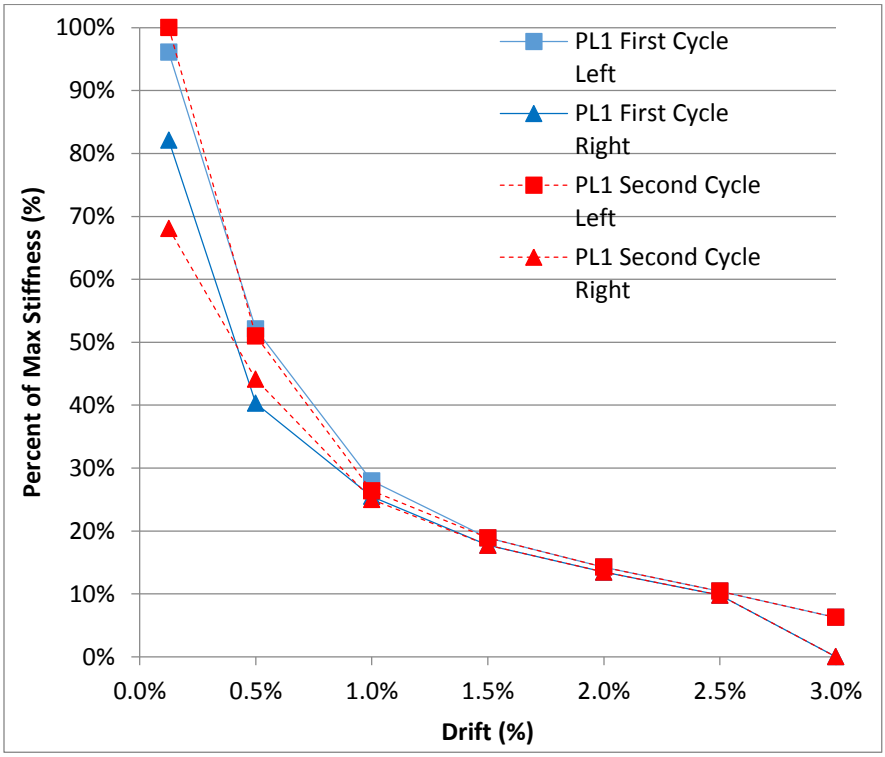

Figure 92 - Wall specimen PL1 stiffness versus drift

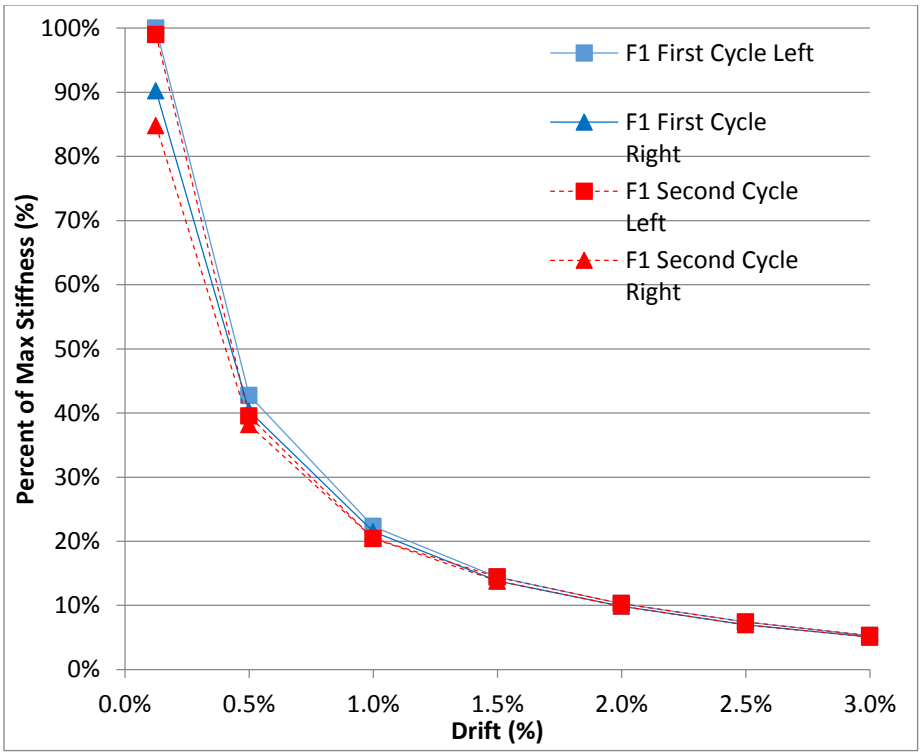

Figure 93 - Wall specimen F1 stiffness versus drift

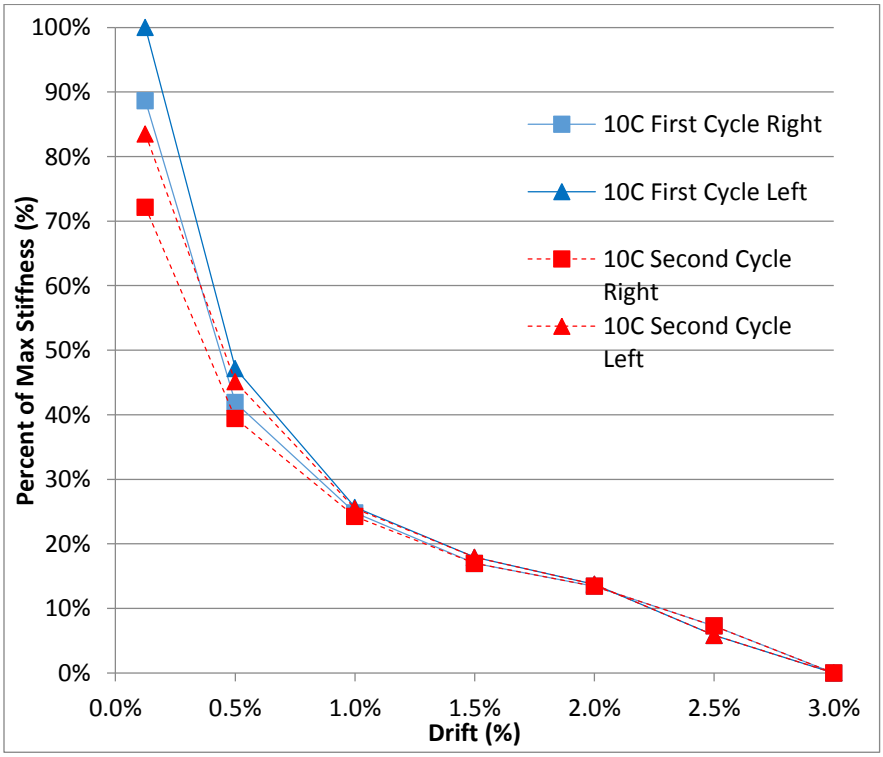

Figure 94 - Wall specimen 10C stiffness versus drift

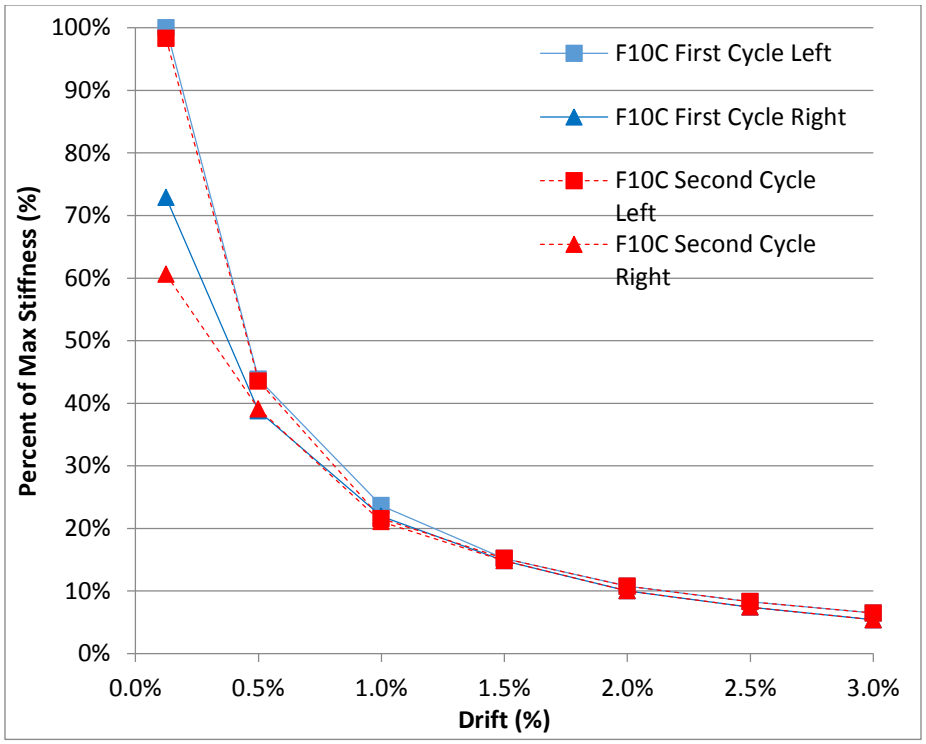

Figure 95 - Wall specimen F10C stiffness versus drift

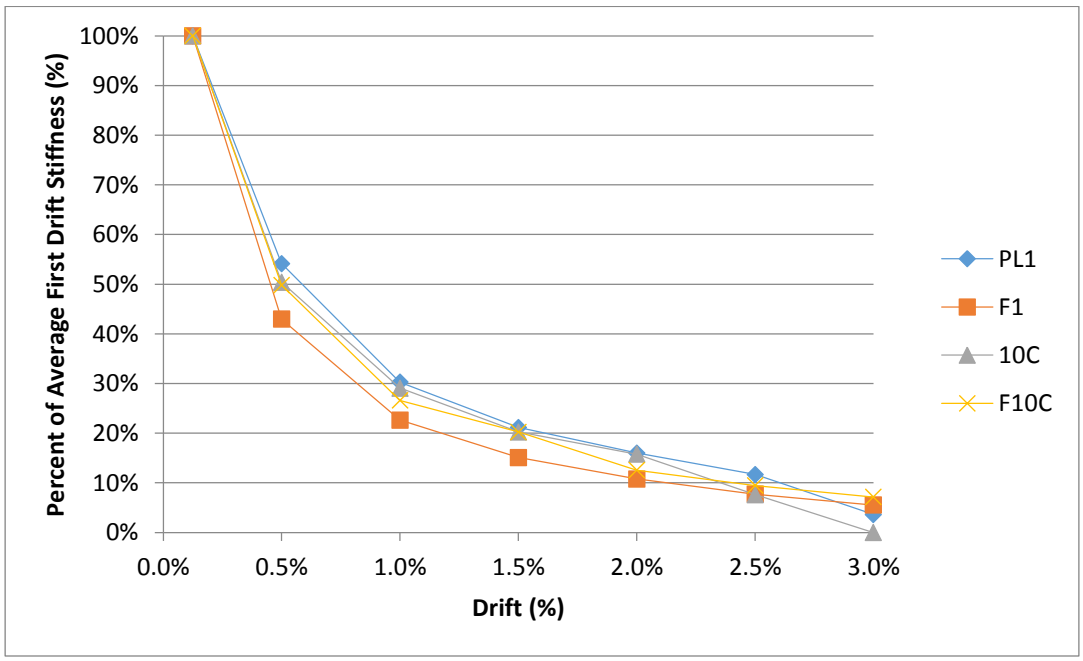

Figure 96 - Percent of average first drift stiffness values for all wall specimens

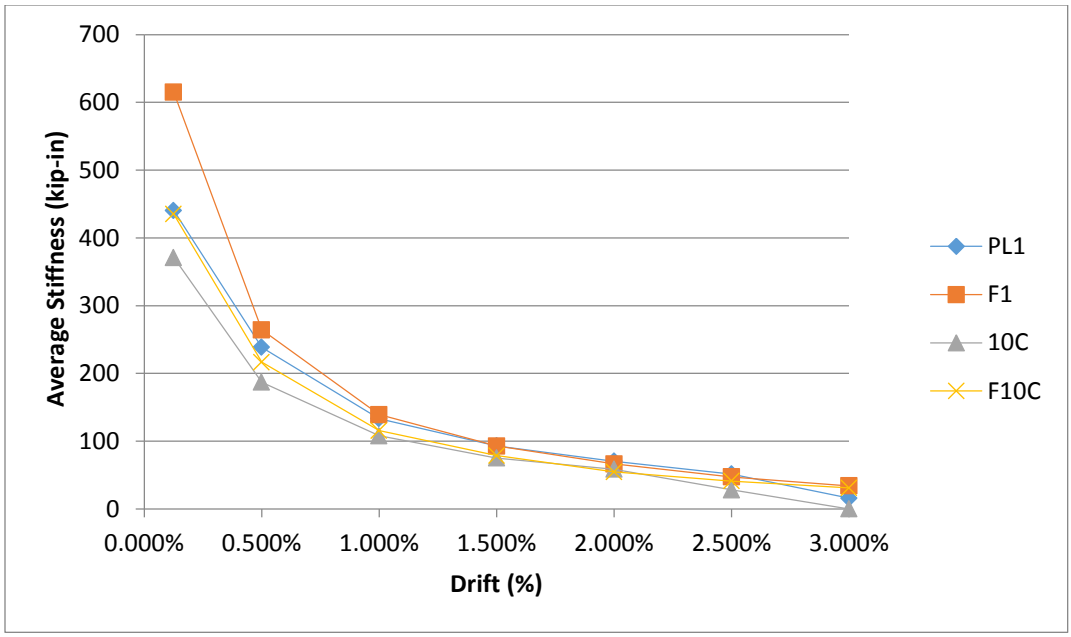

Figure 97 - Average stiffness versus drift for all wall specimens

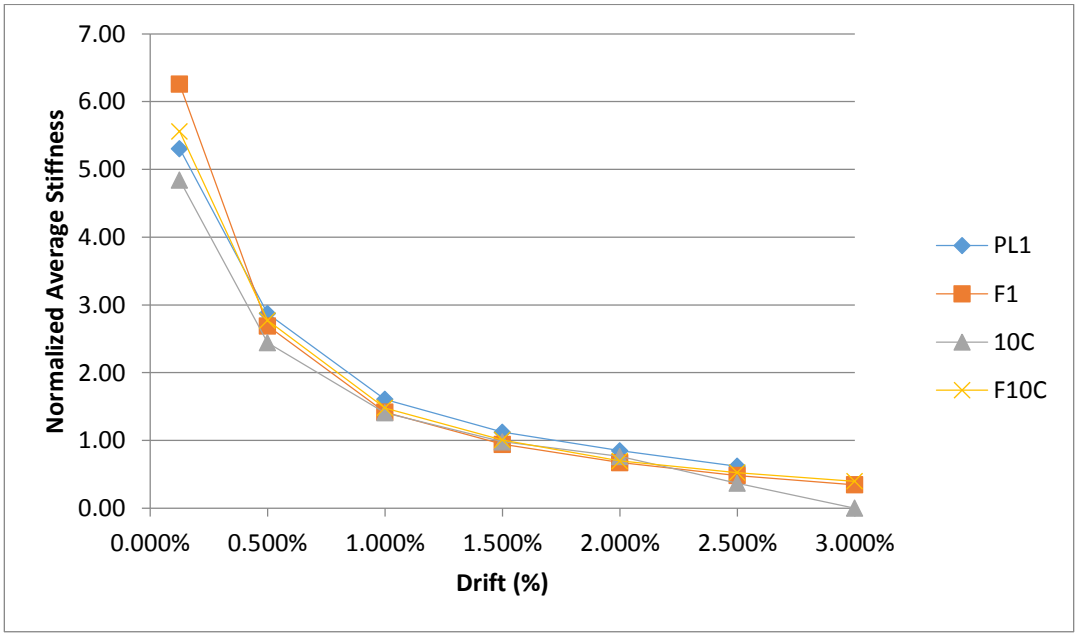

Figure 98 - Normalized average stiffness versus drift for all wall specimens

The first cycle at a given drift percentage should exhibit a larger stiffness value because fewer deformations existed prior to the second cycle at the same drift. This was the case in all cycles of all specimens except for the first drift percentage of PL1. These

deformations cause stiffness loss and are evident in all of the walls' plots. Deformations causing stiffness loss can also be observed when looking at the loading from the positive sides compared to the negative sides. After the wall is loaded first from the positive side it causes deformations and therefore stiffness loss which is noted by observing a higher stiffness value at similar cycles for the positive direction. Observing the average first drift stiffness values in Table 16, it is evident that the initial stiffness of walls increases if fibers are present and decreases when rubber is present. After the initial stiffness values, specimen F1 experienced the largest rate of decrease in average stiffness. This loss of stiffness is caused by the fibers preventing cracks from completely closing because the fibers bridge the cracks. Specimen PL1 experienced the least amount of loss in stiffness. Table 17 illustrates the percentage stiffness loss at each drift for each wall. Overall the wall specimens containing fibers tended to lose stiffness at a slightly quicker rate than those without fibers. The stiffness values also correlated with the observed damage, yielding, and cracking for all wall specimens.

Table 17 - Percentage of Average First Drift Stiffness at Each Drift

Drift %	Displacement (in)	PL1	F1	10C	F10C
0.125%	0.045	100%	100%	100%	100%
0.50%	0.18	54%	43%	50%	50%
1.00%	0.36	30%	23%	29%	27%
1.50%	0.54	21%	15%	20%	20%
2.00%	0.72	16%	11%	16%	13%
2.50%	0.9	12%	8%	8%	9%
3.00%	1.08	4%	6%	0%	7%

4.3.10 Energy Dissipation Capacity

The total energy dissipation capacity or toughness and the total normalized energy dissipation capacity of the wall specimens can be found in Table 18 and Figure 99. Energy dissipation capacity is one of the most important characteristics of a shear wall. The amount of energy absorbed is determined by calculating the area under the curve during a loading cycle for the lateral load versus displacement hysteresis loop. A plot showing the energy dissipation versus drift can be seen in Figure 100. A plot showing the normalized energy dissipation with respect to the compressive strength versus the drift percentage can be seen in Figure 101. To illustrate the effects of a repeated drift cycle, separate lines are plotted using the repeated drift cycle values. It can be noted that the energy dissipated in the first cycle of a repeated drift percentage is slightly larger. The lower energy dissipation in the second cycle of a repeated drift percentage is due to the loss in stiffness and strength the wall experienced from the previous cycle. Viewing the first figure, it can be seen that the PL1 and F1 wall specimens dissipate the most energy throughout the entirety of the test. This is consistent with the peak load experienced for both walls as they experienced the largest loadings. In the second figure, the energy dissipation for each wall is normalized with respect to each walls compressive strength respectively. Wall specimen PL1 dissipated the most energy with respect to its compressive strength. Walls containing rubber dissipated the least amount of energy. It can also be noted that the amount of energy dissipated was greatest for each wall at the cycle in which it was determined to have reached its drift capacity, denoting its failure (80% of the peak load).

Table 18 - Wall Energy Dissipation Capacities

Wall	Total Energy Dissipation	Normalized Total Energy Dissipation
PL1	129.095	1554.797
F1	112.266	1142.364
10C	58.005	757.411
F10C	41.477	530.147

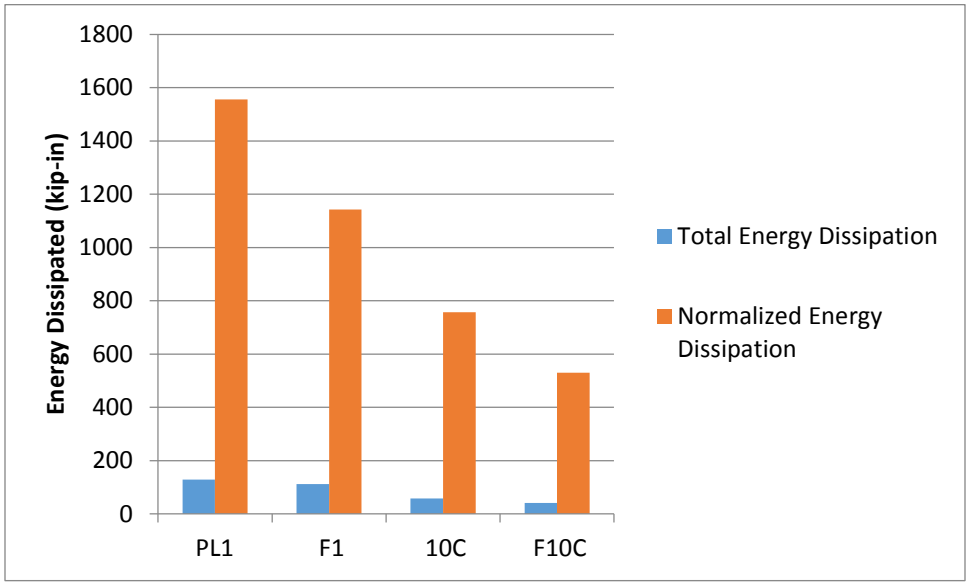

Figure 99 - Total energy dissipation and normalized total energy dissipation for all wall specimens

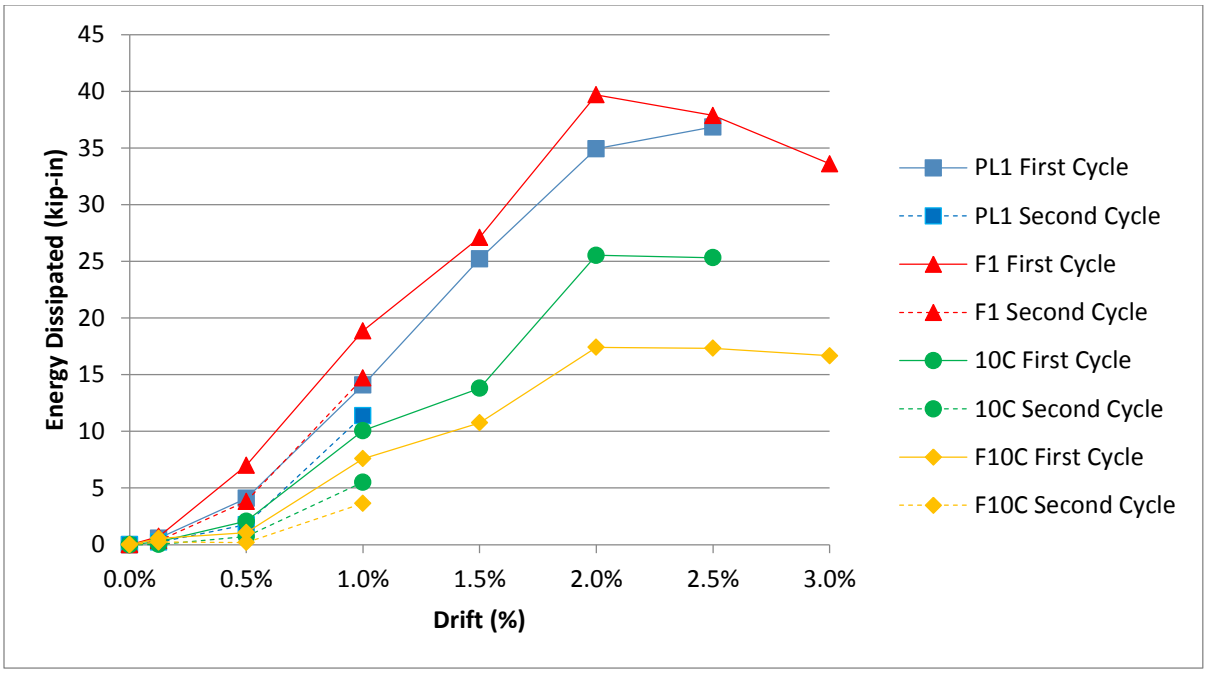

Figure 100 – Energy dissipated versus drift percentage for all wall specimens

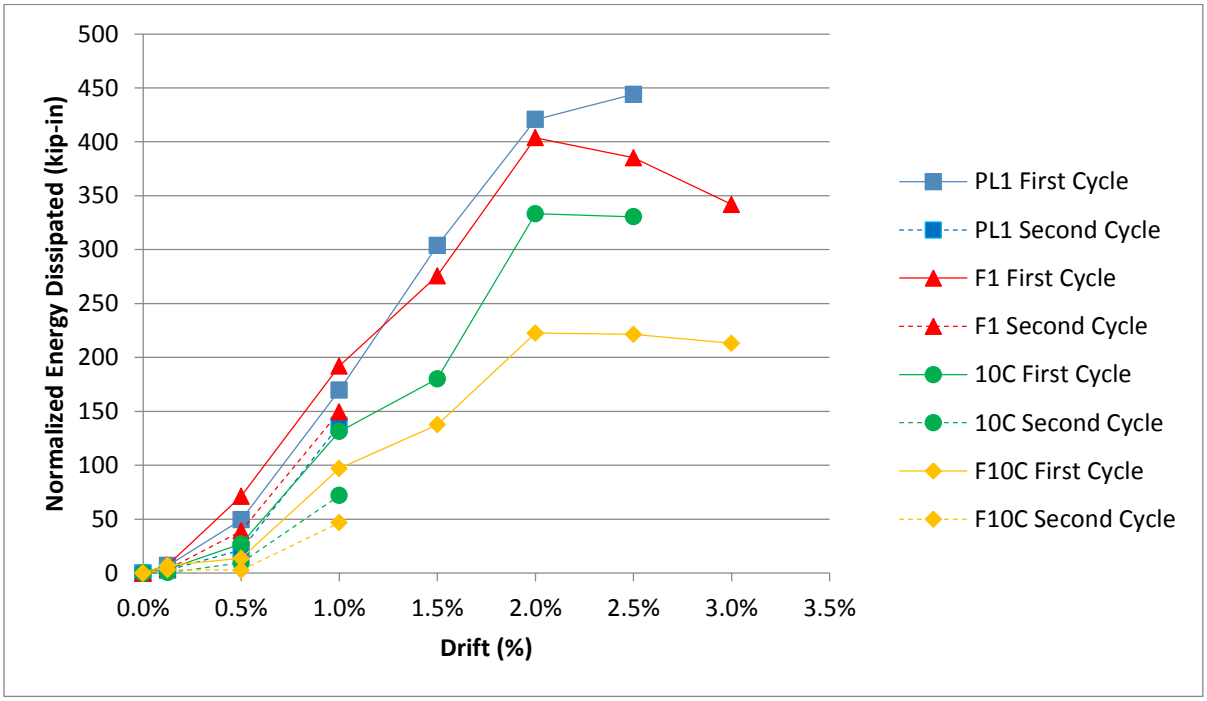

Figure 101 – Normalized energy dissipated versus drift percentage for all wall specimens

4.3.11 Damage Progression in Wall Specimens

The damage progression in the wall specimens was dependent on the mix composition. While all of the walls experienced damage and crack progression and ultimately failure, the peak load, shear stress, capacity, and behavior differed. The test results for each wall can be found in Table 19 and Figures 102-106. The peak shear stress is expressed in terms of $\sqrt{f'_c}$ to more easily compare the values to the other wall specimens. The drift capacity of each wall was taken as the drift percentage in which 80% of the peak load was sustained in both directions for the final time. This 80% is based on previous research done by Mindess et al. where it was found that the cube compressive strength was approximately 80% of the cylinder strength (Mindess, Young, & Darwin, Concrete, 2003). In Figures 107-110 the crack progression is noted by drawing on the wall face with two different colors. Each color was assigned a loading direction and also the cycle number at which cracks began and ended. The walls' damage progressions and results will be discussed in the following sections.

Table 19 - Wall specimen test results

	PL1		F1		10C		F10C	
	+	-	+	-	+	-	+	-
Peak Load (kips)	52.2	49.3	52.8	50.9	42.6	41.7	44.6	42
Peak Shear Stress (psi)	435	411	440	424	355	348	372	350
Peak Shear Stress (in √(f'))	6.55	6.19	5.60	5.39	5.79	5.67	5.94	5.59
Drift at Peak Load (%)	2.0%	2.0%	1.0%	1.0%	2.0%	2.0%	1.0%	1.5%
Drift Capacity (%)	2.5%		2.0%		2.0%		2.0%	
Final Drift (%)	3.0%	2.5%	3.0%	3.0%	2.5%	2.5%	3.0%	3.0%
Failure Mode	Sliding Shear		Sliding Shear		Diagonal Tension		Sliding Shear	

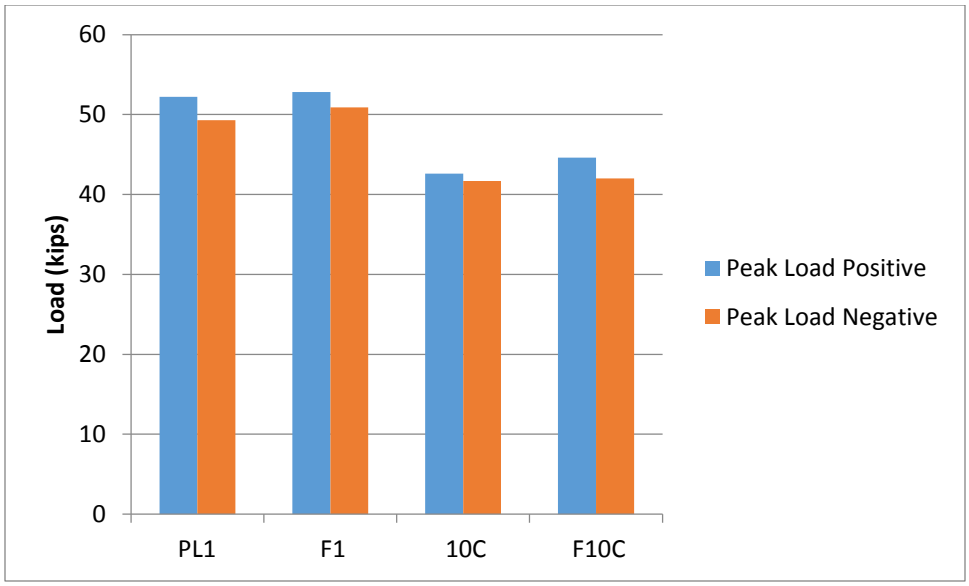

Figure 102 - Peak loads for walls

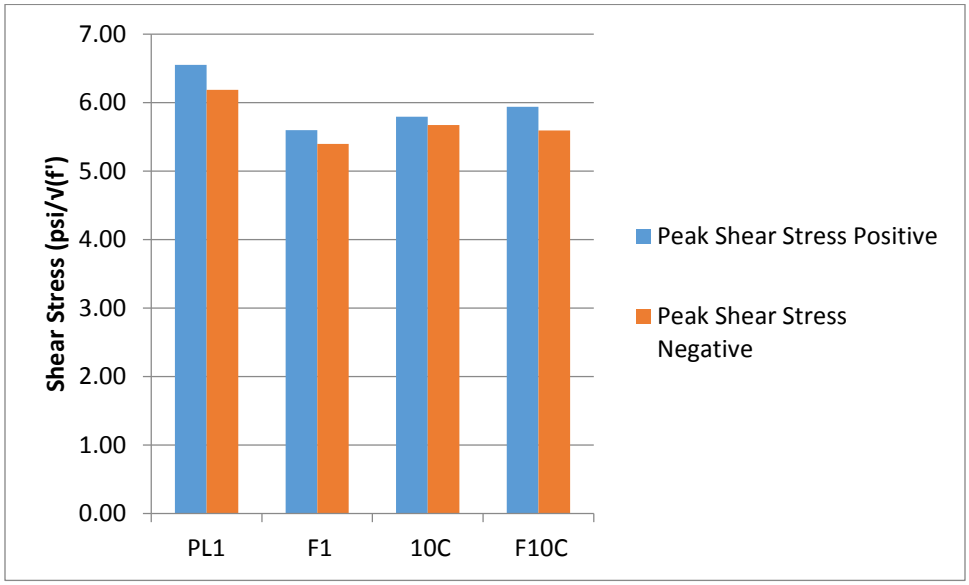

Figure 103 - Peak shear stresses for walls

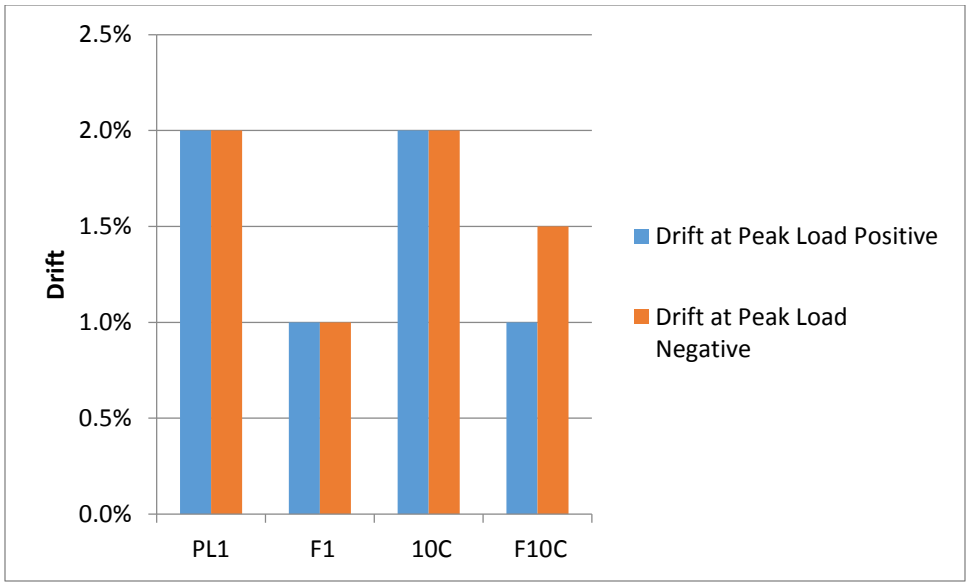

Figure 104 – Drift at peak loads for walls

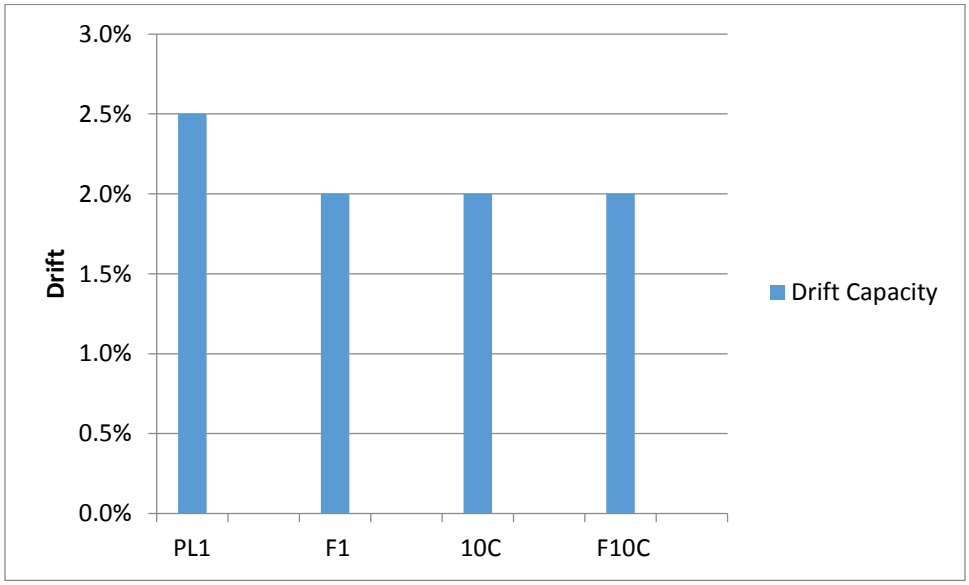

Figure 105 – Drift capacity for walls

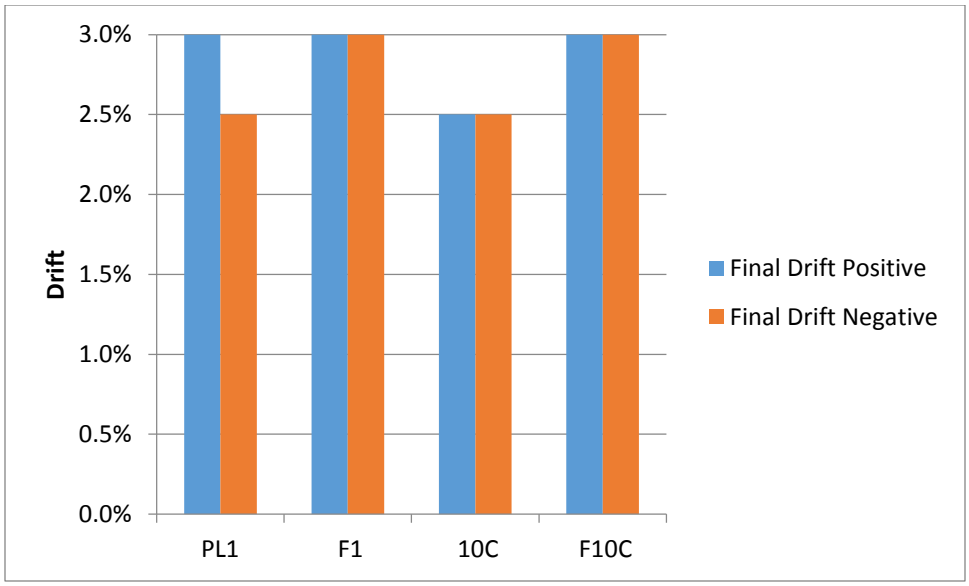

Figure 106 – Final drifts for walls

PL1 Wall Specimen Damage Progression: Wall specimen PL1 was cast using the mix design described in Table 2. During the progression of the test the minor cracks formed during the first few cycles. These minor cracks became longer and some ultimately formed major cracks. At a drift of 2%, damage to the boundary elements just above the wall and foundation intersection began to form, causing crushing and spalling of concrete in the compression zone as well as further yielding of the vertical reinforcement in the tension zone. Also occurring at this drift increment was the formation of two major diagonal cracks. The formation of minor cracks drastically slowed prior to this. Immediately prior to the major cracks occurring is also when peak load was experienced, which transpired at 2%. In the final loading cycles, the extent of the damage in the major cracks and boundary areas became even more evident as the cracks grew larger and boundary areas experienced further section loss. The PL1 wall specimen experienced the most significant section loss in the boundary areas as the boundary reinforcement became completed exposed. The web also began to experience some concrete spalling and reinforcement yielding and slip. The wall

specimen was deemed as a failure due to sliding shear before reaching a drift of 3%. Wall failure was taken as when the wall could not sustain 80% of the peak load for an entire cycle. The test was terminated at a drift of 3% when it could only sustain 76% of its peak loading. The PL1 wall specimen reached a peak load of 52.2 kips at a drift of 2%. The peak shear stresses of the PL1 wall specimen were $6.55\sqrt{f'_c}$ and $6.19\sqrt{f'_c}$ for the positive and negative loading direction respectively constituting an average peak shear stress of $6.37\sqrt{f'_c}$. The crack progression, the boundary and base damage, and the damage after the final cycle are shown in Figure 107.

(a)

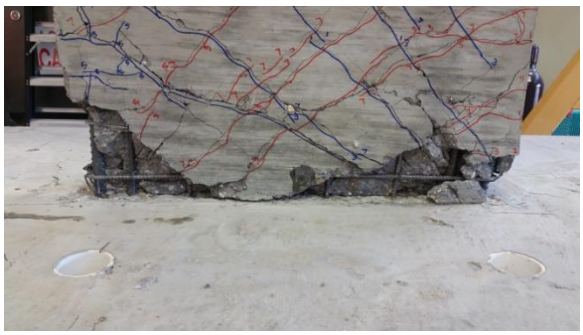

(b)

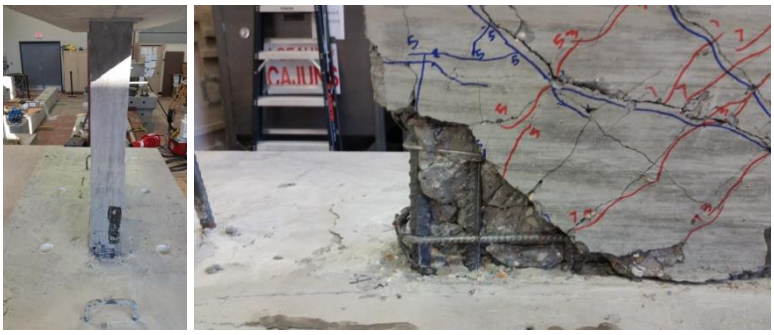

(c)

(d)

Figure 107 - Wall specimen PL1 (a) wall (b) base (c) left boundary (d) right boundary

F1 Wall Specimen Damage Progression: Wall specimen F1 was cast using the mix design described in Table 2. Minor diagonal cracks were difficult to observe due to the fibers causing micro-cracking. These micro cracks are much smaller in width compared to normal minor cracks found in walls without fibers. These minor and micro cracks became longer but never formed what was deemed as a major crack in the web area. It was also observed that the overall crack lengths on the web of the wall were not as long and far reaching as specimens without fibers. At a drift of 1%, damage to the boundary elements just above the wall and foundation intersection began to form, causing crushing and spalling of concrete in the compression zone as well as further yielding of the vertical reinforcement in the tension zone. Immediately prior to this occurring is when peak load was experienced, which transpired at 1%. The spalling and crushing of the concrete was not as severe as the

specimens containing no fibers due to the fibers bridging the crack gaps keeping them from growing larger. Damage was also more prominent in the boundary areas in comparison to the web of the wall contrary to specimens without fibers. Specimens that did not contain fibers experienced major cracks in the web as well as significant damage to the boundary elements. Specimens with fibers only experienced significant damage in the boundary elements. In the final loading cycles, the extent of the damage in the boundary areas became even more evident as the cracks and crushing intensified and experienced further section loss. Vertical hairline cracks also formed in the boundary areas further contributing to its deterioration. The hairline cracks are vertical because cracks orient themselves in the direction of the force placed on that given area. The boundary elements experienced extreme vertical compression and tension due to large drifts causing lateral tensile stresses and thus the given crack orientation. It is important to note that no major diagonal cracking occurred. The wall specimen was deemed as a failure due to sliding shear at a drift before reaching a drift of 2.5%. Wall failure was taken as when the wall could not sustain 80% of the peak load for an entire cycle. The test was terminated at a drift of 3% when it could only sustain 70% of its peak loading. The F1 wall specimen reached a peak load of 52.8 kips at a drift of 1%. The peak shear stresses of the F1 wall specimen were $5.60\sqrt{f'_c}$ and $5.40\sqrt{f'_c}$ for the positive and negative loading direction respectively constituting an average peak shear stress of $5.50\sqrt{f'_c}$. The crack progression, the boundary and base damage, and the damage after the final cycle are shown in Figure 108.

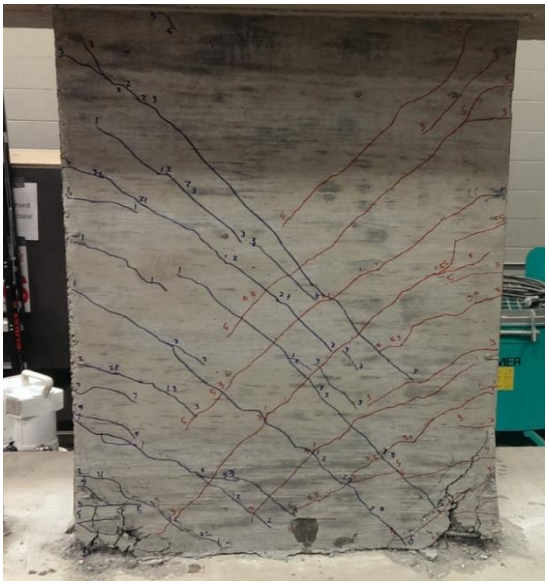

(a)

(b)

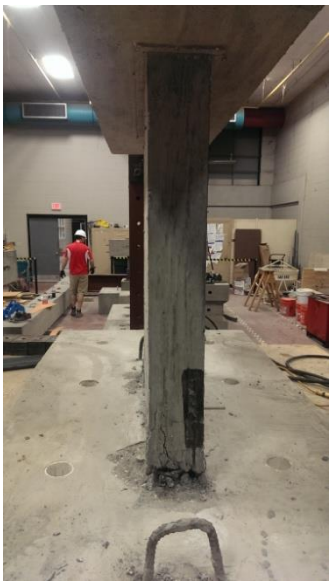

(c)

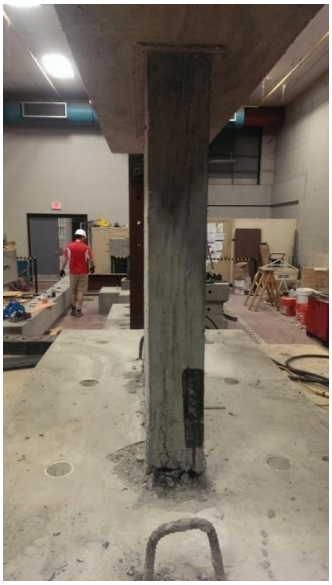

(d)

Figure 108 - Wall Specimen F1(a) wall (b) base (c) left boundary (d) right boundary

10C Wall Specimen Damage Progression: Wall specimen 10C was cast using the mix design described in Table 2. During the progression of the test the minor cracks formed during the first few cycles. It should be noted that wall specimen 10C had the earliest onset of minor cracking in comparison to the other walls. These minor cracks became longer and

some ultimately formed major cracks. At a drift of 2%, damage to the boundary elements just above the wall and foundation intersection began to form, causing crushing and spalling of concrete in the compression zone as well as further yielding of the vertical reinforcement in the tension zone. Numerous major cracks at this drift also began to form in both directions. These major cracks were extremely large and ultimately dominated the failure mode. Immediately prior to this occurring is when peak load was experienced, which transpired at 2%. In the final loading cycles, the extent of the damage in the major cracks and boundary areas became even more evident as the cracks grew larger and boundary areas experienced some section loss. The web also began to experience significant concrete spalling. The major cracks in this specimen were the largest and most prominent out of all of the wall specimens. In the end, the major cracks had formed an "x" on the face of the web spanning from the foundation to midway up the wall. The cracks not only affected the face of the wall but significant major cracking formed on the sides of the wall a quarter of the way to half way up the wall specimen. The wall specimen was deemed as a failure due to a diagonal tension failure before reaching a drift of 2.5%. Wall failure was taken as when the wall could not sustain 80% of the peak load for an entire cycle. The test was terminated at a drift of 2.5% when it could only sustain 77% of its peak loading. The 10C wall specimen reached a peak load of 42.6 kips at a drift of 2%. The peak shear stresses of the 10C wall specimen were $5.79\sqrt{f'_c}$ and $5.67\sqrt{f'_c}$ for the positive and negative loading direction respectively constituting an average peak shear stress of $5.73\sqrt{f'_c}$. The crack progression, the boundary and base damage, and the damage after the final cycle are shown in Figure 109.

(a)

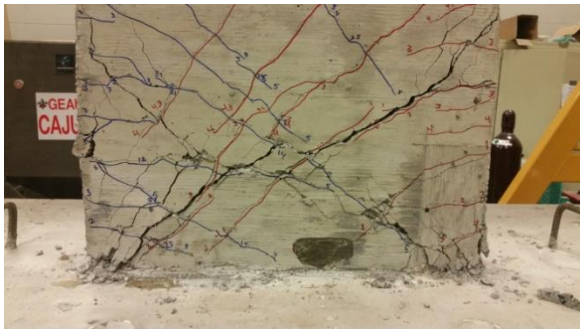

(b)

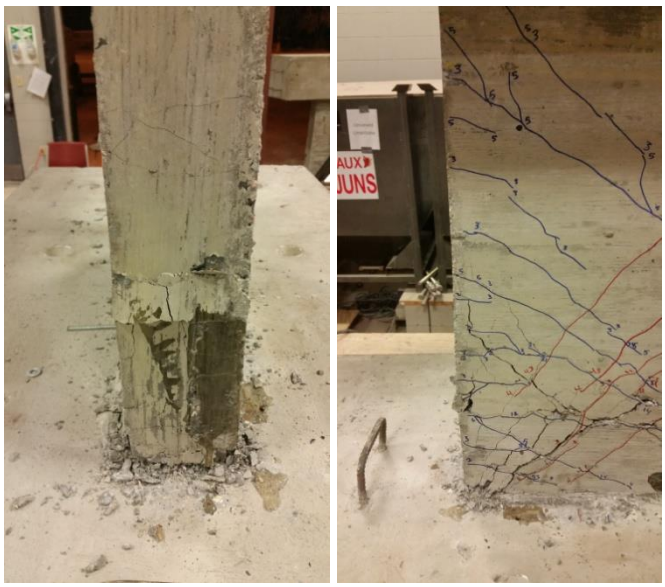

(c)

(d)

Figure 109 - Wall Specimen 10C(a) wall (b) base (c) left boundary (d) right boundary

F10C Wall Specimen Damage Progression: Wall specimen F10C was cast using the mix design described in Table 2. Minor diagonal cracks were difficult to observe due to the fibers causing micro-cracking. These micro cracks are much smaller in width compared to normal minor cracks found in walls without fibers. These minor and micro cracks became longer but never formed what was deemed as a major crack in the web area. It was also observed that the overall crack lengths on the web of the wall were not as long and far reaching as specimens without fibers. At a drift of 1%, damage to the boundary elements just above the wall and foundation intersection began to form, causing crushing and spalling of concrete in the compression zone as well as further yielding of the vertical reinforcement in the tension zone. Immediately prior to this occurring is when peak load was experienced. The spalling and crushing of the concrete was not as severe as the specimens containing no fibers due to the fibers bridging the cracks, keeping them from growing larger. Damage was also more

prominent in the boundary areas than in the web of the wall contrary to specimens without fibers. In the final loading cycles, the extent of the damage in boundary areas became even more evident as the cracks grew larger and boundary areas experienced further section loss. Vertical hairline cracks also formed in the boundary areas contributing further to its deterioration. It is important to note that no major diagonal cracking occurred. The wall specimen was deemed as a failure due to sliding shear before reaching a drift of 2.5%. Wall failure was taken as when the wall could not sustain 80% of the peak load for an entire cycle. The test was terminated at a drift of 3% when it could only sustain 75% of its peak loading. The F10C wall specimen reached a peak load of 44.6 kips at a drift of 1%. The peak shear stresses of the F10C wall specimen were $5.94\sqrt{f'_c}$ and $5.59\sqrt{f'_c}$ for the positive and negative loading direction respectively constituting an average peak shear stress of $5.76\sqrt{f'_c}$. The crack progression, the boundary and base damage, and the damage after the final cycle are shown in Figure 110.

(a)

(b)

(c)

(d)

Figure 110 - Wall Specimen F10C(a) wall (b) base (c) left boundary (d) right boundary

Summary of Damage Progression for All Walls: After observing the damage progressions for the four wall specimens some key notes can be made. The walls that exhibited the hysteretic behavior also showed a pinching effect causing stiffness loss. All of the walls exhibited hysteretic behavior and pinching except for the 10C wall which did not experience pinching due to its sudden diagonal tension failure. For the three walls that failed due to sliding shear, dowels could have been placed in these walls to suspend the failure until a later

drift. More data would have been able to be collected prior to failure if dowels were used. The PL1 wall specimen had the highest shear stresses, highest drift capacity, and dissipated the most energy. The wall specimens that contained rubber tended to have larger cracks, cause more severe web cracking and damage as opposed to damage in the boundary elements, and were subjected to the lowest load capacities which can be contributed lower compressive strength and rubber walls having less vertical reinforcement. Wall specimens containing fibers had less spalling with shorter cracks and crack lengths than walls without fibers. Fiber walls were also subjected to slightly higher loadings when compared to walls with the same reinforcement. Damage to walls containing fibers was found to be more prominent in the boundary elements than in the web. This resulted in more boundary section loss and vertical hairline cracks that did not appear in walls without fibers. Walls that did not contain fibers experienced similarly significant boundary element damage but the web damage was more significant than walls with fibers due to major cracks forming. Fiber walls also tended to reach their peak load at an earlier drift percentage. Because of this, fiber walls exhibited the same or better ductility than walls without fibers containing the same reinforcement. The fibers also kept minor and micro cracks from forming major cracks commonly found in the walls without fibers.

4.4 Summary

Testing of the shear beams and shear walls yielded a plethora of results that were analyzed to determine the characteristics and properties of the specimens and mixes. Analysis of the tested shear beams determined shear strengths, concrete contribution to shear strength coefficients, mix properties, and behaviors of each mix. Analysis of the tested shear

walls determined the behavior and characteristics of the four selected mixes when used in low-rise shear walls subjected to a cyclic loading.

CHAPTER 5: Conclusions and Recommendations

5.1 Summary

Previous studies have examined the characteristics and behaviors of fibers and rubber in concrete as well as reinforced concrete low-rise shear walls. Research has detailed the fresh and hardened concrete properties affected by these two materials. 22 concrete beams were tested using mixes with differing amounts of fibers and rubber in them. The beams were designed to fail in shear by applying a single downward point load at midspan using a MTS Universal Testing Machine. Using the recorded load and displacement data the behavior of each beam and the shear strength contribution for each mix were determined. Four concrete walls were also tested using four of the 22 beam mixes. The four selected mixes were chosen based on the comparable compressive strengths and mix constituents. The walls were designed to fail in shear by applying a lateral load to a top block cast on top of the shear wall. The walls were tested on a modular strong-block test system within a rigid steel frame so that the load could be applied by a hydraulic actuator. During testing the displacement at 10 selected locations, the loads placed on the walls at each displacement, and the behavior were recorded and analyzed. The data from both the beams and walls were compared after analysis and conclusions were made.

For the shear beams both the fibers and rubber contributed to the concretes shear strength. For all mixes that included fibers and/or rubber the shear strengths increased 12% to 56% in comparison to the plain concrete mixes. The beams containing rubber failed quickly after the first crack while beams containing fibers exhibited strain hardening characteristics and tended to level out for a significant amount of time before failing after first cracking. The beams containing fibers also increased the shear strength such that a flexural failure played a

part in the failure mode in all but one beam. For the shear wall tests the behavior and data were similar to the shear beams. The walls containing rubber experienced lower strengths, a brittle failure with severe spalling and damage, and dissipated a low amount of energy. The walls containing fibers exhibited strain hardening characteristics leading to a ductile failure mode, higher strengths, and little web damage. In Section 5.2, a discussion of the conclusions for the shear beams and shear walls will be discussed.

5.2 Conclusions

5.2.1 Fresh and Hardened Concrete Properties

1. Shear beam and wall mixes containing rubber saw a decrease in unit weight, compressive strength, tensile strength, and modulus of elasticity. An increase in air content was also recorded.
2. Shear beam and wall mixes containing fibers saw an increase in unit weight, compressive strength, tensile strength, and modulus of elasticity. A minimal change in air content was also recorded.
3. Shear beam and wall mixes containing fibers and rubber saw an increase in unit weight, compressive strength, tensile strength, and modulus of elasticity when compared to rubber only mixes. A minimal change in air content was also recorded.

5.2.2 Shear Strength Contributions

1. The normalized concrete's contribution to shear strength increased an average of 26.0% when rubber was added. For the one beam that was able to be analyzed containing fibers and rubber, the shear strength increased by 56.3%. If an increase in shear strength is desired for a given beam application, the addition of fibers and/or rubber may be a viable option.

2. The mix with the largest normalized concrete contribution to shear strength contained 1% fibers and 15% coarse/fine rubber. The normalized concrete contribution to shear strength was increased by over 56% in comparison to plain concrete.

5.2.3 Effects of Fibers and Rubber in Beams and Walls

1. Shear beam mixes containing rubber failed at lower loads than those without rubber or those that contained fibers as well. After cracking, concrete beams containing only rubber could not sustain a significant load for an extended period of time. This can be attributed to the loss of aggregate interlock when soft rubber replaces hard rock aggregates, the poor bond between rubber and cement, and the increased air content. These properties also contribute to its low post crack shear strength. Shear wall mixes containing rubber had larger and more severe web cracking in comparison to the boundary damage, lower load capacities, a longer time reaching peak load, and had the lowest initial stiffness. The loss of aggregate interlock, poor bond between the rubber and cement, and increased air content is believed to contribute to the severe and early cracking as well as the strength losses. Walls containing rubber also experienced the least amount of base rotations and dissipated the least amount of energy.
2. Shear beam mixes containing fibers sustained the largest loadings. When the beams first cracked the fibers exhibited strain hardening behavior enabling them to sustain high loads and large displacements for a significant period of time. Mixes that contained fibers also tended to form more significant vertical flexure cracks as opposed to diagonal shear cracks leading to the majority of the beams containing fibers having a flexural failure mode. Shear wall mixes containing fibers had

increased shear deformation capacities based on higher loads experienced prior to yielding in the boundary elements in comparison with walls of the same reinforcement and no fibers. During testing the walls with fibers had less spalling, smaller and more numerous minor and micro cracks, no major cracks, and more severe boundary damage in comparison to the web. The fibers contributed to this effect by bridging the cracks in the web which increased the webs damage tolerance. The fiber wall specimens also experienced higher load capacities, were quicker to reaching peak load, had an increased initial stiffness but a slightly higher rate of stiffness loss after cracking, exhibited a more exaggerated pinching effect due to some strain hardening, and had a more ductile failure mechanism. Flexural cracks formed in the boundary elements of walls containing fibers. This may be attributed to the increased shear strength caused by fibers such that flexural cracking began to occur in a wall designed to fail in shear. Walls containing fibers also experienced the largest rotations which correlated with the largest percent losses in stiffness prior to yielding. Subsequent to yielding the large base rotations may be attributed to the extreme boundary damage which was the worst in walls containing fibers in comparison to web damage which enabled the walls to rotate upon the base more.

3. Plain concrete walls dissipated the most energy prior to failure. This is due to the plain concrete wall sustaining 80% of its peak load at a higher drift cycle than the other three wall specimens. Prior to the 2% drift cycle, wall specimen F1 dissipated the most overall energy. Therefore it can be concluded that prior to yielding fibers are more effective at dissipating energy than rubber or plain concrete. The plain concrete wall also experienced the highest shear strains.

4. The three walls specimens that failed in sliding shear exhibited hysteresis behavior and a pinching effect caused by stiffness loss from the cyclic loadings. Shear sliding caused significantly exaggerated pinching and the effect would have been less evident if sliding would not have occurred. Sliding directly contributed to 30% to 40% of the recorded displacements of the top of the walls during the testing of wall specimens PL1, F1, and F10C.
5. The concretes behavior when subjected to extreme shear loads in reversed cycles affects the properties of the fibers and rubber concrete due to the repeated degradation in comparison to other applications such as beams. While much of the behavior and properties between the walls were similar, some were not. The repeated degradation and damage of the rubber decreased aggregate interlock further and the bond between the rubber and cement became even more critical. The repeated degradation and damage of the fibers when the cracks opened and closed inhibited some strain hardening ultimately affecting its ability to display vastly superior energy dissipation, toughness, and ductility.
6. While dependent on the application and desired characteristics, walls containing fibers are a more viable option in comparison to walls containing rubber due to its ability to dissipate more energy, its failure mode, behavior during loading, and its increased compressive, tensile, and shear strengths. Fiber concrete walls also improve damage and deformation capacities and can simplify reinforcement design in both the web and boundary elements. Fiber walls would be extremely desirable in seismic areas because of these characteristics, most notably its ductile failure mode. It should

be noted however that fiber walls performed similarly to plain walls so it is unlikely that the addition of fibers to the mix is necessary due to increased cost.

5.3 Recommendations

Further experimental research and analysis is suggested regarding the following items:

1. For research pertaining specifically to low-rise shear walls, dowels should be used when appropriate to prevent sliding displacement if possible. Sliding caused exaggerated data output and could have affected the analysis of the overall results. The addition of dowels would enhance the focus on the behavior of the walls web and boundaries while in shear instead of the joint between the foundation and wall.
2. Future research should focus on the highest performing mixes of the existing 22 mixes instead of all 22. Future research should also limit its focus to different volume fractions of either fibers or rubber instead of both to limit the amount of variables. Further research should be done on the role cyclic loading degradation plays into the change in behavior and properties for fiber and rubber concrete
3. Ensure that the amount of water reducer used in the beams and walls is the same to limit mix variability.
4. The beams should be redesigned so that the shear strength of the beam will be met far in advance of any possible flexural failure so that all mixes can be analyzed for their contribution to concrete shear strength.

BIBLIOGRAPHY

(1992). In T. Paulay, & N. M. Priestly, Seismic Design of Reinforced Concrete and Masonry Buildings (pp. 668-669). New York: Wiley Interscience.

ACI Committee 318. (2011). Building code requirements for structural concrete (ACI 318-2011) and commentary. Farmington Hills: American Concrete Institute.

Aiello, M., & Leuzzi, F. (2010). Waste tyre rubberized concrete: Properties at fresh and hardened state. Waste Management, 30, 1696-1704.

Aktan, A. E., & Bertero, V. V. (1985). RC Structural Walls: Seismic Design for Shear. Journal of Structural Engineering, 1775-1791.

Albano, C.; Camacho, N.; Reyes, J.; Feliu, J.L.; Hernandez, M. (2005). Influence of scrap rubber additon to Portland I concrete composites: destructive and non-destructive testing. Compos. Struct., 71, 439-446.

Aoyama, H. (1991). Design Philosophy for Shear in Earthquake Resistance in Japan. International Workshop on Concrete in Earthquake. Houston: University of Houston.

ASTM. (2010a). "Standard test method for air content of freshly mixed concrete by the pressure method." *ASTM Standard C231*. ASTM International, West Conshohocken, PA, 2003, DOI: 10.1520/C0231_C0231M-10, www.astm.org.

ASTM. (2010b). "Standard test method for compressive strength of concrete cylinders cast in place in cylindrical molds." *ASTM Standard C873*. ASTM International, West Conshohocken, PA, 2010, DOI: 10.1520/C0873-C0873M-10A, www.astm.org

ASTM. (2011a). "Standard specifications for steel fibers for fiber-reinforced concrete." *ASTM Standard A820.* ASTM International, West Conshohocken, PA, 2011, DOI: 10.1520/A820_A0820M-11, www.astm.org

ASTM. (2011b). “Standard test method for splitting tensile strength of cylindrical concrete specimens.” *ASTM Standard C496*. ASTM International, West Conshohocken, PA, 2011, DOI: 10.1520/C0496_C0496M-11, www.astm.org

ASTM. (2012a). "Standard test method for density, relative density (specific gravity), and absorption of coarse aggregate." *ASTM Standard C127*. ASTM International, West Conshohocken, PA, 2003, DOI: 10.1520/C0127-12, www.astm.org.

ASTM. (2012b). "Standard test method for density, relative density (specific gravity), and absorption of fine aggregate." *ASTM Standard C128*. ASTM International, West Conshohocken, PA, 2003, DOI: 10.1520/C0128-07A, www.astm.org.

ASTM. (2013a). “Standard specification for chemical admixtures for concrete.” *ASTM Standard C494*. ASTM International, West Conshohocken, PA, 2011, DOI: 10.1520/C0494_C0494M-13, www.astm.org

ASTM. (2013b). “Standard specification for chemical admixture for use in producing flowing concrete.” *ASTM Standard C1017*. ASTM International, West Conshohocken, PA, 2011, DOI: 10.1520/C1017_C1017M, www.astm.org

ASTM. (2014). “Standard practice for making and curing concrete test specimens in the laboratory.” *ASTM Standard C192*. ASTM International, West Conshohocken, PA, 2014, DOI: 10.1520/C0192-C0192M-14, www.astm.org

ASTM. (2015). “Standard specification for Portland Cement.” *ASTM Standard C150/C150M-15*. ASTM International, West Conshohocken, PA, 2014, DOI: 10.1520/C0150_C0150M-15, www.astm.org

Athanasopoulou, A. (2010). Shear Strength and Drift Capacity of Reinforced Concrete and High-Performance Fiber Reinforced Concrete Low-Rise Walls Subjected to Displacement Reversals. Ann Arbor: University of Michigan.

Balaguru, P., Narahari, R., & Patel, M. (1992). Flexural toughness of steel fiber reinforced concrete. ACI Mater. J., 89(6), 541-546.

Barda, F., Hanson, J. M., & Corley, W. G. (1977). Shear Strength of Low-Rise Walls with Boundary Elements. ACI Specifal Publications, 149-202.

Bencardino, F., Rizzuti, L., Spadea, G., & Swamy, R. N. (2008). Stress-strain behavior of steel fiber-reinforced concrete in compression. J. Mater. Civ. Eng., 20(3), 255-263.

Benton, J. (2015). Modular Strong Block Test System.

Bhargava, P., Sharma, U. K., & Kaushik, S. K. (2006). Compressive stress-strain behavior of small scale steel fibre reinforced high strength concrete cylinders. J. Adv. Concr. Technol., 109-121.

Biel, T. D., & Lee, H. (1996). Magnesium Oxychloride Cement Concrete with Recycled Tire Rubber. Transportation Research Record 1561, 6-12.

Biskinis, D. E., Roupakias, G. K., & Fardis, M. N. (2004). Degradation of Shear Strength of Reinforced Concrete Members with Inelastic Cyclic Displacements. ACI Structural Journal, 773-783.

Building code requirements for structural concrete (ACI 318-11) and commentary. (2011). Farmington Hills: American Concrete Institute.

Canbolat, B. A., Parra-Montesinos, G. J., & Wight, J. K. (2005). Experimental Study on Seismic Behavior of High-Performance Fiber Reinforced Cement Composite Coupling Beams. ACI Structural Journal, 159-166.

Cardenas, A. E., & Magura, D. D. (1973). Strength of High-Rise Shear Walls--Rectangular Cross Section. Detroit: American Concrete Institute.

Cardenas, A. E., Hanson, J. M., Corley, W. G., & Hognestad, E. (1973). Design Provisions for Shear Walls. ACI Journal, 221-230.

Chandrangsu, K., & Naaman, A. E. (2003, June). Comparison of tensile and bending response of three high performance fiber reinforced cement composites. (A. E. Naaman, & H. W. Reinhardt, Eds.) Proceeding pro 030: high performance fiber-reinforced cement composites (HPFRCC4), RILEM Publications, 259-274.

Chao, S.-H., Naaman, A. E., & Parra-Montesinos, G. J. (2006, November-December). Bond Behavior of Strand Embedded in Fiber Reinforced Cementitious Composites. PCI Journal, 56-71.

Chompreda, P., & Parra-Montesinos, G. (2005). Deformation Capacity and Shear Strength of Fiber Reinforced Cement Composite Flexural Members Subjected to Displacement Reversals. Ann Arbor: University of Michigan.

Chu, M., Feng, P., & Ye, L. (2012). Study on Improvement for Seismic Behavior of Reinforced Concrete Shear Walls. Advanced Materials Research, pp. 1396-1401.

Collins, M., & Mitchell, D. (1986). A Rational Approach to Shear Design: The 1984 Canadian Code Provisions. ACI Journal.

Corinaldesi, V., & Moriconi, G. (2011). Characterization of self-compacting concretes prepared with different fibers and mineral additions. Cement and Concrete Composites, 33(5), 596-601.

Cottrell, A. H. (1964). Proc. Roy. Soc. A282. 2.

Dhonde, H. B., Mo, Y. L., Hsu, T. T., & Vogel, J. (2007). Fresh and hardened properties of self-consolidating fiber-reinforced concrete. ACI Mater. J., 104(5), 491-500.

Earthquake Hazards Program. (2015). Retrieved from United States Geological Survey: http://earthquake.usgs.gov/

Eldin, N. N., & Senouci, A. B. (1993, November). Rubber-Tire Particles as Concrete Aggregate. Journal of Materials in Civil Engineering, 5(4), 478-496.

Eldin, N. N., & Senouci, A. B. (1993, November). Rubber-Tire Particles As Concrete Aggregate. Journal of Materials in Civil Engineering, 5(4), 478-497.

Environmental Protection Agency. (2013, August 2). Wastes - Resource Conservation - Common Wastes & Materials - Scrap Tires. Retrieved from U.S. Environmental Protection Agency Web Site: http://www.epa.gov/epawaste/conserve/materials/tires/faq.htm

Eom, T.-S., Park, H.-G., Kim, J.-Y., & Lee, H.-S. (2013). Web Crushing and Deformation Capacity of Low-Rise Walls Subjected to Cyclic Loading. ACI Structural Journal, 575-584.

Ezeldin, A. S., & Balaguru, P. N. (1992). Normal and high-strength fiber reinforced concrete under compression. J. Mater. Civ. Eng., 4(4), 415-429.

Farrar, C. R., & Baker, W. E. (1990). Stiffness and Hysteretic Energy Loss of a Reinforced-Concrete Shear Wall. Experimental Mechanics, 95-100.

Farrar, C. R., & Baker, W. E. (1993). Experimental Assessment of Low-Aspect-Ratio, Reinforced Concrte Shear Wall Stiffness. Earthquake Engineering and Structural Dynamics, 373-387.

Fintel, M. (1991). Shearwalls - An Answer for Seismic Resistance? Concrete International, 48-53.

Fischer, G., & Li, V. C. (2002). Effect of Matrix Ductility on Deformation Behavior of Steel Reinforced ECC Flexural Members Under Reversed Cyclic Loading Conditions. ACI Structural Journal, 781-790.

Ghaly, A. M., & Cahill(IV), J. D. (2005). Correlation of strength, rubber content, and water to cement ratio in rubberized concrete. Canada Journal of Civil Engineering, 32, 1075-1081.

Greifenhagen, C., & Lestuzzi, P. (2005). Static Cyclic Tests on Lightly Reinforced Concrete Shear Walls. Engineering Structures, 1703-1712.

Hannant, D. J. (2003). Fibre-reinforced concrete. (J. Newman, & B. S. Choo, Eds.) Advanced concrete technology set, 6/1-6/17.

Helfet, J. L., & Harris, B. (1972). J. Mater. Sci. 7, 494.

Helminger, N. (2014). Material and Flexural Properties of Fiber-reinforced Rubber Concrete.

Hsu, L. S., & Hsu, C. T. (1994). Stress-strain behavior of steel-fiber high-strength concrete under compression. ACI Struct. J., 91(4), 448-457.

Huang, B., Li, G., Pang, S.-S., & Eggers, J. (2004, May/June). Investigation into Waste Tire Rubber-Filled Concrete. Journal of Materials in Civil Engineering, 187-194.

Kabeyasawa, T., & Matsumoto, K. (1992). Tests and Analysis of Ultra-High Strength Reinforced Concrete Shear Walls. Earthquake Engineering, Tenth World Conference, (pp. 3291-3297). Rotterdam.

Kanda, T., & Li, V. (1998). Interface Property and Apparent Strength of a High Strength Hydrophilic Fiber in Cement Matrix. ASCE Journal of Materials in Civil Engineering, 10(1), 5-13.

Khaloo, A. R., Dehestani, M., & Rahmatabadi, P. (2008). Mechanical properties of concrete containing a high volume of tire-rubber particles. Waste Management, 28, 2472-2482.

Khatib, Z. K., & Bayomy, F. M. (1999, August). Rubberized Portland Cement Concrete. Journal of Materials in Civil Engineering, 206-213.

Khuntia, M., Stojadinovic, B., & Goel, S. C. (1999). Shear Strength of Normal and High Strength Fiber Reinforced Concrete Beams without Stirrups. ACI Structural Journal, 282-289.

Kim, D. j., Naaman, A. E., & El-Tawil, S. (2008). Comparitive flexural behavior of four fiber reinforced cementitious composites. Cement and Concrete Composites, 30, 917-928.

Kim, K., & Parra-Montesinos, G. (2003). Behavior of HPFRCC Low-Rise Walls Subjected to Displacement Reversals. Ann Arbor, Michigan, USA.

Krolicki, J., Maffei, J., & Calvi, G. M. (2011). Shear Strength of Reinforced Concrete Walls Subjected to Cyclic Loading. Journal of Earthquak Engineering, 30-71.

Kwak, Y. K., Eberhard, M. O., Kim, W., & Kim, J. (2002). Shear Strength of Steel Fiber-Reinforced Concrete Beams Without Stirrups. ACI Structural Journal, 530-538.

Lefas, I. D., Kotsovos, M. D., & Ambraseys, N. N. (1990). Behavior of Reinforced Concrete Structural Walls: Strength, Deformation Characteristics, and Failure Mechanism. ACI Structural Jounal, 23-31.

Lehmans, D., Moehle, J., & Mahin, S. (2004). Experimental Evaluation of the Seismic Performance of Reinforced Concrete Bridge Columns. Journal of Structural Engineering, 869-879.

Li, V. C. (1992). A Simplified Micromechanical Model of Compressive Strength of Fiber-Reinforced Cementitious Composites. Cement & Concrete Composites, 14, 131-141.

Li, V. C., Wu, C., Wang, S., Ogawa, A., & Saito, T. (2002, September-October). Interface Tailoring for Strain-Hardening Polyvinyl Alcohol-Engineered Cementitious Composite (PVA-ECC). ACI Materials Journal, 463-472.

Maalej, M., Hashida, T., & Li, V. C. (1995). Effect of Fiber Volume Fraction on the Off-Crack-Plane Fracture Energy in Strain-Hardening Engineered Cementitious Composites. Journal of the American Ceramic Society, 78(12), 3369-3375.

Mansour, M., & Hsu, T. T. (2005). Behavior of Reinforced Concrete Elements under Cyclic Shear. I: Experiments. Journal of Structural Engineering, 44-53.

Mansur, M. A., Chin, M. S., & Wee, T. H. (1999). Stress-strain relationship of high-strength fiber concrete in compression. J. Mater. Civ. Eng., 11(1), 21-29.

Matamoros, A., & Sozen, M. (2003). Drift Limits of High-Strength Concrete Columns Subjected to Load Reversals. Journal of Structural Engineering, 297-313.

Mindess, S., Young, J., & Darwin, D. (2003). Concrete. New Jersey: Prentice Hall.

Morton, J., & Groves, G. W. (1974). ibid 9, 1436.

Morton, J., & Groves, G. W. (1974). The Cracking of Composites Consisting of Discontinuous Ductile Fibres in a Brittle Matrix - Effect of Fibre Orientation. Journal of Material Sciences, 1436-1445.

Morton, J., & Groves, G. W. (1976). The effect of metal wires on the fracture of a brittle-matrix composite. Journal of Materials Science 11, 617-622.

Mydin, M. A., & Soleimanzadeh, S. (2012). Effect of polypropylene fiber content on flexural strength of lightweight foamed concrete at ambient and elevated temperatures. Adv. Appl. Sci. Res., 3(5), 2837-2846.

Naaman, A. E. (2003, Novemeber). Engineered Steel Fibers with Optimal Properties for Reinforcement of Cement Composites. Journal of Advanced Concrete Technology, 1(3), 241-252.

Narayanan, R., & Darwish, I. Y. (1987). Use of Steel Fibers as Shear Reinforcement. ACI Structural Journal, 216-227.

Nataraja, M. C., Dhang, N., & Gupta, A. P. (1999). Stress strain curve for steel-fiber reinforced concrete under compression. Cem. Concr. Compos., 21(5-6), 383-390.

Noushini, A., Samali, B., & Vessalas, K. (2013). Effect of polyvinyl alcohol (PVA) fibre on dynamic and material properties of fibre reinforced concrete. Construction and Building Materials, 49, 374-383.

Oesterle, R. G., Fiorato, A. E., Aristizabal-Ochoa, J. D., & Corley, W. G. (1980). Hysteretic Response of Reinforced Concrete Structural Walls. pp. 243-273.

Oesterle, R., Fiorato, A. E., Johal, L. S., Carptenter, J. E., Russel, H. G., & Corley, W. G. (1976). Earthquake Resistant Structural Walls - Tests of Isolated Walls. National Science Foundation, 1-43.

Oesterle, R., Fiorato, A., Johal, L., Carptenter, J., Russel, H., & Corley, W. (1976). Earthquake-Resistant Structural Walls-Test of Isolated Walls. PCA Construction Technology Laboratories/National Science Foundation, 315.

Online Metals. (n.d.). Online Metals. Retrieved May 20, 2015, from OnlineMetals.com: www.onlinemetals.com

Otter, D. E., & Naaman, A. E. (1988). Properties of Steel Fiber Reinforced Concrete under Cyclic Loading. ACI Materials Journal, 254-261.

Ou, Y.-C., Tsai, M.-S., Liu, K.-Y., & Chang, K.-C. (2012, February). Compressive Behavior of Steel-Fiber-Reinforced Concrete with a High Reinforcing Index. Journal of Materials in Civil Engineering, 207-215.

Outwater, J. P., & Murphy, M. C. (1969). 24th Annual Technical Conference, S.P.I. Reinforced Plastics Division.

Palermo, D., & Vecchio, F. J. (2001). Behaviour of Cyclically Loaded Shear Walls.

Pang, X.-B. "., & Hsu, T. T. (1995). Behavior of Reinforced Concrete Membrane Elements in Shear. ACI Structural Journal, 665-679.

Parra-Montesinos, G. J., & Chompreda, P. (2007, March). Deformation Capacity and Shear Strength of Fiber-Reinforced Cement Composite Flexural Members Subjected to Displacement Reversals. Journal of Structural Engineering, 421-431.

Parra-Montesinos, G., Canbolat, G., & Jeyeraman, G. R. (2006). Relaxation of Confinement Reinforcement in Structural Walls Through the Use of Fiber Reinforced Cement Composites. Eighth National Conference on Earthquake Engineering. San Francisco.

Paulay, T. M. (1986). The Design of Ductile Reinforced Concrete Structural Walls for Earthquake Resistance. Earthquake Spectra, 783-823.

Paulay, T., Priestley, M. J., & Synge, A. J. (1982). Ductility in Earthquake Squat Shearwalls. ACI Journal, 257-269.

Pilakoutas, K., & Elnashai, A. (1995). Cyclic Behavior of Reinforced Concrete Cantilever Walls, Part 1: Experimental Results. ACI Structural Journal, 271-281.

Pilakoutas, K., & Elnashai, A. S. (1995). Cyclic Behavior of Reinforced Concrete Cantilever Walls, Part II: Discussions and Theoretical Comparisons. ACI Structural Journal, 425-433.

Popovics, S. (1987). A hypothesis concerning the effects of macro-porosity on mechanical properties of concrete. Proc., SEM/RELIM Int. Conf. on Fracture of Concrete and Rock, 170-174.

Rubber Manufacturers Association. (2013). U.S. Scrap Tire Management Summary 2005-2009. Washington, DC.

Salonikios, T. N., Kappos, A. J., Tegos, I. A., & Penelis, G. G. (1999). Cyclic Load Behavior of Low-Slenderness Reinforced Concrete Walls: Design Basis and Test Results. ACI Structural Journal, 649-661.

Salonikios, T. N., Kappos, A. J., Tegos, I. A., & Penelis, G. G. (2000). Cyclic Load Behavior of Low-Slenderness Reinforced Concrete Walls: Failure Modes, Strength and Deformation Analysis, and Design Implications. ACI Structural Journal, 132-142.

Salonikios, T. N., Kappos, A. J., Tegos, I. A., & Penelis, G. G. (2007). Analytical Prediction of the Inelastic Response of RC Walls with Low Aspect Ratio. Journal of Structural Engineering, 844-854.

Segre, N., & Joekes, I. (2000). Use for tire rubber particles as addition to cement paste. Cement Concrete Res., 30(9), 1421-1425.

Shao, Y., & Shah, S. P. (1997, November-December). Mechanical Properties of PVA FIber Reinforced Cement Composites Fabricated by Extrusion Processing. ACI Materials Journal, 555-564.

Shende, A., & Pander, A. (2011). Experimental Study and Prediction of Tensile Strength for Steel Fiber Reinforced Concrete. International Journal of Civil and Structural Engineering, 910-917.

Soroushian, P., & Bayasi, Z. (1991). Fiber type effects on the performance of steel fiber reinforced concrete. ACI Materials Journal, 88(2), 129-134.

Soulioti, D. V., Barkoula, N. M., Paipetis, A., & Matikas, T. E. (2011). Effects of Fibre Geometry and Volume Fraction on the Flexural Behaviour of Steel-Fibre Reinforced Concrete. Strain, 47, 534-541.

Stevens, N. J., Uzumeri, S. M., & Collins, M. P. (1991). Reinforced Concrete Subjected to Reversed Cyclic Shear - Experiments and Constitutive Method. ACI Structural Journal, 135-146.

Taha, M. M., El-Dieb, A. S., El-Wahab, M. A., & Abdel-Hameed, M. E. (2008, October). Mechanical, Fracture, and Microstructural Investigations of Rubber Concrete. Journal of Materials in Civil Engineering, 640-649.

Thomas, J., & Ramaswamy, A. (2007, May). Mechanical Properties of Steel Fiber-Reinforced Concrete. Journal of Materials in Civil Engineering, ASCE, 385-392.

Topçu, I. B. (1995). The Properties of Rubberized Concretes. Cement and Concrete Research, 25(2), 304-310.

Toutanji, H. A. (1996). The Use of Rubber Tire Particles in Concrete to Replace Mineral Aggregate. Cement and Concrete Composites, 18, 135-139.

Toutanji, H. A., Xu, B., & Gilbert, J. (2010). Impact resistance of poly(vinyl alcohol) fiber reinforced high-performance organic aggregate cementitious material. Cement and Concrete Research, 40(2), 347-351.

U.S. Environmental Protection Agency. (2013). Wastes - Resource Conservation - Common Wastes & Materials - Scrap Tires. Retrieved 2015, from U.S. Environmental Protection Agency: http://www.epa.gov/epawaste/conserve/materials/tires/faq.htm

Vecchio, F. J., & Collins, M. D. (1986). The Modified Compression-Field Theory for Reinforced Concrete Elements Subjected to Shear. ACI Journal, 219-231.

Wallace, J. W. (1994). New Methodology for Seismic Design of RC Shear Walls. Journal of Structural Engineering, 101-130.

Wallace, J. W., & Moehle, J. P. (1989). The 3 March 1985 Chile Earthquake: Structural Requirements for Bearing Walls Buildings. Berkeley.

Ward, R., Yamanobe, K., Li, V., & Backer, S. (1989). Fracture resistance of acrylic fiber reinforced mortar in shear and flexure. In Fracture Mechanics: Application to Concrete. (V. L. Bazant, Ed.) ACI SP-118, 17-68.

Willie, K., & Naaman, A. E. (2012, July-August). Pullout Behavior of High-Strength Steel Fibers Embedded in Ultra-High-Performance Concrete. ACI Materials Journal, 479-487.

Wood, L. S. (1991). Performance of Reinforced Concrete Buildings during the 1985 Chile Earthquake. Earthquake Spectra, 607-638.

Wood, S. L. (1989). Minimum Tensile Reinforcement Requirements in Walls. ACI Structural Journal, 582-591.

Wood, S. L. (1990). Shear Strength of Low-Rise Reinforced Concrete Walls. ACI Structural Journal, 99-107.

Wu, H.-C., & Li, V. C. (1994). Trade-off Between Strength and Ductility of Random Discontinous Fiber Reinforced Cementitious Composites. Cement and Concrete Composites, 16, 23-29.

Zhang, Y., & Wang, Z. (2000). Seismic Behavior of Reinforced Concrete Shear Walls Subjected to High Axial Loading. ACI Structural Journal, 739-750.

Zheng, L., Huo, X. S., & Yuan, Y. (2008, November). Strength, Modulus of Elasticity, and Brittleness Index of Rubberized Concrete. Journal of Materials in Civil Engineering, 692-699.

Zhong, J. X., Mo, Y. L., & Liao, W. I. (2009). Reversed Cyclic Behavior of Reinforced Concrete Shear Walls with Diagonal Steel Grids. ACI Special Publication, pp. 47-60.

APPENDIX A

APPENDIX A Figures

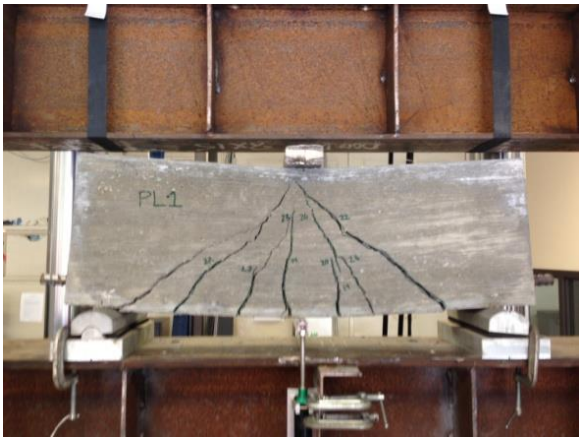

Figure A1 - Beam Specimen PL1

Figure A2 - Beam Specimen 5C

Figure A3 - Beam Specimen 5F

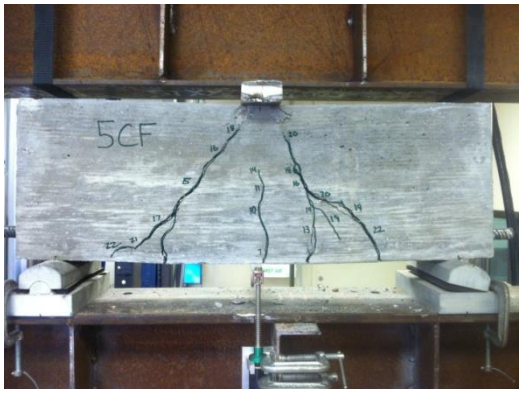

Figure A4 - Beam Specimen 5CF

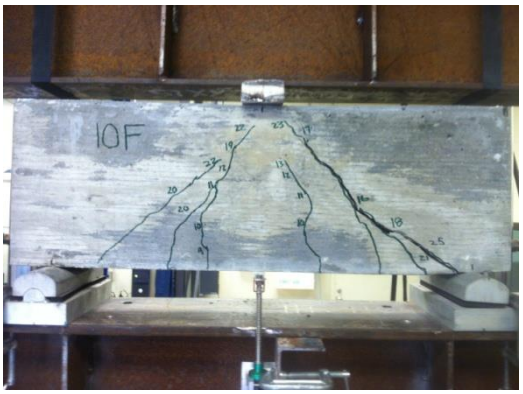

Figure A5 - Beam Specimen 10C

Figure A6 - Beam Specimen 10F

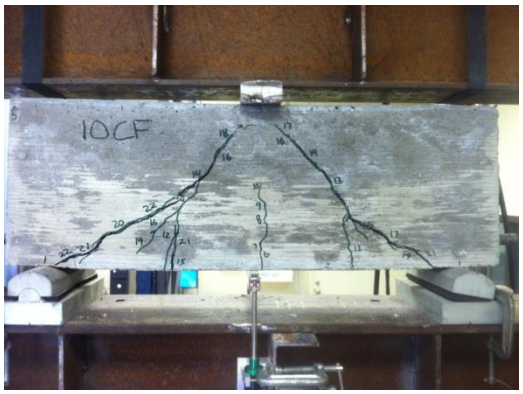

Figure A7 - Beam Specimen 10CF

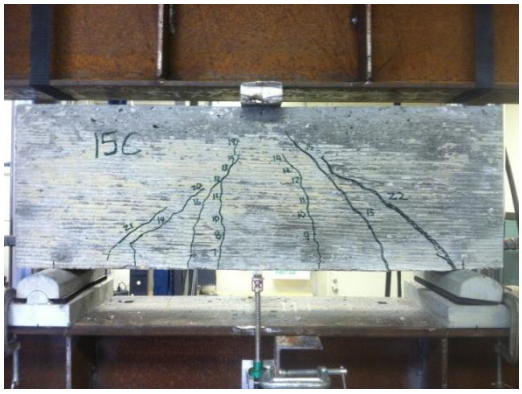

Figure A8 - Beam Specimen 15C

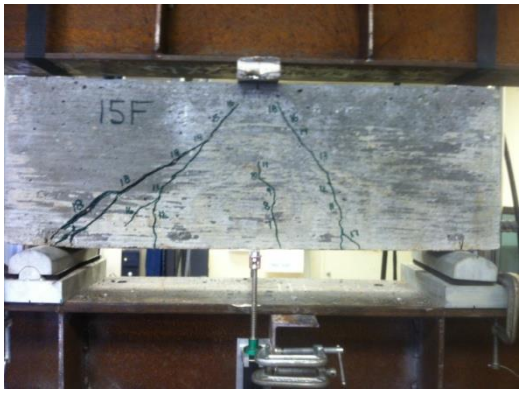

Figure A9 - Beam Specimen 15F

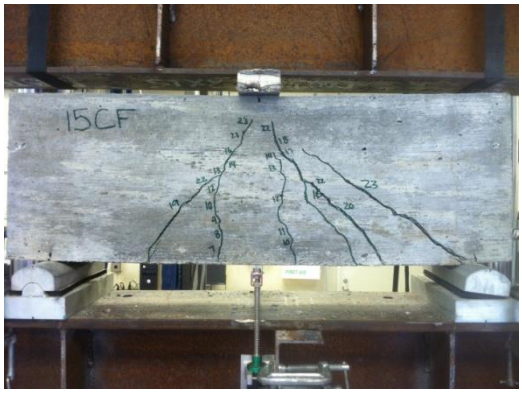

Figure A10 - Beam Specimen 15CF

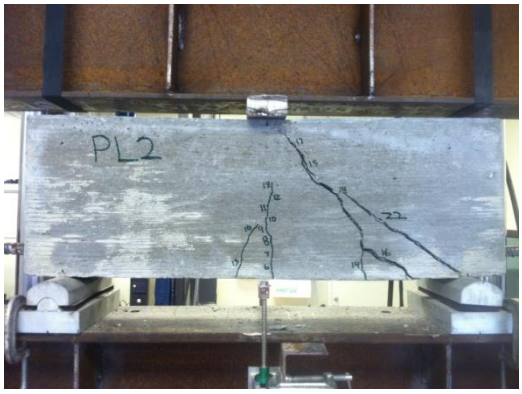

Figure A11 - Beam Specimen PL2

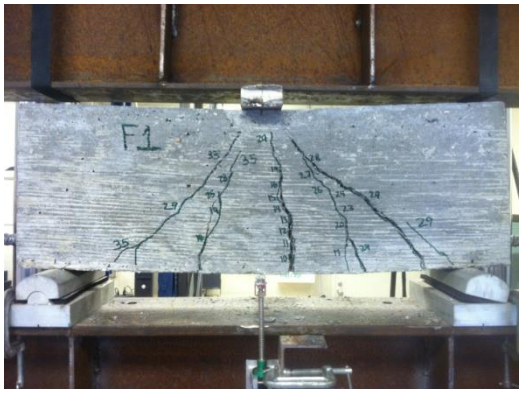

Figure A12 - Beam Specimen F1

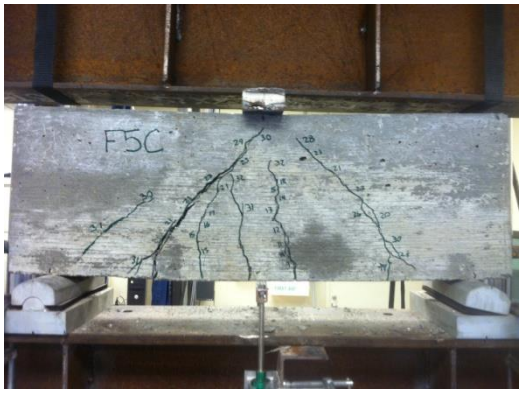

Figure A13 - Beam Specimen F5C

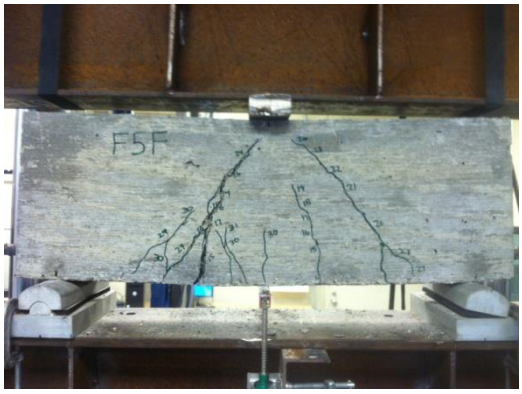

Figure A14 - Beam Specimen F5F

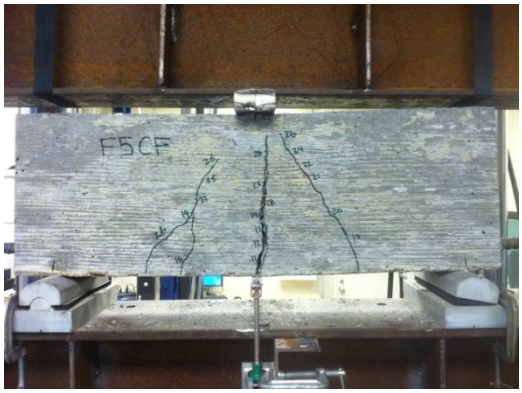

Figure A15 - Beam Specimen F5CF

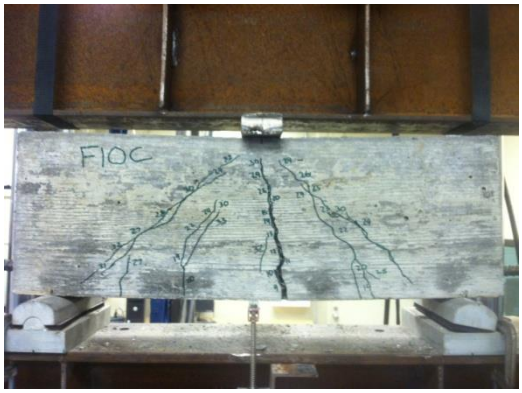

Figure A16 - Beam Specimen F10C

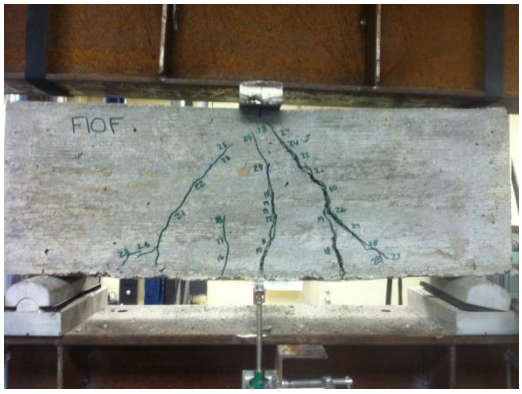

Figure A17 - Beam Specimen F10F

Figure A18 - Beam Specimen F10CF

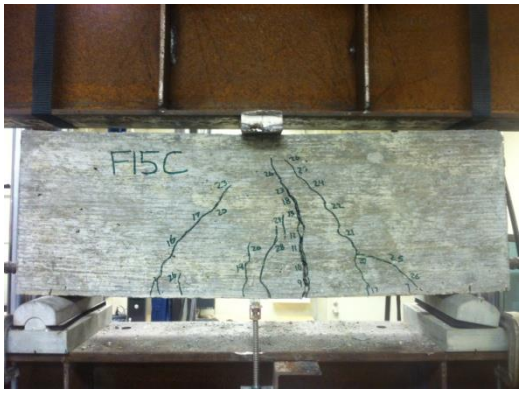

Figure A19 - Beam Specimen F15C

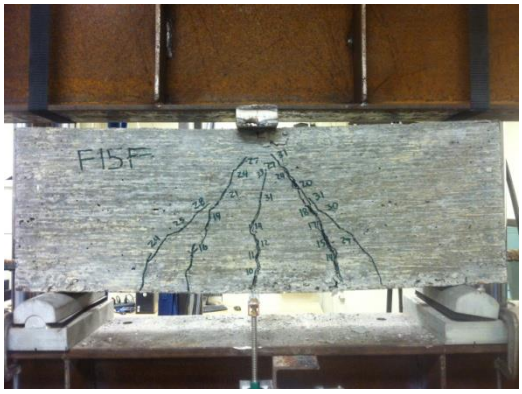

Figure A20 - Beam Specimen F15F

Figure A21 - Beam Specimen F15CF

Figure A22 - Beam Specimen F2

APPENDIX B

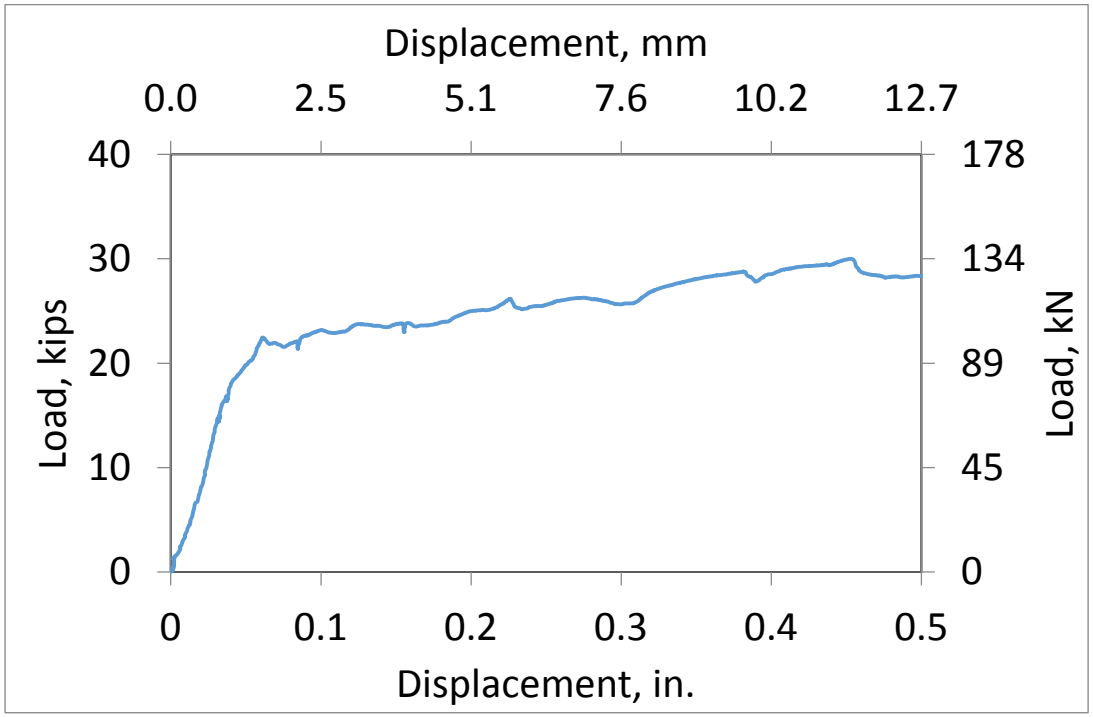

Figure B1 - Beam specimen PL1 Lateral Load Versus Displacement Response

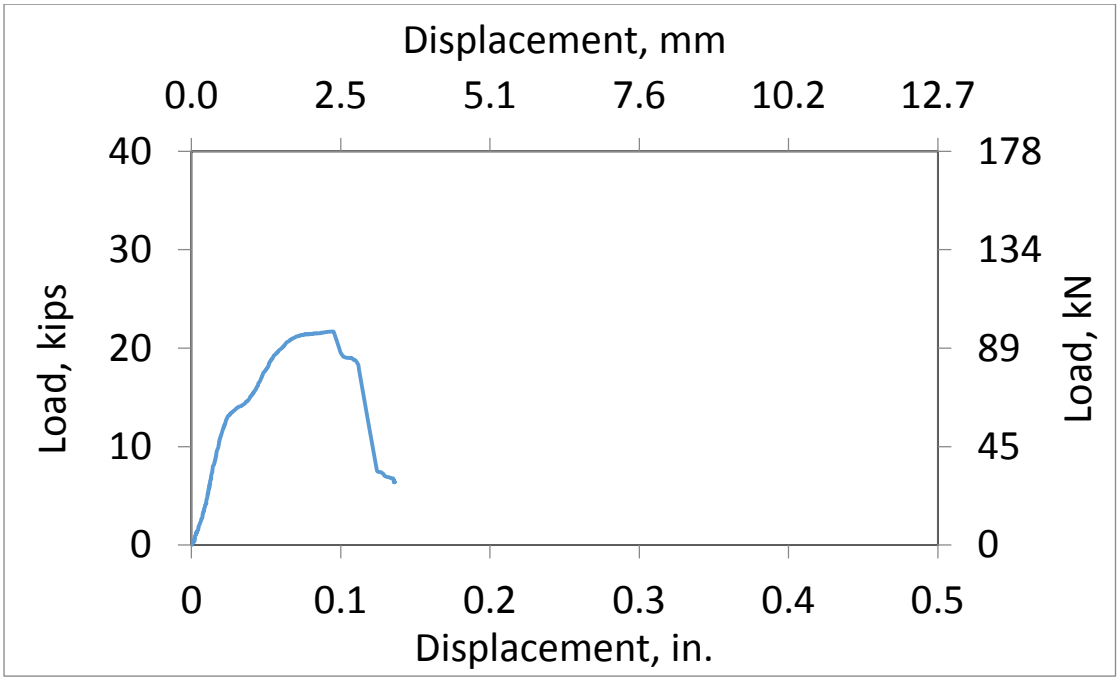

Figure B2 - Beam specimen 5C Lateral Load Versus Displacement Response

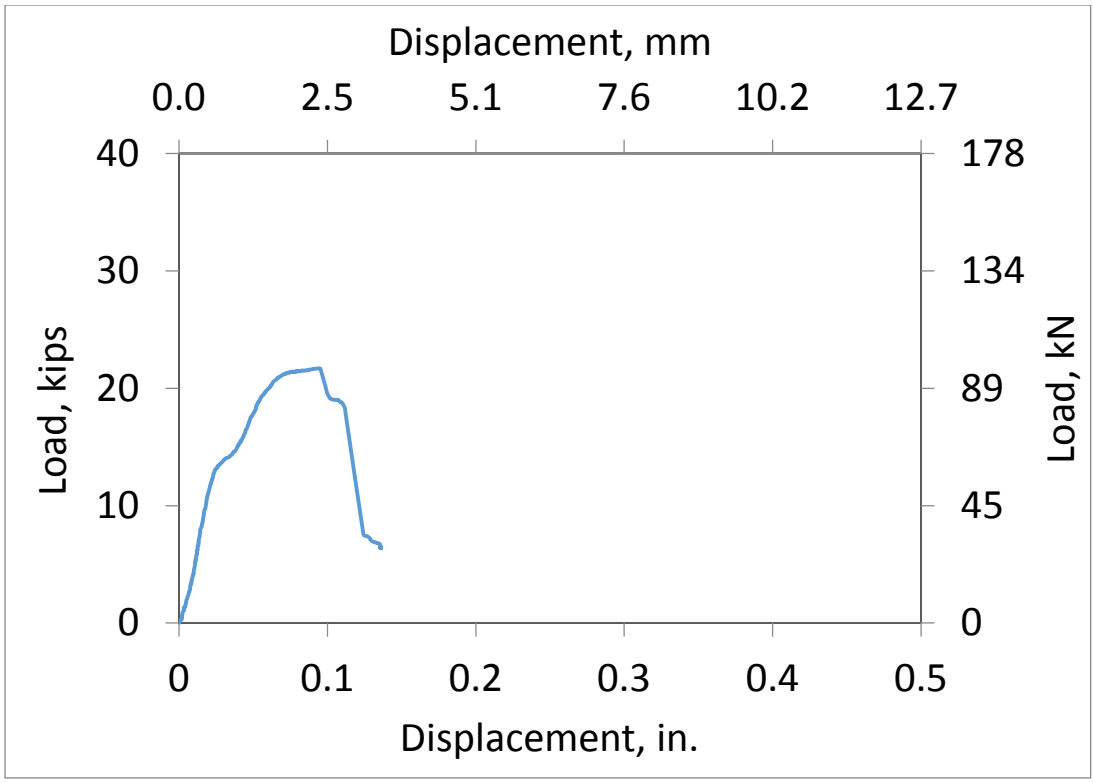

Figure B3 - Beam specimen 5F Lateral Load Versus Displacement Response

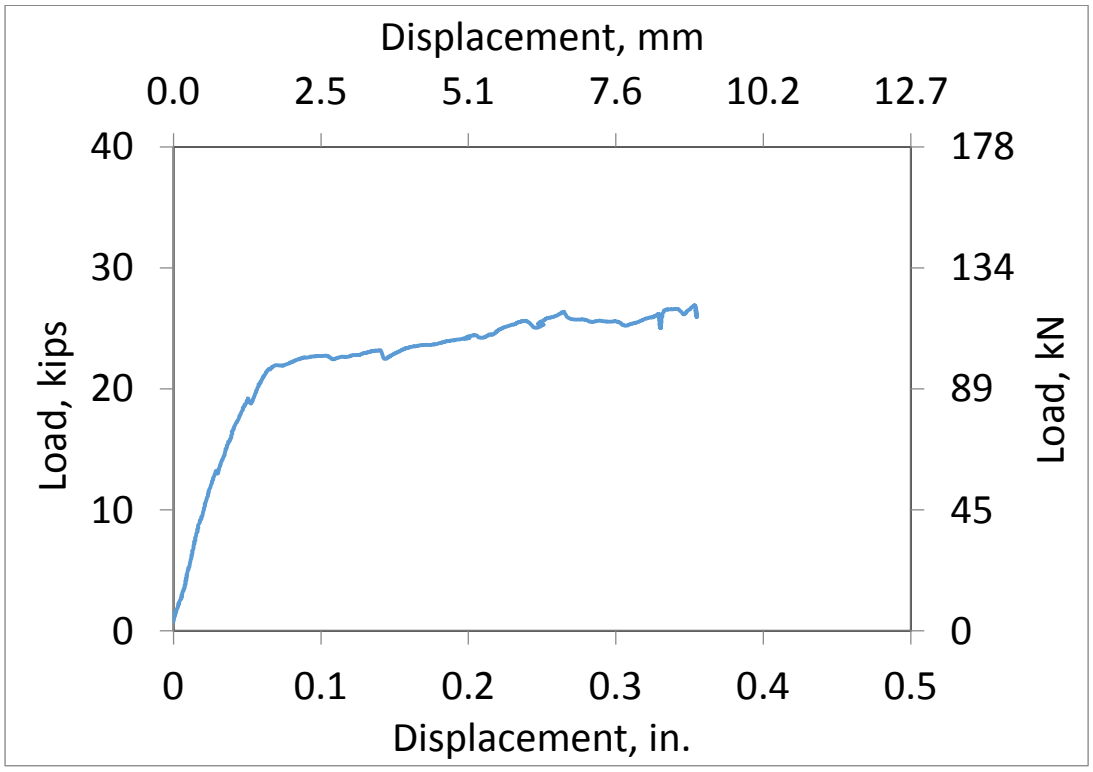

Figure B4 - Beam specimen 5CF Lateral Load Versus Displacement Response

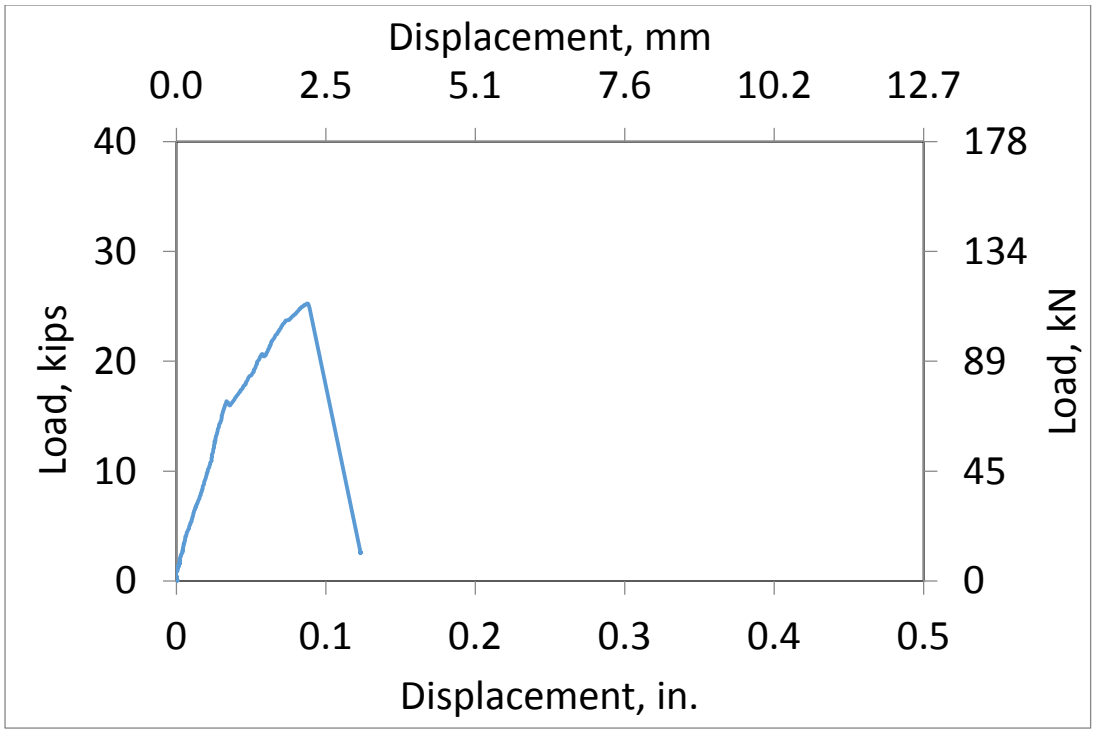

Figure B5 - Beam specimen 10C Lateral Load Versus Displacement Response

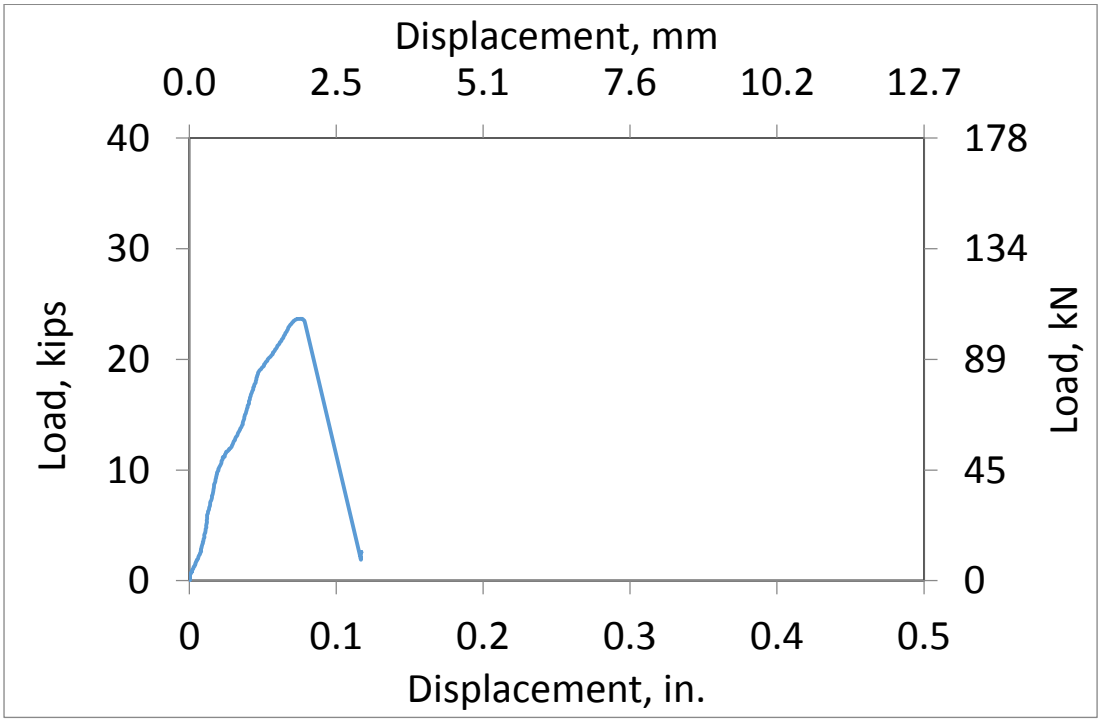

Figure B6 - Beam specimen 10F Lateral Load Versus Displacement Response

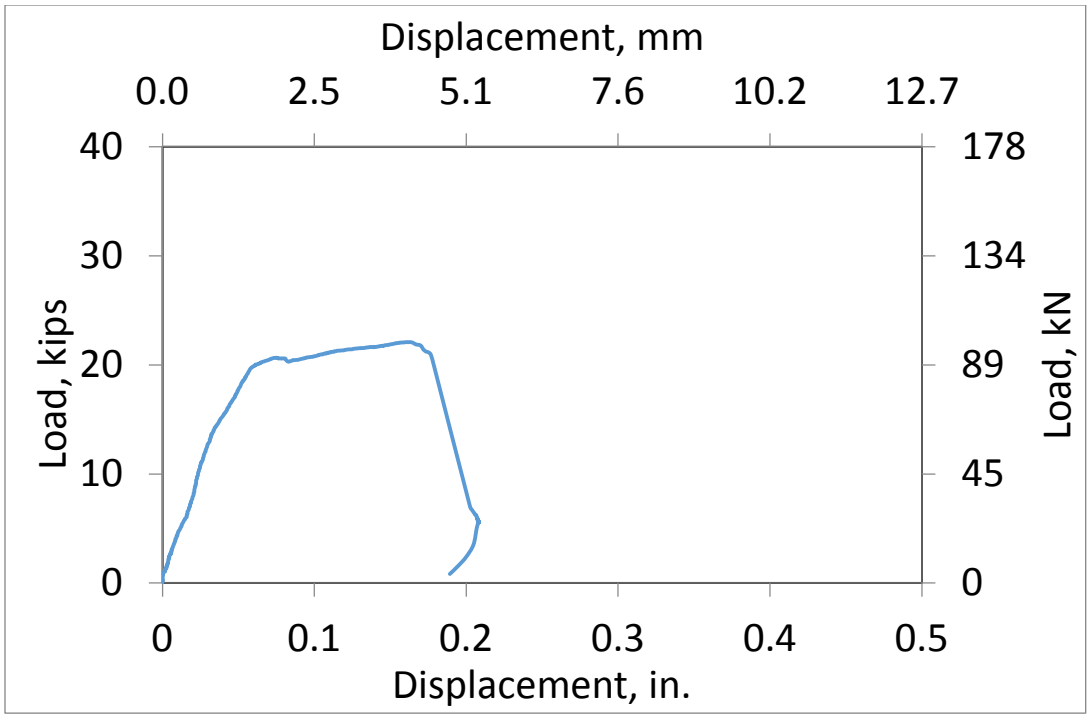

Figure B7 - Beam specimen 10CF Lateral Load Versus Displacement Response

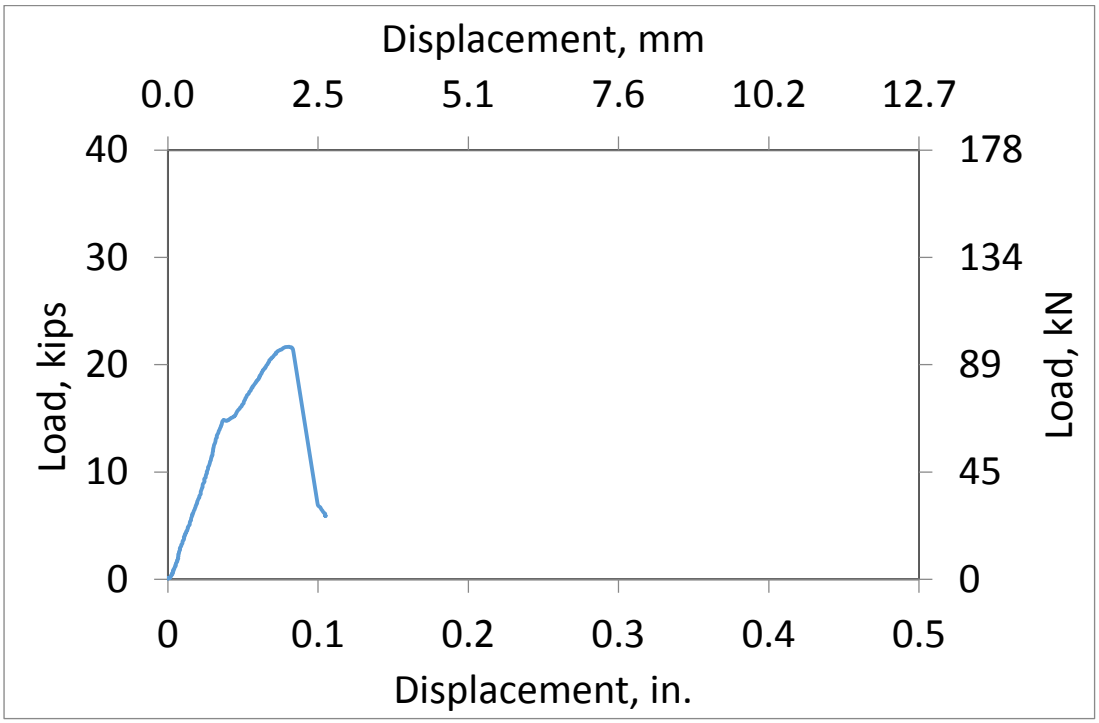

Figure B8 - Beam specimen 15C Lateral Load Versus Displacement Response

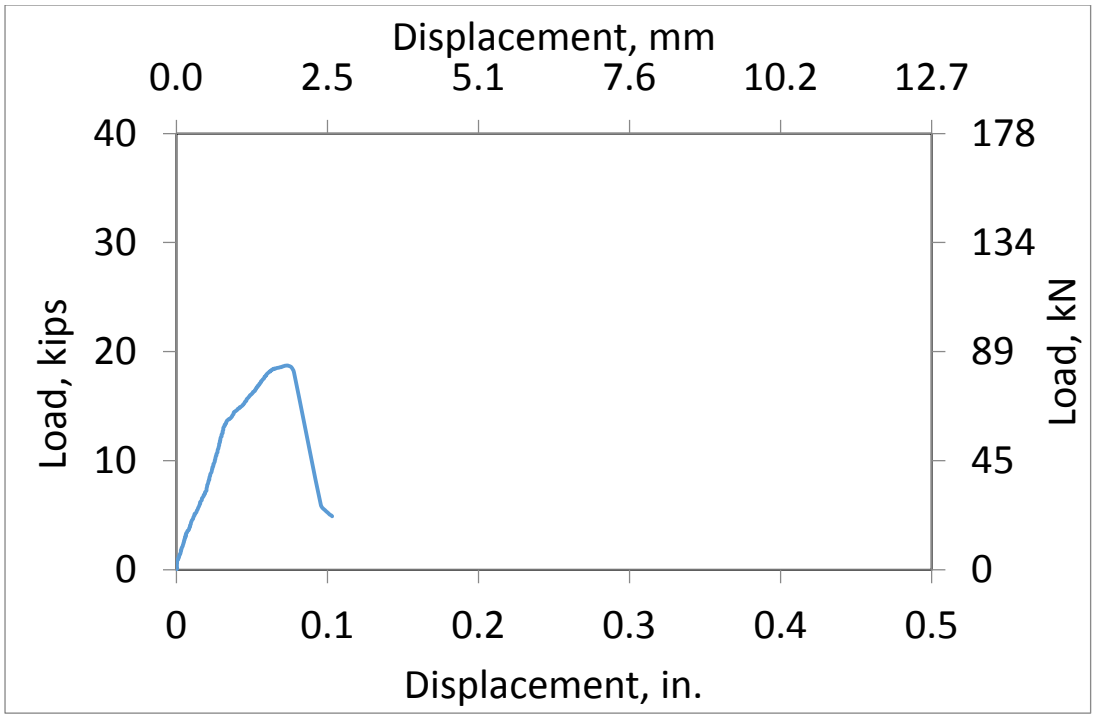

Figure B9 - Beam specimen 15F Lateral Load Versus Displacement Response

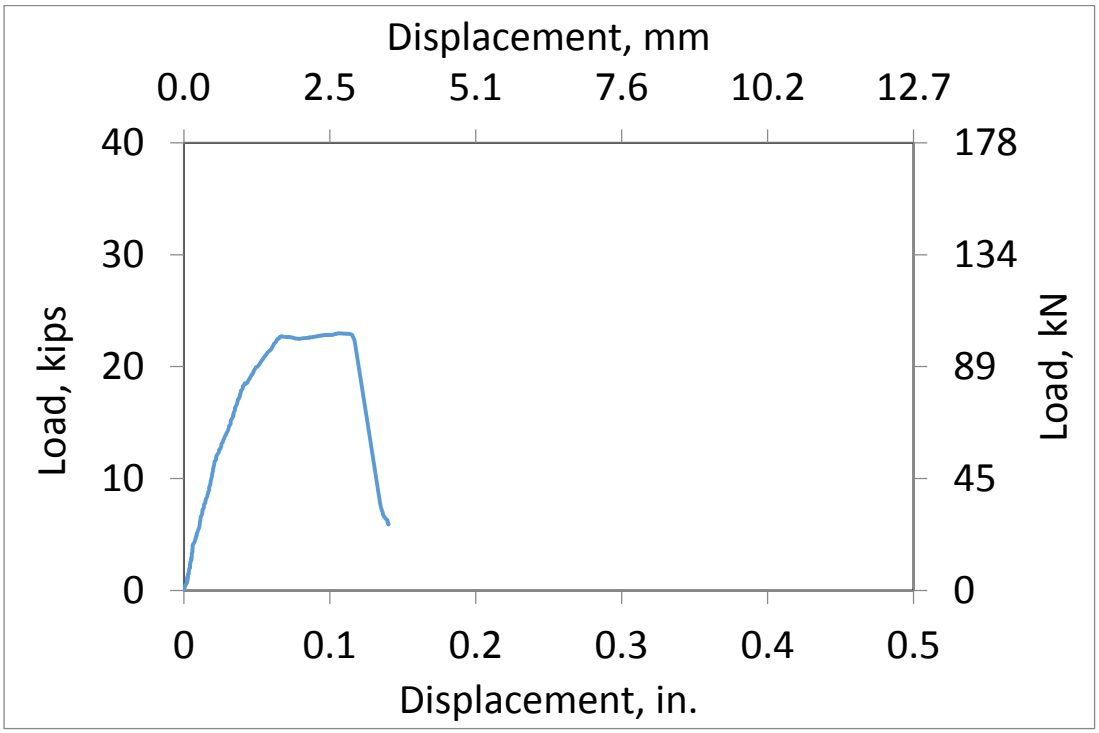

Figure B10 - Beam specimen 15CF Lateral Load Versus Displacement Response

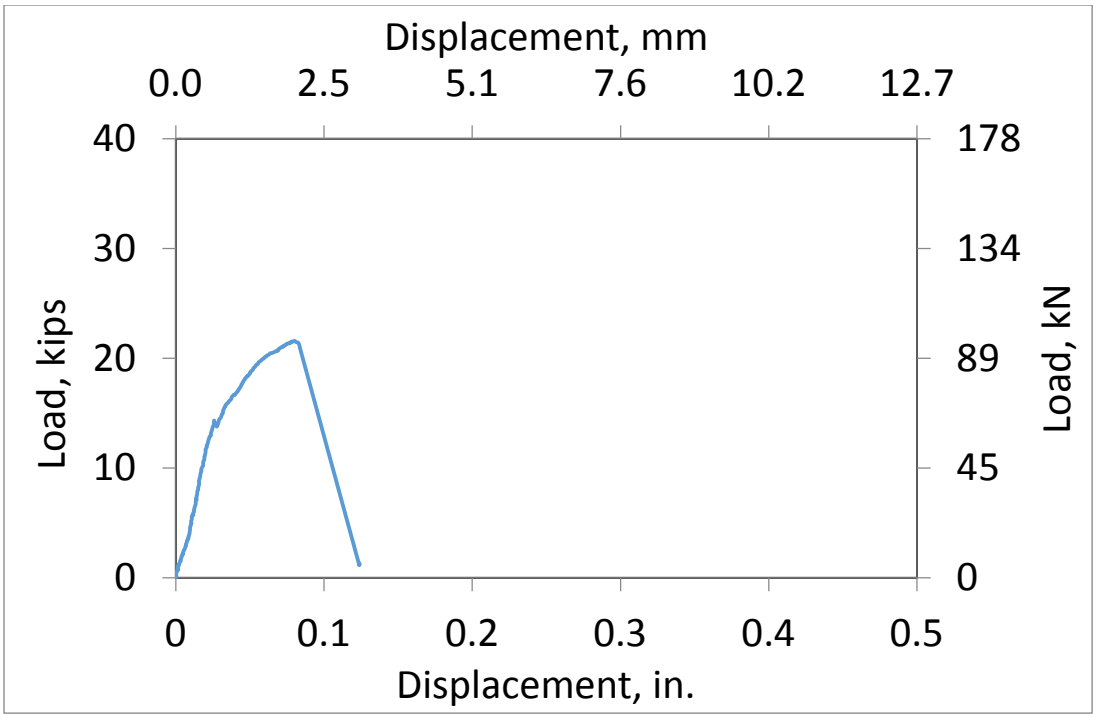

Figure B11 - Beam specimen PL2 Lateral Load Versus Displacement Response

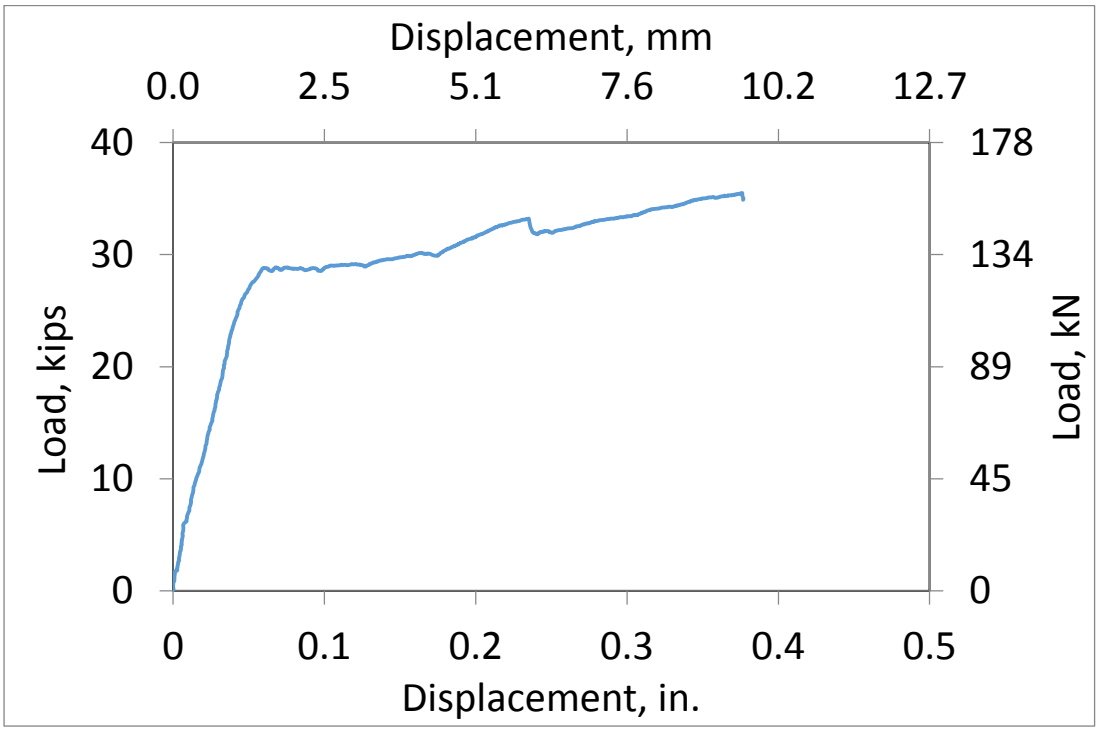

Figure B12 - Beam specimen F1 Lateral Load Versus Displacement Response

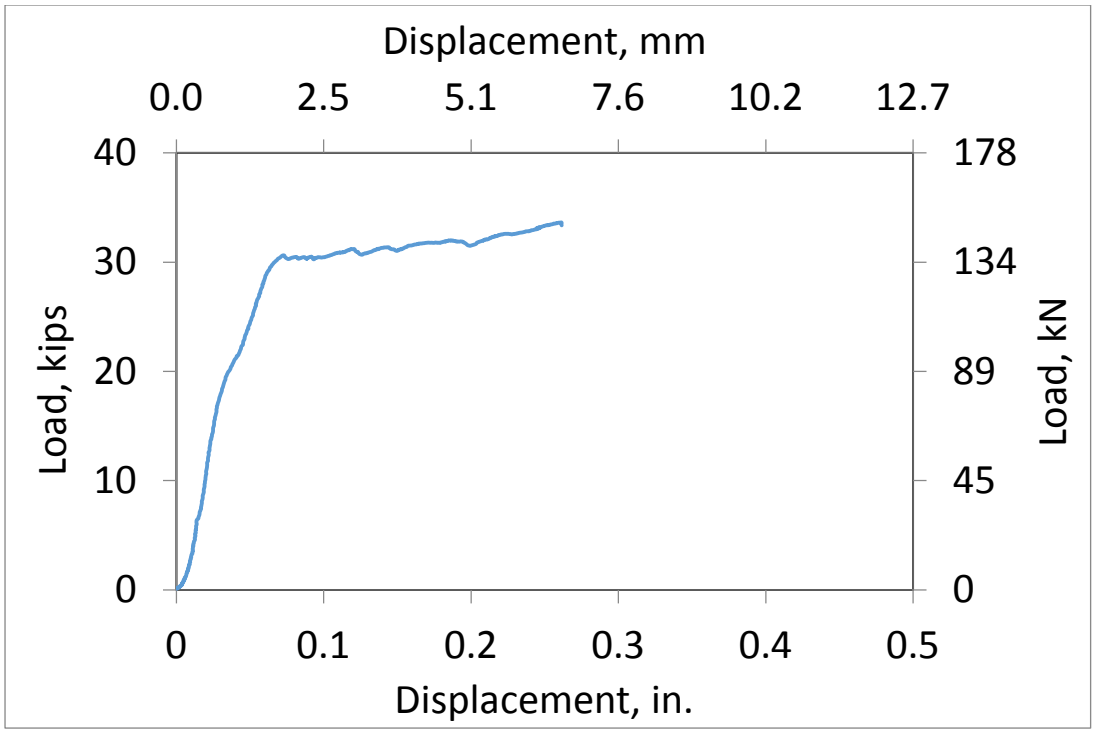

Figure B13 - Beam specimen F5C Lateral Load Versus Displacement Response

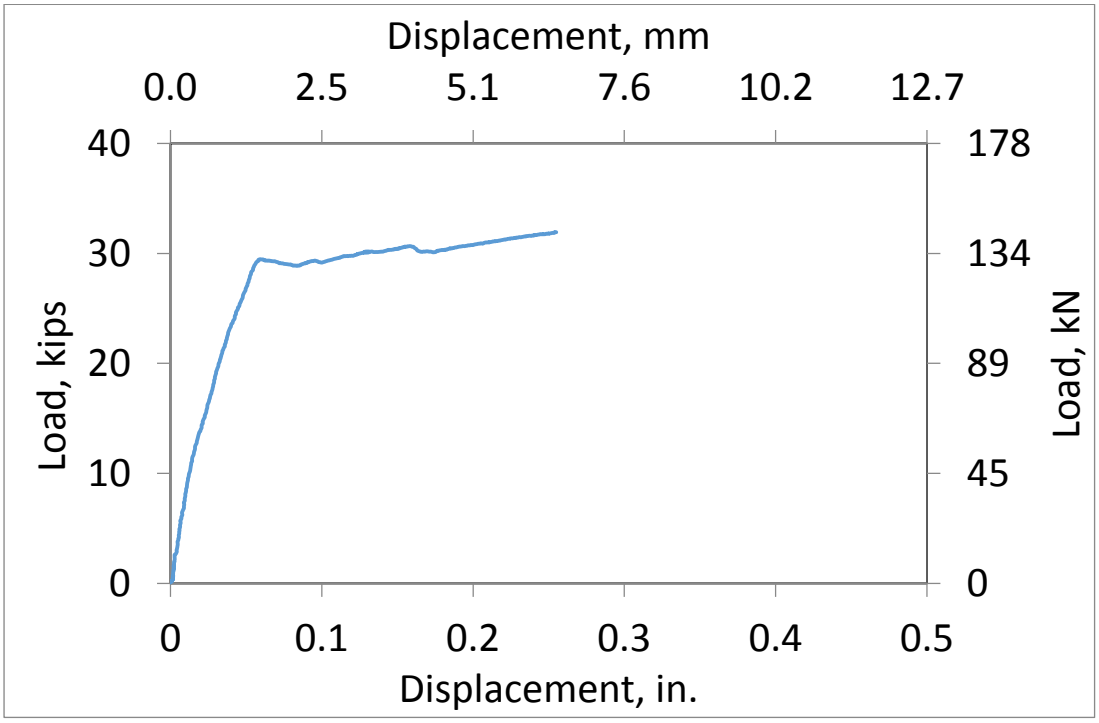

Figure B14 - Beam specimen F5F Lateral Load Versus Displacement Response

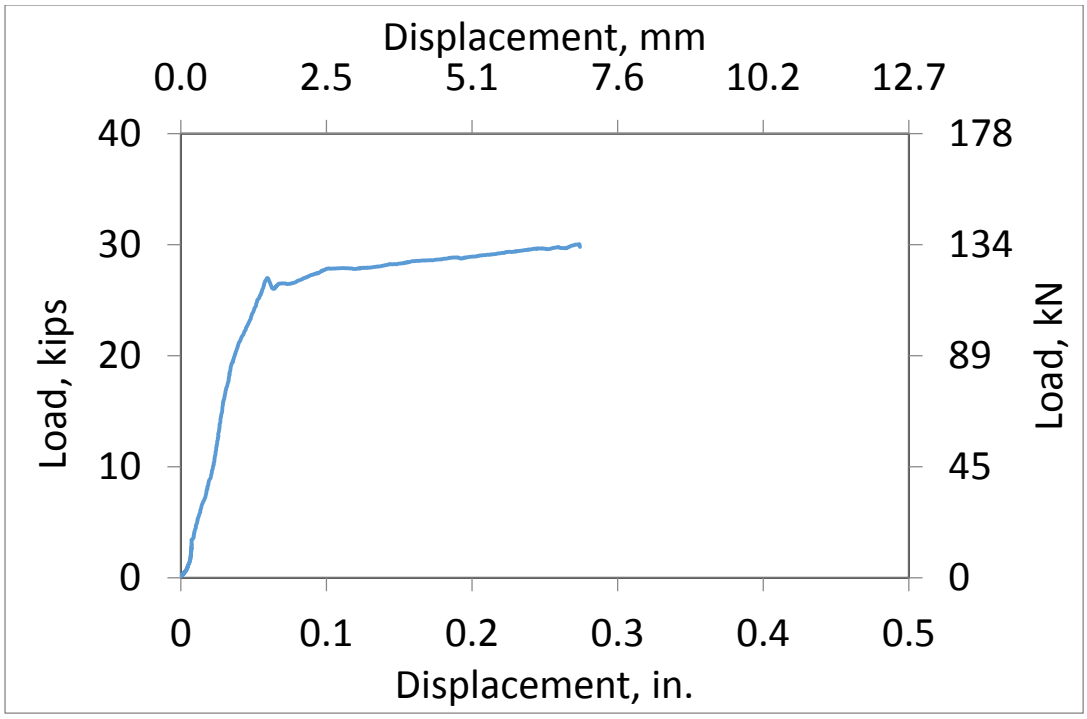

Figure B15 - Beam specimen F5CF Lateral Load Versus Displacement Response

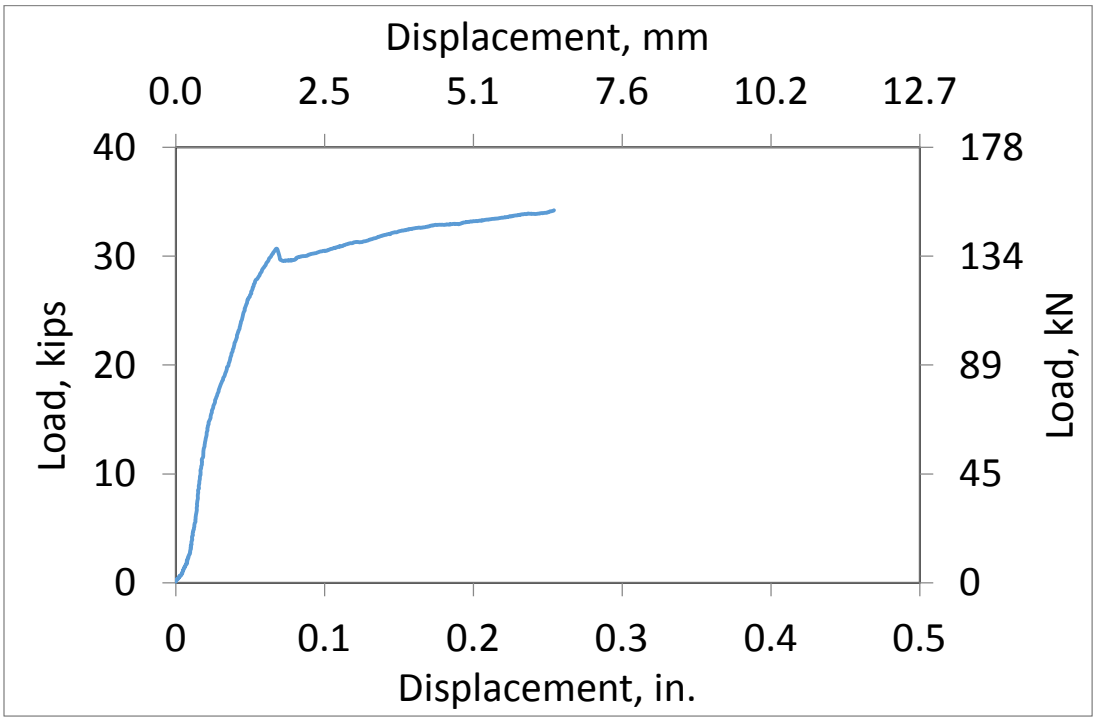

Figure B16 - Beam specimen F10C Lateral Load Versus Displacement Response

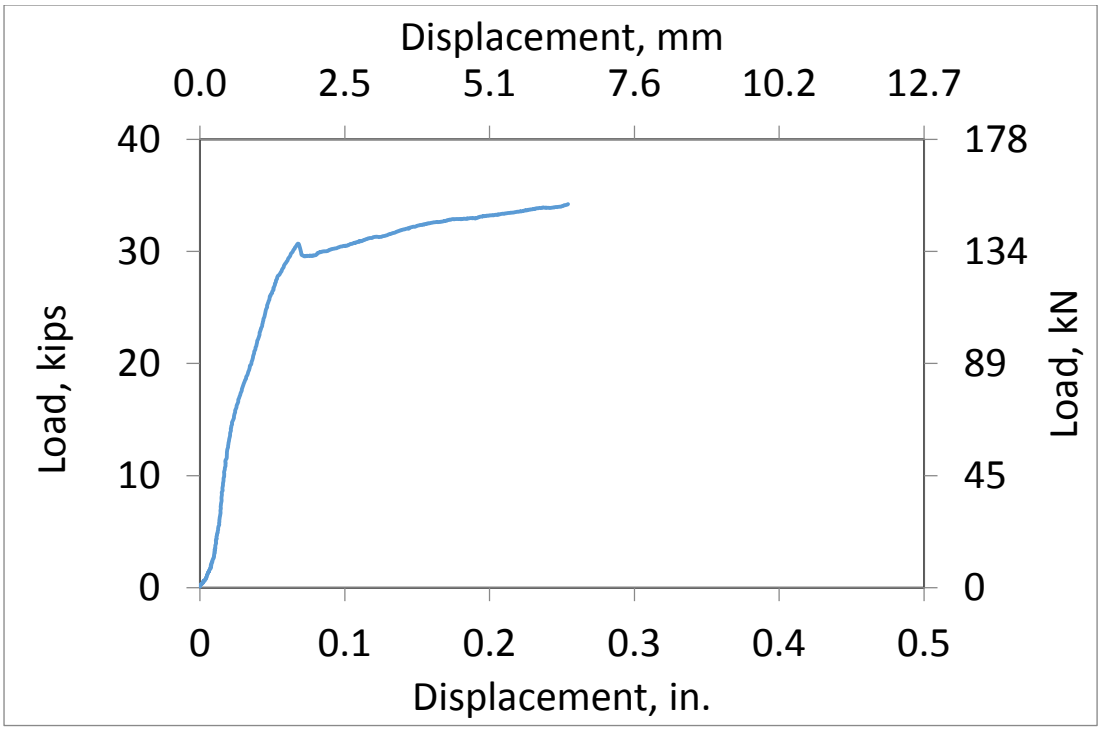

Figure B17 - Beam specimen F10F Lateral Load Versus Displacement Response

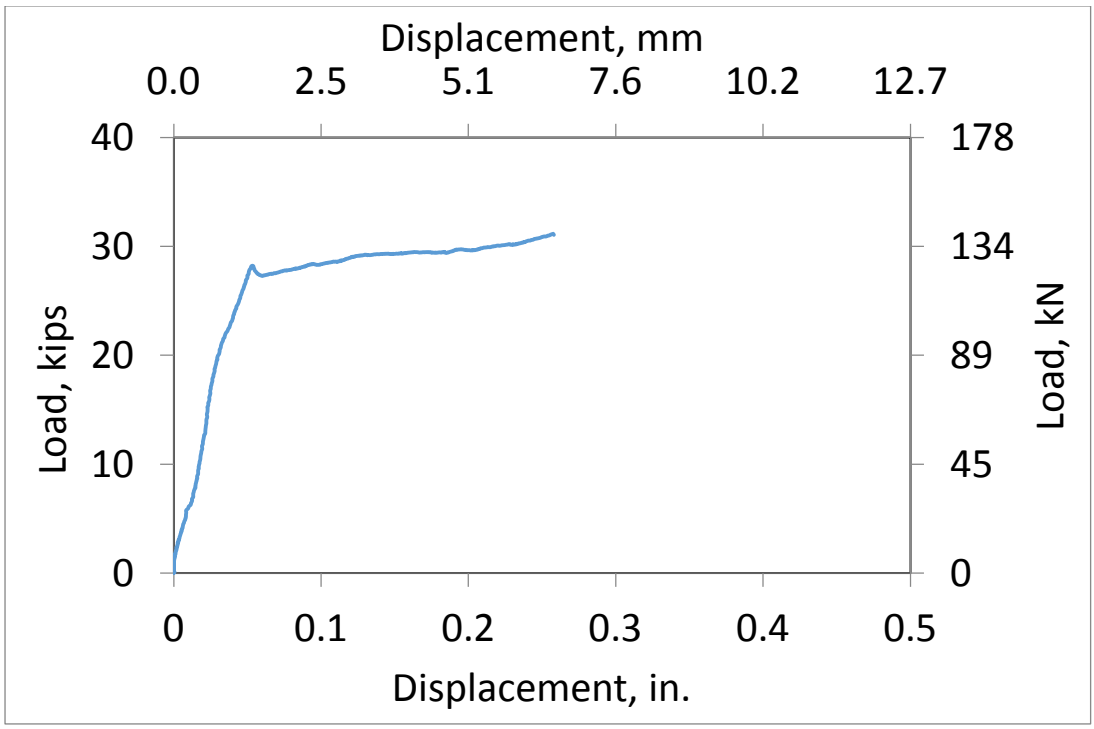

Figure B18 - Beam specimen F10CF Lateral Load Versus Displacement Response

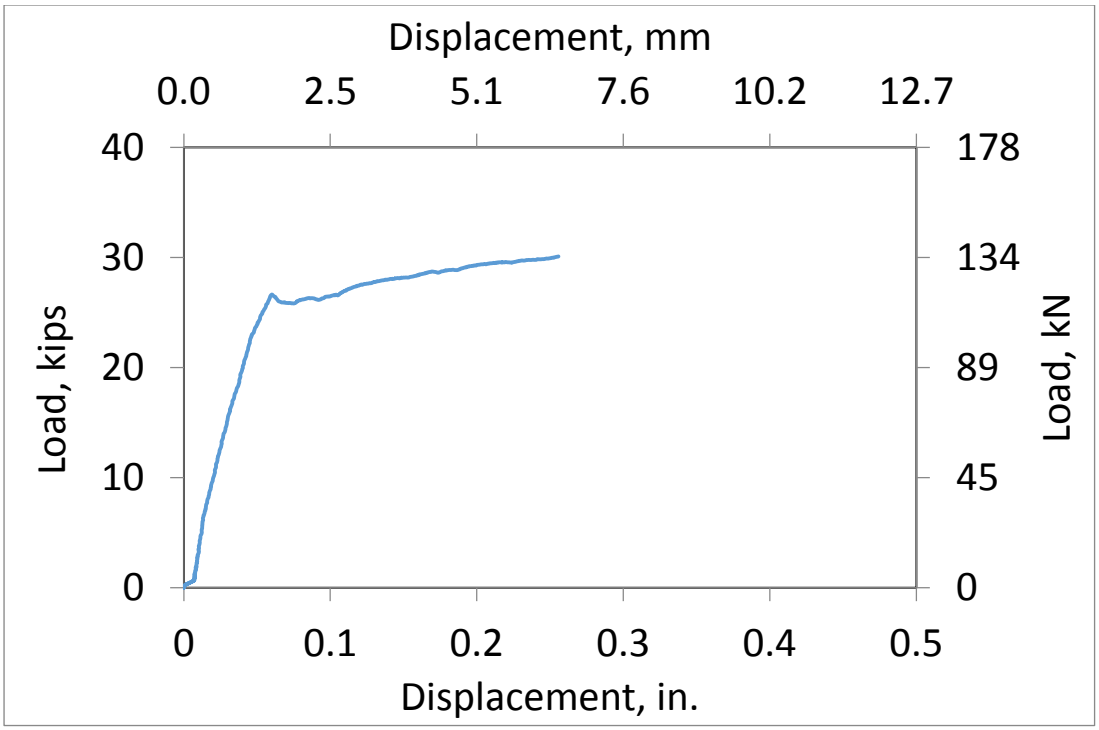

Figure B19 - Beam specimen F15C Lateral Load Versus Displacement Response

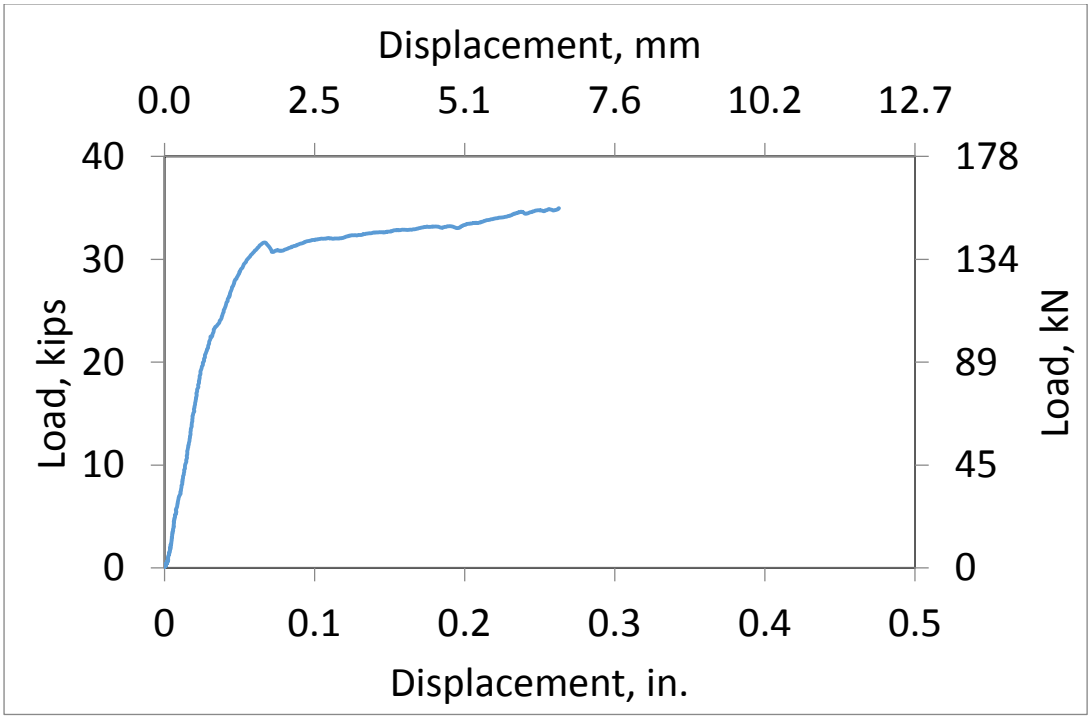

Figure B20 - Beam specimen F15F Lateral Load Versus Displacement Response

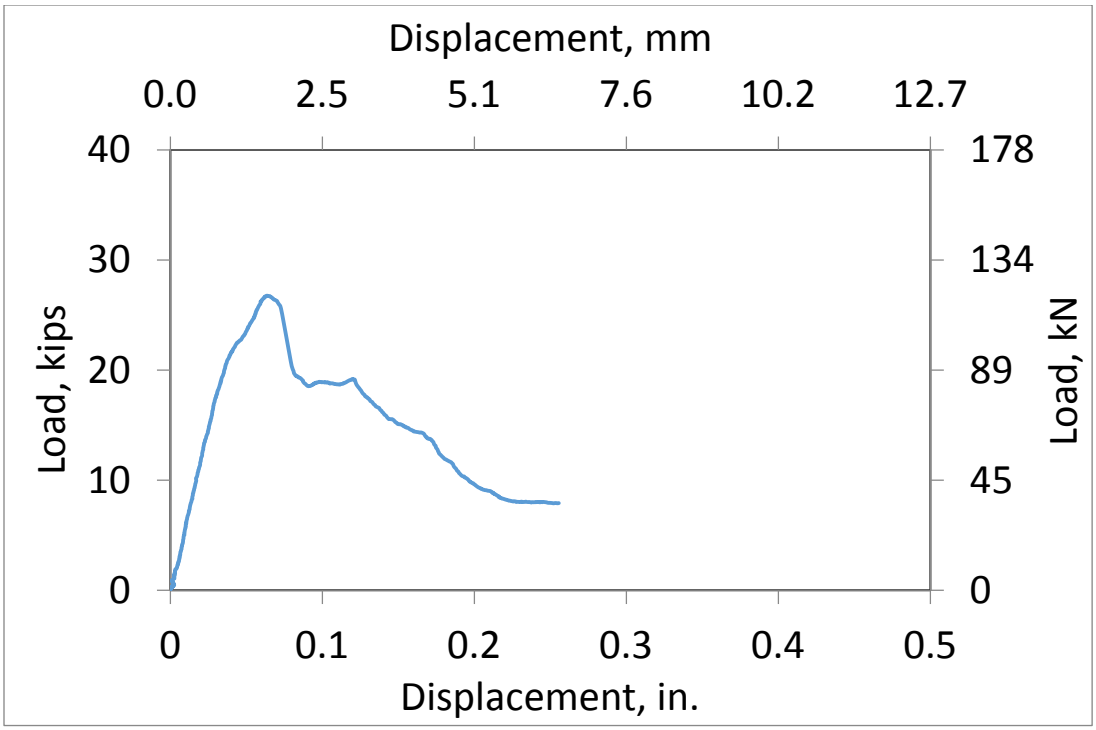

Figure B21 - Beam specimen F15CF Lateral Load Versus Displacement Response

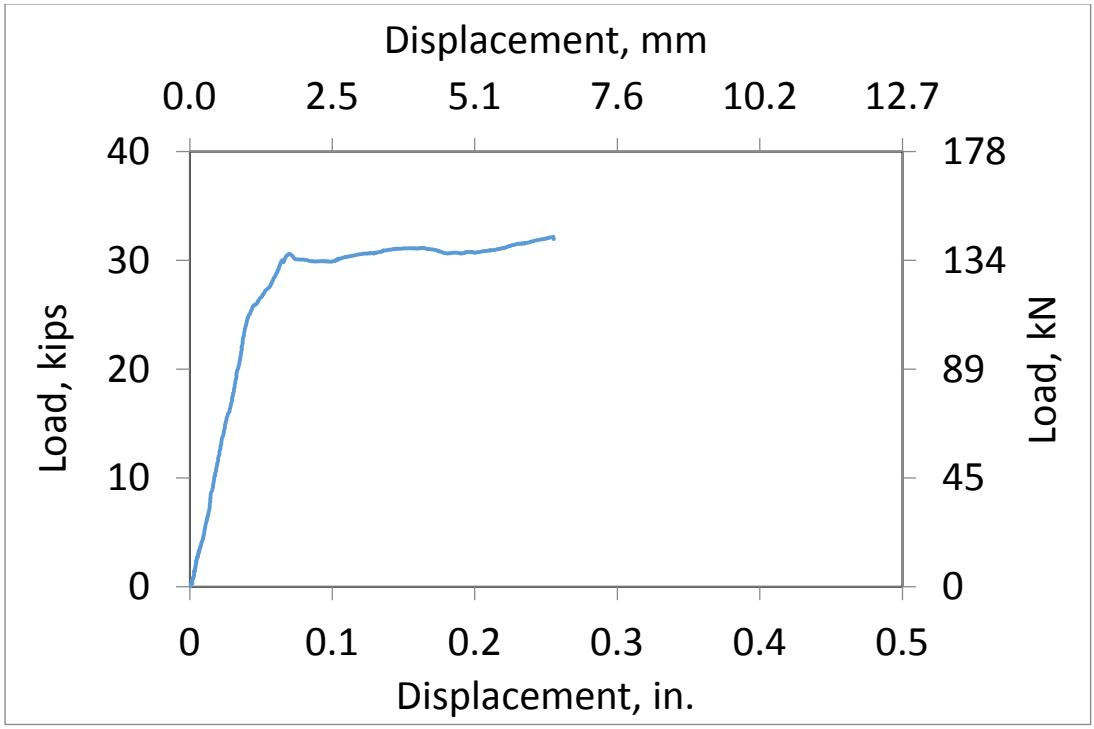

Figure B22 - Beam specimen F2 Lateral Load Versus Displacement Response

Broussard, Dylan W. Bachelor of Science, Millsaps College, Fall 2012; Master of Science, University of Louisiana at Lafayette, Fall 2015; Master of Business Administration, University of Louisiana at Lafayette, Summer 2015
Major: Engineering, Civil engineering option
Title of Thesis: Cyclic Behavior of Small Scale Shear Panels Containing Fiber Reinforced Rubber Concrete
Thesis Director: Dr. Chris Carroll
Pages in Thesis: 220; Words in Abstract: 300

ABSTRACT

Shear beams and shear walls were constructed using varying amounts of steel fibers and rubber to determine the effect of these constituents on concrete when subject to shear loads and reversed cyclic loadings. 22 concrete beams were tested using mixes with differing amounts of fibers and rubber. The beams were designed to fail in shear by applying a single downward point load at midspan using a MTS Universal Testing Machine. Using the recorded load and displacement data the behavior of each beam and the shear strength contribution for each mix were determined. For all mixes that included fibers and/or rubber the shear strengths increased 12% to 56% in comparison to the plain concrete mixes. Four concrete walls were also tested using four of the 22 beam mixes. The four selected mixes were chosen based on the comparable compressive strengths and mix constituents. The walls were designed to fail in shear by applying a lateral load to a top block cast on top of the shear wall. The walls were tested on a modular strong-block test system within a rigid steel frame so that the load could be applied by a hydraulic actuator. During testing, the displacement at 10 selected locations, the loads placed on the walls at each displacement, and the behavior were recorded and analyzed. The walls containing rubber experienced lower strengths, a brittle failure with severe spalling and damage, and dissipated a low amount of energy. The walls containing fibers exhibited strain hardening characteristics leading to a ductile failure mode, higher strengths, and little web damage. Using the findings from this study, it can be

concluded that both fibers and rubber can be used to increase shear strength but only fibers were found to be a viable option for application in walls subject to reverse cyclic loadings.

BIOGRAPHICAL SKETCH

Dylan Broussard was born on June 14, 1990 and grew up in Lafayette, Louisiana. His parents are Matt and Meleesa Broussard. Dylan graduated from Millsaps College in May 2012 with a Bachelor of Science in Engineering Studies. Dylan also graduated from the University of Louisiana at Lafayette in August of 2015 with a Master's of Business Administration. Dylan is a member of ACI and ASCE and plans to continue his involvement in these societies in his professional career. In December 2015, Dylan was awarded a Master of Science in Engineering from the University of Louisiana at Lafayette.